

1-1-2008

## Three-dimensional numerical study of proton exchange membrane fuel cell design

Jianfei Wu

*University of Nevada, Las Vegas*

Follow this and additional works at: <https://digitalscholarship.unlv.edu/rtds>

---

### Repository Citation

Wu, Jianfei, "Three-dimensional numerical study of proton exchange membrane fuel cell design" (2008). *UNLV Retrospective Theses & Dissertations*. 2437.

<http://dx.doi.org/10.25669/5phq-7o3n>

This Thesis is protected by copyright and/or related rights. It has been brought to you by Digital Scholarship@UNLV with permission from the rights-holder(s). You are free to use this Thesis in any way that is permitted by the copyright and related rights legislation that applies to your use. For other uses you need to obtain permission from the rights-holder(s) directly, unless additional rights are indicated by a Creative Commons license in the record and/or on the work itself.

This Thesis has been accepted for inclusion in UNLV Retrospective Theses & Dissertations by an authorized administrator of Digital Scholarship@UNLV. For more information, please contact [digitalscholarship@unlv.edu](mailto:digitalscholarship@unlv.edu).

THREE-DIMENSIONAL NUMERICAL STUDY OF PROTON EXCHANGE  
MEMBRANE FUEL CELL DESIGN

by

Jianfei Wu

Bachelor of Engineering in Automation Engineering  
Nanjing University of Technology, China  
2005

A thesis submitted in partial fulfillment  
of the requirements for the

**Master of Science Degree in Mechanical Engineering**  
**Department of Mechanical Engineering**  
**Howard R. Hughes College of Engineering**

**Graduate College**  
**University of Nevada, Las Vegas**  
**December 2008**

UMI Number: 1463540

### INFORMATION TO USERS

The quality of this reproduction is dependent upon the quality of the copy submitted. Broken or indistinct print, colored or poor quality illustrations and photographs, print bleed-through, substandard margins, and improper alignment can adversely affect reproduction.

In the unlikely event that the author did not send a complete manuscript and there are missing pages, these will be noted. Also, if unauthorized copyright material had to be removed, a note will indicate the deletion.

**UMI**<sup>®</sup>

---

UMI Microform 1463540

Copyright 2009 by ProQuest LLC.

All rights reserved. This microform edition is protected against unauthorized copying under Title 17, United States Code.

ProQuest LLC  
789 E. Eisenhower Parkway  
PO Box 1346  
Ann Arbor, MI 48106-1346



**Thesis Approval**  
The Graduate College  
University of Nevada, Las Vegas

November 21, 20 08

The Thesis prepared by

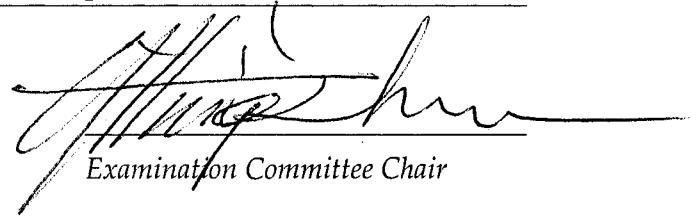
Jianfei Wu


**Entitled**

Three-dimensional Numerical Study of Proton Exchange Membrane Fuel  
Cell Design

is approved in partial fulfillment of the requirements for the degree of

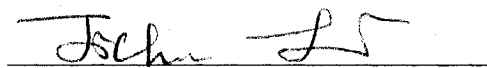
Masters of Science in Mechanical Engineering

  
Examination Committee Chair

  
Dean of the Graduate College

  
Examination Committee Member

  
Examination Committee Member

  
Graduate College Faculty Representative

## ABSTRACT

### **Three-Dimensional Numerical Study of Proton Exchange Membrane Fuel Cell Design**

by

Jianfei Wu

Dr. Yitung Chen, Examination Committee Chair  
Associate Professor of Department of Mechanical Engineering  
University of Nevada, Las Vegas

Performance of proton exchange membrane (PEM) fuel cells is dependent of a set of complex physical and chemical processes occurring simultaneously. Bipolar plates are important components of PEM fuel cells because they are the first stage of the flow distribution system. A non-uniform flow distribution across the active reaction area within PEM fuel cells will probably lead to an unbalanced use of the precious catalyst, and a lower overall efficiency of the device than expected. A three-dimensional numerical model has been developed to evaluate the PEM fuel cell including the current collectors, flow channels, gas diffusion layers, and membrane. This model takes into account the multi-component fluid flow in porous medium, electrochemical kinetics and water transport across membrane by electro-osmosis, diffusion and convection. Different fuel cell design cases, associated with their own bipolar plate designs, have been studied. Numerical results from the developed model show that the predicted polarization curve is in very good agreement with the experimental data. Results also show that the fluid flow distribution in the baseline design is very non-uniform, which is not favorable for the use

of catalyst and the high efficiency fuel cell. In order to improve the fuel cell efficiency, the bipolar plate design has been optimized, which then greatly increases the current density or power of fuel cell under the same operating conditions compared with the baseline design. Parametric study of the fuel flow rate on the current density has also been performed. Results reveal that the flow rate of fuel or air greatly influences the water content distribution within the proton exchange membrane, thus significantly impacting the performance of the PEM fuel cell. Generally, uniform fluid flow inside the entire plates and the proper humidity of the fuel cell are significantly important to the high performance PEM fuel cell.

## TABLE OF CONTENTS

ABSTRACT.....	iii
LIST OF FIGURES .....	vii
NOMENCLATURE .....	ix
ACKNOWLEDGEMENTS.....	xii
CHAPTER 1 INTRODUCTION .....	1
1.1 Background and History .....	1
1.2 Fuel Cell Review.....	2
1.3 PEMFC .....	4
1.4 Fundamentals of Fuel Cell.....	6
1.5 Thesis Motivation .....	10
1.6 Literature Review.....	11
1.6.1 Bipolar Plate.....	15
1.6.2 PEM Membrane .....	16
1.6.3 Gas Diffusion Layer and Catalyst.....	18
1.6.4 Water and Humidity.....	20
1.7 Research Objectives.....	23
1.8 Outline of Thesis.....	24
CHAPTER 2 PEMFC MODEL AND VALIDATION.....	25
2.1 PEMFC Model.....	25
2.1.1 Electrochemical Equations.....	27
2.1.2 Mass Conservation Equation .....	30
2.1.3 Momentum Conservation Equation .....	31
2.1.4 Species Conservation .....	31
2.1.5 Energy Conservation.....	33
2.1.6 Water Model .....	33
2.2 Numerical Method .....	35
2.2.1 Computational Domain.....	35
2.2.2 Boundary Conditions .....	39
2.2.3 PEM Model.....	41
2.2.4 Numerical Techniques .....	43
2.3 PEMFC Model Validation .....	45
2.3.1 Available Published Experimental Work.....	45
2.3.2 CFD Data from Other Research Groups.....	47
2.3.3 PEMFC Model Validation .....	49

CHAPTER 3	BASELINE DESIGN OF PEMFC .....	52
3.1	Design Description.....	52
3.2	Boundary Conditions .....	57
3.3	Results and Discussion .....	59
3.3.1	Velocity Distribution .....	59
3.3.2	Temperature Distribution.....	60
3.3.2.1	Bipolar Plate.....	60
3.3.2.2	Gas Channel Temperature.....	65
3.3.2.3	Catalyst Temperature .....	68
3.3.3	Hydrogen Mass Fraction.....	73
3.3.4	Oxygen Mass Fraction .....	76
3.3.5	Water Content .....	80
3.3.6	Current Density .....	83
CHAPTER 4	AN IMPROVED DESIGN OF PEMFC .....	85
4.1	Design Description.....	85
4.2	Results and Discussion .....	87
4.2.1	Velocity.....	87
4.2.2	Temperature .....	88
4.2.2.1	Bipolar Plate.....	89
4.2.2.2	Catalyst Temperature.....	93
4.2.3	Hydrogen Mass Fraction.....	98
4.2.4	Current Density .....	101
CHAPTER 5	CONCLUSIONS AND RECOMMENDATIONS .....	103
5.1	Conclusions.....	103
5.2	Recommendations.....	105
REFERENCES...	.....	106
VITA.....	.....	112



## LIST OF FIGURES

Fig. 1.1	Schematic of the PEMFC [7].....	5
Fig. 1.2	Fuel cell polarization curve [10].....	10
Fig. 1.3	Schematic view of a PEMFC and its computational domain [11] .....	12
Fig. 2.1	Schematic View of PEMFC model [49].....	26
Fig. 2.2	Boundary conditions for $\phi_{sol}$ and $\phi_{mem}$ [49].....	28
Fig. 2.3	Front view of single channel PEMFC (Unit: mm) .....	36
Fig. 2.4	Computational mesh .....	38
Fig. 2.5	Grid independent Study .....	45
Fig. 2.6	Schematic of single cell [58] .....	46
Fig. 2.7	Cell V-I curves for PEMFC at 50 °C, 1 atm: A and C cells with Nafion-impregnated and asreceived Prototech electrodes (0.35 mg Pt/cm <sup>2</sup> , respectively; B cell with GE/HS-UTC membrane and electrode assembly (4 mg Pt/cm <sup>2</sup> ) [58].....	47
Fig. 2.8	Oxygen (a) and hydrogen (b) mass fraction at a 0.37 cell voltage [63] .....	49
Fig. 2.9	Comparison of the V-I curves with experiment data.....	50
Fig. 2.10	Oxygen mass fraction in gas channel and GDL .....	51
Fig. 3.1	Schematic view of single pack PEMFC .....	53
Fig. 3.2(a)	Top view of bipolar plate .....	53
Fig. 3.2(b)	Top view of gas channel .....	54
Fig. 3.2(c)	Assembly view of bipolar plate, gas channel and membrane .....	54
Fig. 3.3	Dimensions of bipolar plate design (unit: in).....	56
Fig. 3.4(a)	Computational mesh of bipolar plate and gas channel.....	56
Fig. 3.4(b)	Computational meshes of bipolar plate, gas channel and MEA .....	57
Fig. 3.4(c)	Computational mesh of the whole single pack fuel cell .....	57
Fig. 3.5	Velocity distribution between channels.....	60
Fig. 3.6	Anode bipolar plate temperature at 0.4V.....	63
Fig. 3.7	Cathode bipolar plate temperature at 0.8V.....	65
Fig. 3.8	Gas channel temperature .....	68
Fig. 3.9	Cathode catalyst layer temperature at 0.4V.....	71
Fig. 3.10	Cathode catalyst temperature at 0.8V.....	72
Fig. 3.11	Anode catalyst hydrogen mass fraction at 0.4V .....	75
Fig. 3.12	Anode gas channel hydrogen mass fraction .....	76
Fig. 3.13	Cathode oxygen mass fraction at 0.4V.....	78
Fig. 3.14	Cathode gas channel oxygen mass fraction.....	79
Fig. 3.15	Cathode catalyst water at 0.4V .....	82
Fig. 3.16	Cathode gas channel water mass fraction at 0.4V .....	82
Fig. 3.17	Current density flow rate curves at 0.4V and 0.8V .....	84
Fig. 4.1	Schematic view of bipolar plate design.....	86
Fig. 4.2	Improved design of PEMFC.....	87

Fig. 4.3	Computational mesh-part view.....	87
Fig. 4.4	Velocity distribution between channels.....	88
Fig. 4.5	Cathode bipolar plate temperature at 0.4V.....	91
Fig. 4.6	Anode bipolar plate temperature at 0.8V.....	93
Fig. 4.7	Cathode catalyst temperature at 0.4V.....	95
Fig. 4.8	Cathode catalyst temperature at 0.8V.....	97
Fig. 4.9	Anode catalyst hydrogen mass fraction at 0.4V.....	99
Fig. 4.10	Cathode catalyst water mass fraction at 0.4V.....	101
Fig. 4.11	Normalized current density under different $\zeta$ .....	102

## NOMENCLATURE

$a$	water activity
$A_m, A_{ch}$	membrane area and channel cross section area (m <sup>2</sup> )
$b$	Tafel slop
$c$	molar concentration (g-mole/cm <sup>3</sup> )
$D_{ij}$	binary diffusivity (cm <sup>2</sup> /s)
$E^0$	standard potential under 25 °C, 1 atm
$F$	Faraday constant (96487 C/mol)
$\Delta G^0$	standard free energy (kJ/mol)
$\Delta H$	stored chemical energy (kJ/mol)
$I, I_{ref}$	current (A) and reference current (A/m <sup>2</sup> )
$i$	current density (A/m <sup>3</sup> )
$i_{sol}, i_{mem}$	solid phase and membrane phase current density (A/m <sup>3</sup> )
$j_{an}^{ref}, j_{cat}^{ref}$	volumetric reference exchange current density (A/m <sup>3</sup> )
$K$	absolute permeability
$K_r$	relative permeability
$k^{eff}$	effective heat conductivity (W/m-K)
$M_{w,H_2}$	molecular weight of hydrogen
$M_{w,H_2O}$	molecular weight of water

$M_{w,O_2}$	molecule weight of oxygen
$N$	molar flux vector (g-mol/cm <sup>2</sup> -s)
$n$	unit vector
$p_c$	capillary pressure (Pa)
$p_{H_2}, p_{O_2}$	hydrogen and oxygen gas pressure (Pa)
$R$	gas constant (8.314 J/K-mol)
$R_{tot}$	fuel cell total electric resistance (ohm)
$r_w$	condensation rate
$s$	liquid water saturation
$T$	absolute temperature (K)
$U_i$	velocity vector
$V_{cell}$	fuel cell operating voltage (V)
$V_{oc}$	fuel cell open circuit voltage or ideal voltage (V)
$w$	weight fraction
$X, x_i$	molar fraction and molar fraction of species $i$
$\alpha_a, \alpha_c$	anode and cathode transfer coefficient
$\varepsilon$	porosity
$\sigma_{sol}, \sigma_{mem}$	solid and membrane field conductivity (Siemens)
$\sigma$	surface tension (N/m <sup>2</sup> )
$\phi_{sol}, \phi_{mem}$	solid phase and membrane field potential (V)
$\varphi, \varphi_i$	fuel cell efficiency and ideal fuel cell efficiency

$\gamma$	concentration dependence
$\eta_{mas}$	mass transport limit loss potential (V)
$\eta_{ohm}$	ohmic loss potential (V)
$\eta_{pol}$	activation loss potential (V)
$\lambda$	water content
$\theta_c$	contact angle
$\rho_i$	density of component $i$ ( $\text{kg/m}^3$ )
$\zeta_a, \zeta_c$	anode and cathode stoichiometric ratio
$\mu_i$	viscosity of component $i$ (kg/m-s)
$\mu_l$	liquid water viscosity (kg/m-s)

## ACKNOWLEDGEMENTS

First and foremost I would like to express the deepest appreciation to my honorific advisor, Dr. Yitung Chen, who has continuously supported me through my thesis and research work with his patience and knowledge. Without his motivation, encouragement and valuable guidance, this thesis would not have been completed or written. I would like to thank Dr. Jianhu Nie for his assistance, generosity and advice. He encouraged me to develop research skills and greatly assisted me with scientific writing. I want to thank Dr. Robert Boehm and Dr. Jichun Li for their valuable suggestions and help in many ways.

I would like to express my appreciation to Dr. Hsuan-Tsung Hsieh. He has given me valuable advice and guidance on technical and non-technical problems. I also thank Dr. Huajun Chen, and Dr. Taide Tan. Their suggestions help me a lot in my graduate study and research work. I am also thankful for all my friends in Las Vegas.

Last, but not least, I want to thank my parents Zhihua Wu and Hongying Yao, my grandmother Youying Chen, my uncle Zhicheng Wu and aunt Yingchun Si for their unconditional support and selfless love. I extend my thanks to my girlfriend Lin Han for her 5 years of continuous love and support.

## CHAPTER 1

### INTRODUCTION

#### 1.1 Background and History

Due to the increasing demand for energy consumption and the energy related environmental pollution problems, renewable energy has become one of the hottest topics in the 21st century. It is very important to one nation's future energy dependence and to the dependence of industry and economic development in the long run. There are many renewable energy forms, such as solar, wind, hydraulic, geothermal and tidal energy. However, the accomplishment is still very limited due to the current techniques and hence they are not widely used yet.

Hydrogen, as an energy carrier, is considered to be a very promising method to use renewable energy, and to solve the energy demand and environmental pollution problems. Hydrogen can be produced from water, biomass, or natural gas molecules through steam reforming and electrolysis. It can be used in almost every application where fossil fuel is being used today, without harmful emissions. It becomes the choice of fuel for many energy applications due to its high reactivity with an appropriate catalyst, and a wide range of production from other energy sources.

A fuel cell is an electrochemical device that can convert the chemical energy of a reaction directly into electrical energy. It is deemed as a promising pathway towards

renewable energy system. In 1838-1842, Sir William Grove and Christian Friedrich Schonbein invented the first fuel cell as an electrical energy conversion device [1]. It has many advantages, such as low to zero emission power generation, high theoretical efficiency, adaptable features, reliability and quiet operation. It can continuously produce electricity as long as supplied with the fuel and oxidant [2].

## 1.2 Fuel Cell Review

Fuel cells can be generally classified into several types, depending on the used electrolyte and catalyst and their operating temperatures [3]:

- Alkaline Fuel Cell (AFC)
- Molten Carbonate Fuel Cell (MCFC)
- Phosphoric Acid Fuel Cell (PAFC)
- Proton Exchange Membrane Fuel Cell (PEMFC)
- Solid Oxide Fuel Cell (SOFC).

The alkaline fuel cell (AFC) was developed in the early 1960's, under the Apollo project by U.S. National Aeronautics and Space Administration (NASA) [3]. AFC's electrolyte is a potassium hydroxide (KOH) solution, which operates between 65 and 250°C. It has the excellent performance compared to other candidate fuel cells due to its active electrode kinetics and its flexibility to use a wide range of catalysts. However, AFC requires the high purity fuel and oxidant, which limits its application in many areas.

Molten carbonate fuel cell (MCFC) uses alkali carbonate, such as potassium, sodium and lithium salts as its electrolyte, operating from 600 °C to 700 °C [3]. The MCFC uses



a cheaper nickel catalyst rather than other expensive metals. However, its electrolyte is very corrosive, so that stainless steel is required for the cell hardware.

The phosphoric acid fuel cell (PAFC) is one of the well developed fuel cells, which uses 100% phosphoric acid ( $\text{H}_3\text{PO}_4$ ) as the electrolyte and operates from 150 °C to 220 °C [3]. It has thermal, chemical and electrochemical stability advantages, which makes it one the first type of fuel cells to be commercialized. However, the PAFC is not very efficient at generating electricity alone and it is less powerful than other fuel cells. Therefore, PAFC is typically used for stationary power generation or some large vehicles.

The solid oxide fuel cell (SOFC) uses a non-porous metal oxide electrolyte, which operates in the range 650 °C to 1000 °C [3]. The solid electrolyte feature allows its flexible shape, and has no corrosion problem compared to liquid electrolyte, as well as no flooding problem. However the operating temperature is significantly high and the preheating of the inlet air is necessary. The difference of thermal expansion between each parts of the cell cause many problems, such as the sealing and choice of material. Finally, it leads to lower performance than other cells.

The proton exchange membrane fuel cell (PEMFC), also known as the solid polymer or polymer electrolyte fuel cell, has received increasing attention. A PEMFC uses a proton exchange membrane as the electrolyte, which has high proton conductivity when it is properly hydrated. A PEMFC generally uses hydrogen as the fuel and air as the oxidant and the product is purely water and it operates around 50 °C to 80 °C. Of the different types of fuel cells, PEMFC has the advantages of low operating temperature and high power density. So it has been considered the leading candidate for use as a non-polluting power source, especially for transportation and automotive applications. The

PEMFC has already attracted lots of research interest. Currently the thermal and water management is the key issue to the cell performance [4]. Under low operating temperature it has the low CO tolerance, which is the CO poisoning problem of the catalyst. The membrane also needs to be hydrated to keep the high conductivity for the protons but excess water can cause the membrane to flood, which then prevents the fuel and air transport to the catalyst layer.

### 1.3 PEMFC

PEMFC is primarily composed of nine parts and elements: two current collectors, two gas channels, two gas diffusion layers, two catalyst layers and the polymer electrolyte membrane, as is shown in Fig. 1.1.

Electrolyte is one of the most important parts in various types of fuel cells. The PEMFC has an acidic polymeric membrane, which allows the protons to pass but repels electrons. Usually, Nafion<sup>®</sup> from DuPont is selected as the membrane material, which consists of the fluoro-carbon backbone, attached with sulfonic acid ( $\text{SO}_3^-$ ) groups [5]. So, the higher the fixed-charge concentration, the better the protonic conductivity. It is also very important to keep the membrane humidified while operating, because the conductivity is directly related to the water content. Another important parameter is the membrane thickness. It should be kept very thin in order to decrease the ohmic losses and typically, the membrane thickness is kept in the range of 5-200  $\mu\text{m}$  [6].

It is necessary to use a catalyst in order to enhance the electrochemical reaction in the low operating temperature PEMFC. The catalyst is usually the platinum supported by the carbon particles. Those particles are normally mixed with some electrolyte material to

ensure the migration process through the catalyst layer. The chemical reactions depend on surface area, and the higher porosity provides more surface area, a larger surface is better.

The gas diffusion layer (GDL) or gas diffusion electrode is characterized by its thickness and porosity. It usually consists of the carbon paper or carbon cloth, where the gas is transported to the catalyst layer and electrons are carried out.

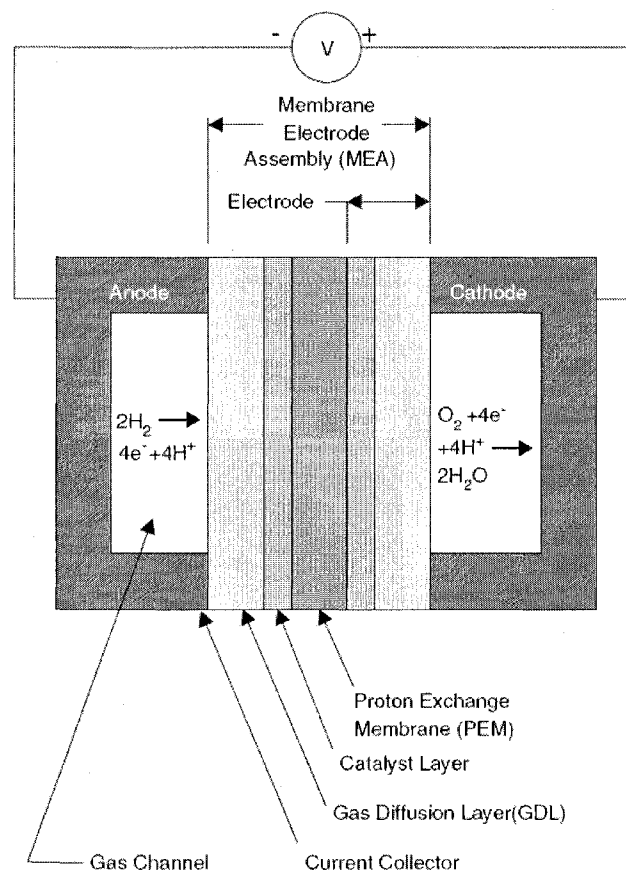


Fig. 1.1 Schematic of the PEMFC [7]

Bipolar plate is used to support and separate different cells in fuel cell stack. Its gas channels deliver the fuel or air to the gas diffusion layers. It is obvious that the channel's

area should be large, which can increase the fuel diffusion. However considering the conductive limitation of the electrons through the bipolar plate, this is not always the true, because thin rims will increase the system electric resistance.

#### 1.4 Fundamentals of Fuel Cell

Fuel cell is a complicated energy converting device, with coupled mass and heat transport, chemical, and electrochemical processes. In order to obtain the high performance fuel cell, lots of designing issues need to be taken into account, such as the channels dimensions, temperature distribution, humidity level, water management, gas transport through porous media, catalyst material and membrane conductivity.

The electrochemical reactions (reduction and oxidization) taking place at the electrode can be expressed as:



During the reaction, the change of the standard free energy is  $\Delta G^0$ , which is expressed as [3]:

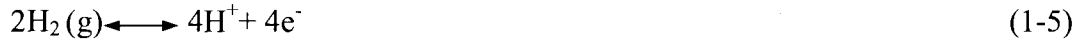
$$\Delta G^0 = -nFE^0 \quad (1-3)$$

where F is the Faraday constant (96487 C/mol),  $E^0$  is standard potential under the standard state (25 °C and 1 atm). Generally, the cell potential  $V_{oc}$  is defined by the Nernst equation:

$$V_{oc} = E^0 - \frac{RT}{nF} \ln \frac{C_C^c D_D^d}{A_A^a B_B^b} \quad (1-4)$$

Where  $R$  is the gas constant,  $T$  is the operating temperature, and  $A_A$ ,  $B_B$ ,  $C_C$  and  $D_D$  are the species activities.

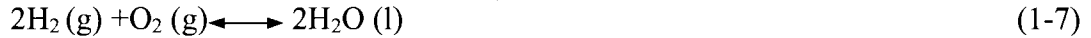
For a PEMFC, the reactants are hydrogen and air. Hydrogen flows through the anode side channels and diffuses into the anode gas diffusion layer, then contacts with the anode side catalyst layer, where it splits into protons and electrons:



Then  $\text{H}^+$  ions migrate through the membrane, arrive at the cathode catalyst layer, and react with the oxygen, which is from the cathode side gas diffusion layer.



The overall reaction could be expressed as:



The standard free energy for this reaction is  $\Delta G^0 = -237.1 \text{ kJ/mol}$  [8] and the standard potential is  $E^0 = 1.229 \text{ V}$ . It is calculated by the Nernst equation by taking partial pressure and temperature into account.

Each energy conversion device has an efficiency, and the traditional thermal power generator's efficiency is limited by the theoretical Carnot cycle efficiency (less than 50%). In order to get the high efficiency, a high temperature difference is required for those thermal power generators. The efficiency definition  $\varphi$  is the amount of useful energy produced, which is  $\Delta G$ , divided by the change in the stored chemical energy, that is  $\Delta H$ .

$$\varphi = \frac{\Delta G}{\Delta H} \quad (1-8)$$

Under the standard condition (25 °C, 1 atm),  $\Delta H$  equals to 285.8 kJ/mol according to the thermodynamics data. Then for the H<sub>2</sub>/O<sub>2</sub> fuel cell, the ideal efficiency under the standard conditions is:

$$\varphi_i = \frac{237.1}{285.8} = 83\% \quad (1-9)$$

This's much higher than any thermal cycle efficiency, even though the actual efficiency  $\varphi_{act}$  will be lower than  $\varphi_i$ , due to the irreversible losses.  $\varphi_{act}$  is expressed as:

$$\varphi_{act} = \frac{V_{cell}}{V_{oc}} \times 83\% \quad (1-10)$$

Where  $V_{cell}$  is the actual cell voltage,  $V_{oc}$  is the idea cell voltage or the open circuit cell voltage, which is determined by the Nernst equation. Generally, there are three main losses:

(1) Activation polarization  $\eta_{pol}$ ,

The activation energy barrier has to be overcome for the electrochemical reaction. Based on experimental investigations, the current  $i$  and voltage  $\eta_{pol}$  has an exponential relation. The Tafel equation describes the semi-empirical relationship [9]:

$$\eta_{pol} = a + b \log i \quad (1-11)$$

Where  $a$  is the constant,  $b$  is the Tafel slope, and  $i$  is the current. However this simple relation is not valid at low overpotential (less than 50 mV). A more accurate expression for the current and overpotential relation is the Butler-Volmer equation [9]:

$$i = i_0 \left[ \exp\left(\alpha_a \frac{F \eta_{pol}}{RT}\right) - \exp\left(-\alpha_c \frac{F \eta_{pol}}{RT}\right) \right] \quad (1-12)$$

Where  $i_0$  is the reference exchange current density,  $\alpha_a$  and  $\alpha_c$  are the anode and cathode transfer coefficients, which refer to the symmetry of the energy barrier;  $F$  is Faraday constant; and  $R$  and  $T$  are the gas constant and cell temperature, respectively.

(2) Ohmic heat  $\eta_{ohm}$

There exists ion transport resistance inside of the electrolyte and the electrode so that the ohmic loss is expressed as:

$$\eta_{ohm} = iR_{tol} \quad (1-13)$$

Where the  $R_{tol}$  is the total cell resistance including the electronic and contact resistances.

(3) Mass transport limitation  $\eta_{mas}$

When the reactant consumption rate is very high, which exceeds the transport limit from the bulk to the electrode surface, the reactant concentration will decrease, which then leads to the potential loss. So improving the diffusion rate of the reactant species through the porous media is critical to lower the mass transport limit losses.

Fig. 1.2 shows the polarization curve for a single PEMFC. The current density of the fuel cell decreases when the actual cell voltage increases. There are three regions for different losses. In Region I, the activation polarization loss is significant, which is controlled by the electrode kinetics of the reaction; in Region II, which is generally the fuel cell operating region, the ohmic loss dominates, and the ohmic loss is proportional to the current density. This is due to the cell resistance of the ions in electrolyte; in Region III, where the current density is very high, the mass transport of reactants to the electrode reaches its limit, and then the concentration limit loss becomes the predominant factor.

Finally, the actual cell potential could be summarized as:

$$V_{act} = V_{cell} - |\eta_{pol,a}| - |\eta_{pol,c}| - |\eta_{mas,a}| - |\eta_{mas,c}| - |\eta_{ohm}| \quad (1-14)$$

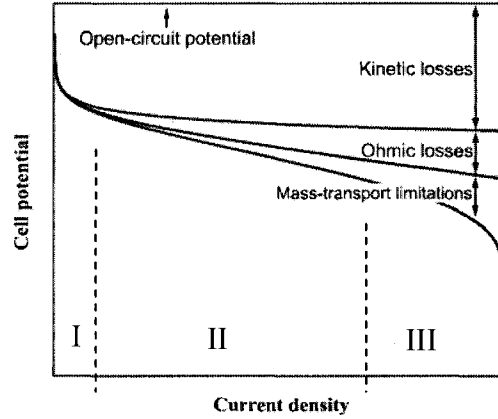


Fig. 1.2 Fuel cell polarization curve [10]

### 1.5 Thesis Motivation

Enhancing fuel cell efficiency and reducing fuel cell cost are two key objectives in research and development of fuel cell technologies. Due to the fuel cell's complexity and highly reactive environment, it is difficult to perform detailed investigations during its operation. It is crucially important to understand the physics inside the fuel cell in order to improve its performance. While the experiments are expensive to implement and subject to practical limitations, cost effective numerical modeling and simulation can provide such information and predict effects of different factors including bipolar plate designs, and various parameters, which leads to shorter design and optimization cycles.

Many numerical models have been developed to predict the cell performance. Some of them focus on the catalyst material, some focus on the membrane performance, while some others concentrate on the channels. However, there are few research publications on the overall PEMFC modeling, in particular, coupled with the bipolar plate design, heat



and mass transfer, electrochemical reaction, and water generation. This motivates the thesis author to develop a numerical model for the entire PEMFC and optimize the cell performance by the various bipolar plate designs and operating parameters. The developed model will give a clear view of the PEMFCs, and help engineers to understand the effects of those parameters, which can significantly improve the cell performance.

## 1.6 Literature Review

There are many coupled processes simultaneously occurring in PEMFCs. Some of them are not fully understood. The developed models aim at giving a clear insight into the complex physical phenomena within PEMFCs. Due to the expensive experimental work and its physical limitations, the numerical method has played a very important role in the fuel cell research history. The computational fluid dynamics (CFD) modeling, coupled with an electrochemical model can predict the multi-species transport processes, and electrochemical reaction processes. A typical PEMFC is schematically shown in Fig. 1.3. It primarily includes the bipolar plates (gas channel), gas diffusion layers, catalyst layers and membrane.

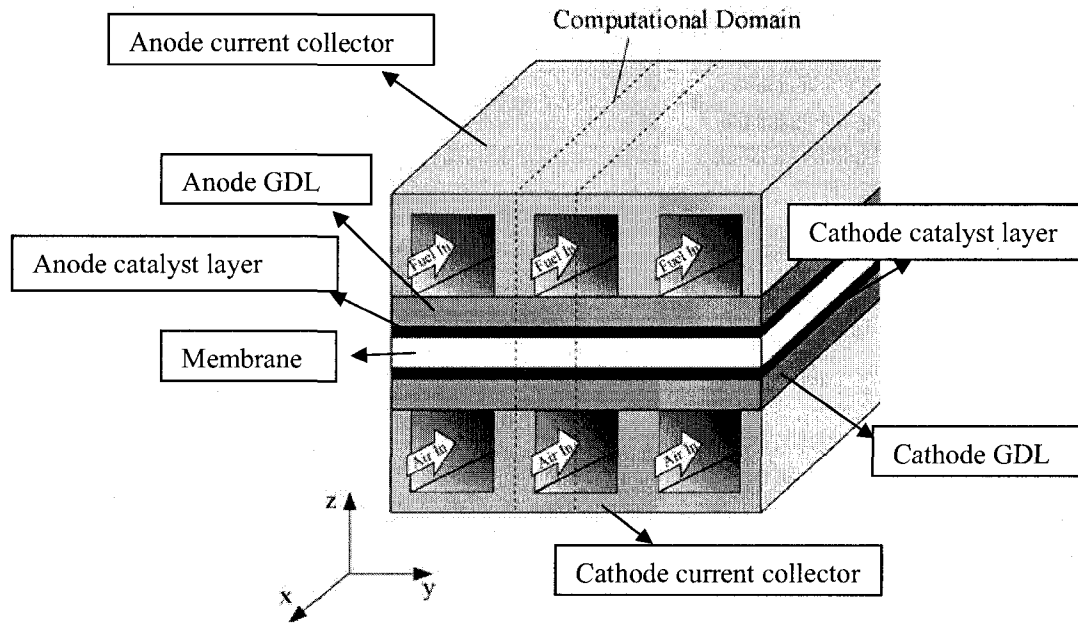


Fig. 1.3 Schematic view of a PEMFC and its computational domain [11]

A number of the numerical models have been reported during the last twenty years. Some of them focus on the specific parts, such as the catalyst layer [12], electrodes [13], the gas diffusion layer [14], and the membrane [15]. Then Bernardi and Verbrugge [16] and Springer et al. [17] developed a one-dimensional fuel cell model, by which the predicted V-I curves agree with the experimental data in the low current density range. Later, some two-dimensional PEMFC models were developed, such as the published work by Kazim et al. [18], Gurau et al. [19] and He et al. [20]. These two-dimensional models can only simulate the plane perpendicular to the flow channels or plane with one flow direction and one direction through the membrane. In addition, these models are limited to provide two-dimensional temperature and reactants information in the actual three-dimensional problem.

Dutta et al. [21], Berning et al. [22], and Jen et al. [23] developed three-dimensional models. Dutta et al. discussed the need to model three-dimensional flow in PEMFCs and developed an integrated flow and current density model to predict current density distributions in the membrane in a straight channel PEMFC. The geometrical model includes diffusion layers on both the anode and cathode sides and the numerical model solves the same primary flow related variables in the main flow channel and the diffusion layer. Predictions revealed that inclusion of a diffusion layer creates a lower and more uniform current density compared to cases without diffusion layers. The results also showed that the membrane thickness and cell voltage have a significant effect on the axial distribution of the current density and net rate of water transport.

Ramousse et al. [24] presented a fuel cell model that takes account of gas diffusion in the porous electrodes, water diffusion and electro-osmotic transport through the polymeric membrane, and heat transfer in both the membrane electrode assembly (MEA) and bipolar plates. This model was constructed by combining independent descriptions of heat and mass transfers in the cell with a third description of coupled charge and mass transfers in the electrodes, which are considered as porous media. The results showed that thermal gradients in the MEA could lead to thermal stresses at high current densities. The feeding gas temperature influence on the cell temperature is also important.

Meng [25] has developed a three-dimensional PEM fuel cell model with a consistent water transport treatment in the membrane electrode assembly (MEA). In this PEM fuel cell model, a conservation equation of the water concentration is solved in the gas channels, gas diffusion layers, and catalyst layers while a conservation equation of the water content is established in the membrane. Since all the other conservation equations

are still developed and solved in the single-domain framework without resort to interfacial boundary conditions, this PEMFC model was termed as a mixed-domain method. Results from this mixed-domain approach showed good accuracy in terms of not only cell performance and current distributions but also water content variations in the membrane.

Mann et al. [26] proposed a generalized steady-state electrochemical model, which accepts as inputs not only values of the operating variables but also cell parameters including active area and membrane thickness. A further feature of this model is the addition of a term to account for membrane aging. This model is a useful tool that allows the addition of parameters for fuel cell geometry and membrane characteristics in the design process.

A three-dimensional CFD model of a PEMFC with serpentine flow field channels was presented by Nguyen et al. [27]. This comprehensive model accounts for the major transport phenomena in a PEMFC: convective and diffusive heat and mass transfer, electrode kinetics, and potential fields. A unique feature of the model is the implementation of a voltage-to-current (VTC) algorithm that solves for the potential fields and allows for the computation of the local activation over-potential. The coupling of the local activation over-potential distribution and reactant concentration makes it possible to predict the local current density distribution more accurately. The simulation results revealed current distribution patterns are significantly different from those obtained in studies assuming constant surface over-potential.

### 1.6.1 Bipolar Plate

The bipolar plates typically have several functions: (1) to distribute the fuel and oxidant within the cell; (2) to facilitate water management within the cell; (3) to separate the individual cells in the stack; and (4) to carry current away from the cell. First of all, one of the specific functions of a bipolar plate is to produce a uniformly distributed flow distribution over the catalyzed electrodes. A non-uniform flow distribution across the bipolar plate surface area will probably lead to an unbalanced use of the expensive catalyst such as platinum or other metals/alloys, and an overall efficiency of the device lower than expected. Therefore, bipolar plates of fuel cells must be properly designed to distribute reactant evenly across the catalyzed reaction surface area, to provide a pathway to collect reaction products, and to provide an electrical conduction path to the reaction sites [11].

A serpentine flow channel is one of the most common and practical channel layouts for a PEMFC. During the reactant flows along the flow channel, it can also leak or cross to neighboring channels via the porous gas diffusion layer due to the high pressure gradient caused by the short distance. A numerical and experimental study has been carried out by Park et al. [28] to investigate the cross flow in a PEMFC. Experimental measurements revealed that the pressure drop in a PEMFC is significantly lower than that without cross flow. Three-dimensional numerical simulation has been performed for wide ranges of flow rate, permeability and thickness of the gas diffusion layer to analyze the effects of those parameters on the resultant cross flow and pressure drop of the reactant streams. Considerable amount of cross flow through gas diffusion layer has been found in

flow simulation and its effect on pressure drop becomes more significant as the permeability and the thickness of gas diffusion layer are increased.

Grigoriev et al. [29] have performed the numerical optimization of the dimensions of channels and current transfer ribs of bipolar plates as well as an analysis of the effects of thickness and porosity of gas diffusion layers. A mathematical model of the transfer processes in a PEMFC has been developed for this purpose. The results are compared with experimental data. Then they suggested some recommendations of the values of operating parameters and some design requirements to increase PEMFC efficiency.

Kumar et al. [30] studied steady state and transient performance of PEMFC stack using different flow field designs in bipolar plates. A three-dimensional transient numerical model of proton exchange membrane fuel cell was developed and the effect of gas flow-field design in the bipolar plates was tested. They also performed the simulations for different flow-field designs in the bipolar plates of PEMFC.

Another important area in bipolar plate design is material selection. Kuo et al. [31] reported a novel composite material for the bipolar plates of PEMFCs. Joseph et al. [32] reported the results of using stainless steel for PEMFC bipolar plates. In addition, as alternative bipolar plate materials for PEMFCs, two types of carbon composite were developed and characterized by Cho et al. [33].

#### 1.6.2 PEM Membrane

In PEMFCs, a key component, the polymer electrolyte membrane, acts as both a separator and an electrolyte in the operating fuel cell. Beuscher et al. [34] discussed PEM membrane requirements in terms of two different parameters: temperature and relative humidity. In their work, effects of these two operating parameters on the proton

conductivity of PEMFC membranes and the resulting effect on fuel cell performance were examined using experimental observations. Numerical simulations were used to assess the influence of water transport properties on the local hydration state of the membrane inside the running fuel cell. Finally, the challenge of longer membrane life is explored by examination of recent studies on reinforced and non-reinforced membranes. These results illustrate the benefit of reinforced membranes in terms of membrane durability and therefore cell lifetime.

The operating temperature of atmospheric PEMFC is limited to 80°C to maintain liquid water for proton transport. However, high temperature operation of a PEMFC (above 80°C) is desirable to reduce the effects of CO present in the reformed gas streams. Jalani et al. [35] developed a proton transport and sorption model, which was used to study the effect of different parameters like the number of acid sites and solvent sorption in the membrane as a function of relative humidity (RH). A phenomenological sorption model developed can predict the water and methanol sorption in the Nafion® membrane. Both water management and thermal management in proton conducting membrane are very important to the performance of PEMFCs. It is of significant importance that the CFD model can accurately simulate these heat and mass transports so that the developed model can be used to identify the optimum operating conditions and guide the PEMFC design.

Carnes et al. [36] analyzed numerical predictions of a recently proposed rational model for transport of protons and water in a PEMFC. The effects of coupling partially saturated gas diffusion electrodes (GDLs) with the membrane are studied in both 1D and 2D contexts. Their numerical results predict a higher current density and more uniform

membrane hydration using a dry cathode instead of a dry anode, and illustrate that the strongest 2D effects are for water vapor transport.

### 1.6.3 Gas Diffusion Layer and Catalyst

Gostick et al. [37] have performed an experiment to measure the absolute gas permeability of several common gas diffusion layer materials for polymer electrolyte membrane fuel cells. Most materials were found to display higher in plane permeability than through-plane permeability. The permeability in the two perpendicular in-plane directions was found to display significant anisotropy. In-plane permeability was also measured as the GDL was compressed to different thicknesses. Typically, compression of a sample to half its initial thickness resulted in a decrease in permeability by an order of magnitude.

Tungsten nitride supported on carbon black was prepared by Zhong et al. [38] from temperature-programmed reaction (TPR) process and is proposed as a catalyst for the oxygen reduction reaction (ORR) in PEMFCs. The as-prepared catalyst was characterized by X-ray diffraction (XRD) and transmission electron microscopy (TEM) techniques. The ORR activities of the catalyst were studied by electrochemical measurements and single cell tests, respectively. The results indicated that the tungsten nitride electrocatalyst exhibited attractive catalytic activity and stability for the ORR in PEMFCs. It is expected to be a promising cathode electrocatalyst for PEMFCs, especially for the comparatively high temperature proton exchange membrane fuel cells.

Numerical simulations were performed by Cheng et al. [39] to investigate the effect on PEMFC performance of Nafion® loading in the catalyst layer. The investigation also considered variations of geometric parameters. A model that accounts for the volume



fractions of Nafion®, the solid catalyst particles, and the void space inside the catalyst layers was incorporated into a three-dimensional computational fluid dynamics code, capable of resolving three-dimensional mass, momentum, and species transport phenomena as well as the electron- and proton-transfer processes in PEMFCs. Numerical results were first compared with experiments, showing close agreement between predictions and measurements. A parametric study on the effects of Nafion® loading and geometric parameters variation was carried out to evaluate the performance of PEMFCs for various parameter combinations.

Electrode material durability is an important factor in limiting the commercialization of PEMFCs. They typically use carbon supported nanometer sized Pt and/or Pt alloy catalysts for both anode and cathode. Electro catalyst surface area loss is due to the growth of platinum particles. Particle size growth is accelerated by potential cycling whether due to artificial potential cycling or by cycling during fuel cell operation. Catalysts were analyzed by X-ray diffraction (XRD) to determine the degree of electro catalyst sintering by Borup et al.[40]. Cathode Pt particle size growth is a function of temperature, test length and potential. The largest increase in cathode Pt particle size was observed during potential cycling experiments and increased with increasing potential. During cycling measurements, catalyst coarsening rates exhibited a linear increase with temperature. Low relative humidity decreased platinum particle growth, but substantially increased carbon loss. Carbon corrosion of the electrode catalyst layer was found to increase with increasing potential and decreasing humidity.

Yong et al. [41] reported that biosynthesis of nano-scale platinum and palladium was achieved via enzymatically mediated deposition of metal ions from solution. The bio-

accumulated Pt(0) and Pd(0) crystals were dried, applied onto carbon paper and tested as anodes in a polymer electrolyte membrane (PEM) fuel cell for power production. Up to 100% and 81% of the maximum power generation was achieved by the bio-Pt and bio-Pd catalysts, respectively, compared to commercial fuel cell grade Pt catalyst. Hence, bio-mineralization could pave the way for economical production of fuel cell catalysts since previous studies have shown that precious metals can be bio-recovered from wastes into catalytically active bio-nanomaterials.

#### 1.6.4 Water and Humidity

Ludlow et al. [42] have performed neutron scattering experiments on a proton exchange membrane fuel cell to assess the ability to quantify water in the membrane and electrode or gas diffusion layers. This study demonstrated the resolution of water content changes within the membrane electrode assembly and membrane alone.

Flooding of the membrane electrode assembly (MEA) and dehydrating of the polymer electrolyte membrane have been the key problems to be solved for PEMFCs. Zhan et al. [43] reported that under steady-state conditions, the liquid water flux through the GDL increases as contact angle and porosity increase and as the GDL thickness decreases. A GDL with a gradient of porosity is more favorable for liquid water discharge from catalyst layer into the gas channel. For the GDL with the same equivalent porosity, the larger the gradient is, the more easily the liquid water is discharged.

Jiao et al. [44] presented a numerical investigation of air–water flow in micro-parallel-channels with PEMFC stack inlet and outlet manifolds for the cathode, using the commercial CFD software package Fluent®. Various air–water flow behaviors inside the straight micro-parallel-channels with inlet and outlet manifolds were simulated and

discussed. The results showed that excessive and unevenly distributed water in different single PEMFCs could cause blockage of airflow or uneven distribution of air along the different flow channels. It was found that for a design with straight-channels, water in the outflow manifold could be easily blocked by air/water streams from the gas flow channels; the airflow could be severely blocked even if there was only a small amount of water in the gas flow channels.

Wood et al. [45] investigated the effectiveness of the direct liquid water injection scheme and the interdigitated flow field design towards providing adequate gas humidification to maintain membrane optimal hydration and alleviating the mass transport limitations of the reactants and electrode flooding. It was found that the direct liquid water injection used in conjunction with the interdigitated flow fields as a humidification technique is an extremely effective method of water management. The forced flow-through-the-electrode characteristic of the interdigitated flow field (1) provides higher transport rates of reactant and products to and from the inner catalyst layers, (2) increases the hydration state and conductivity of the membrane by bringing its anode/membrane interface in direct contact with liquid water and (3) increases the cell tolerance limits for excess injected liquid water, which could be used to provide simultaneous evaporative cooling.

Jang et al. [46] presented that, due to the water management problem, the effects of inlet humidity of reactant fuel gases on both anode and cathode sides on the cell performance are considerable. In their work, due to the blockage effects in the presence of the baffles, more fuel gas in the flow channel can be forced into the gas diffuser layer (GDL) and catalyst layer (CL) to enhance the chemical reactions and then augment the

performance of the PEMFC systems. The effect of liquid water formation on the reactant gas transport was taken into account in the numerical modeling. Predictions showed that the local transport of the reactant gas, the local current density generation and the cell performance can be enhanced by the presence of the baffles. Results revealed that, at low voltage conditions, the liquid water effect is especially significant and should be considered in the modeling. The cell performance can be enhanced at a higher inlet relative humidity, by which the occurrence of the mass transport loss can be delayed with the limiting current density raised considerably.

Yan et al. [47] theoretically studied the water transport phenomena in PEMFCs, mainly investigating the transient behavior in the gas diffusion layer (GDL), catalyst layer (CL) and PEM. In the PEM, both diffusion and electro-osmosis processes were considered, while in the GDL and CL, only the diffusion process was taken into account. The process of water uptake was employed to account for the water transport at the interface between the PEM and CL. The results indicate that the water content in the PEM and the time for reaching the steady state in the start-up process are influenced by the humidification constant,  $k$ , the humidification, and the thickness of PEM. The rise of the  $k$  increases the water content in the membrane and shortens the time for reaching steady state. Insufficient humidification causes relatively small water content and long steady time. When the PEM is thinner, the water is more uniformly distributed, the water content gets higher, and the time for reaching the steady state is distinctly shorter.

To determine the net electro-osmotic drag coefficient of Nafion 115 and Hanwha membrane, Choi et al. [48] measured the fluxes of water discharged from the anode and cathode at different current densities. Also, they investigated the contribution of water

supply for the membrane from the anode and cathode. When the cathode was humidified, water supply for the membrane at low current densities was achieved via the cathode, but the contribution of the anode became more important as current density gradually increased. The net electro-osmotic drag coefficient decreased sharply with current density, but it had a nearly constant value over  $200 \text{ mA cm}^{-2}$ . When the cathode was not humidified, at low current densities, most of water generated at cathode was supplied for the membrane, but water supply from the cathode at high current densities decreased proportionately, and the net electro-osmotic drag coefficient showed larger value.

### 1.7 Research Objectives

The PEMFC is a very complicated electrochemical device. In order to achieve the high fuel cell performance, improved fluid flow, good thermal management and proper humidity level are the promising pathways. During the operation of PEMFC, significant variation of the local current density could exist across the membrane, due to the non-uniform velocity. It can cause a sharp temperature and stress gradient and leads to membrane degradation. In this thesis, four research objectives are pursued, which are listed below:

- Create a single fuel cell model, including the bipolar plates, gas channels, gas diffusion layers, catalyst layers and membrane.
- Simulate the hydrodynamic, heat transfer and electrochemical phenomena to obtain the fuel cell performance information.
- Redesign the bipolar plates in order to achieve the uniform fluid flow in channels and to improve the fuel cell performance.

- Perform the parametric study of different fuel flow rates, to obtain better operating parameters for the PEMFC.

## 1.8 Outline of Thesis

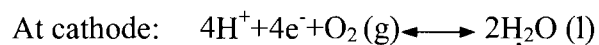
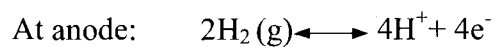
In this thesis, the three-dimensional CFD model has been developed and a parametric study is performed. Chapter 2 will discuss the PEMFC modeling including the fundamentals of the electrochemistry and fuel cells. This model is validated using a three-dimensional single channel PEMFC case. Chapter 3 discusses the baseline design of the single unit PEM fuel cell. Different velocity, temperature, and water content distributions are investigated. Influence of the flow rate on the fuel cell current density distribution has also been studied. Chapter 4 focuses on the improved design case with the uniform velocity distribution in channels. The improvement in current density and other performance is discussed by comparing with the baseline design case. Chapter 5 concludes the current research, and some recommended future work is summarized.

## CHAPTER 2

### PEMFC MODEL AND VALIDATION

#### 2.1 PEMFC Model

A schematic view of the PEMFC is shown in Fig. 2.1. A PEMFC can be divided into nine zones: bipolar plates (anode/cathode current collectors), anode/cathode gas channels, anode/cathode gas diffusion layers, anode/cathode catalyst layers and membrane. The hydrogen gas mixture flows through the anode gas channels. Then it diffuses into the porous gas diffusion layers and contacts with active surface in the catalyst layer. In the anode catalyst layer, hydrogen is split into the hydrogen ions and electrons. Under the influence of the electrical field inside the PEMFC, hydrogen ions migrate through the polymer electrolyte membrane while electrons are transferred back to the anode current collector through the anode gas diffusion layer. Then electrons pass through the external circuit and reach the cathode current collector. In cathode side, the oxygen mixture flows through the cathode gas channel and diffuses through the cathode GDL. After that, oxygen contacts the active surface in the cathode catalyst layer. In the cathode catalyst layer, oxygen, electrons and hydrogen ions combine and form the water. The chemical reactions can be expressed as:



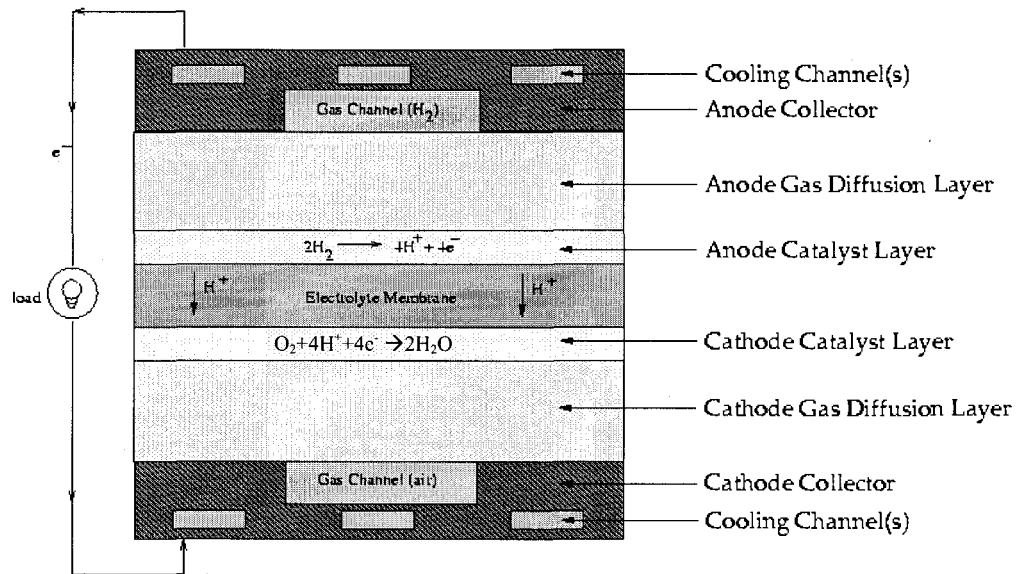
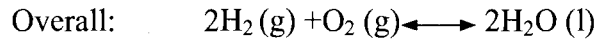


Fig. 2.1 Schematic View of PEMFC model [49]

In order to model PEMFCs, it is necessary to understand the mass, momentum and energy transport, electrochemical reactions and charge balance inside the fuel cell.

However, it is impossible to take every single detail of the whole process into account.

Some basic assumptions are necessary to simplify the PEM model, including:

- Non-isothermal operation
- Ideal gas mixtures
- Steady-state operation
- Isotropic electrodes and membrane
- Neglect contact resistance of current collector and MEA
- Incompressible flow
- Laminar flow



### 2.1.1 Electrochemical Equations

In PEMFCs, some of the most important parts are the catalyst layers, where the electrochemical reactions take place. The driving force of the electrochemical reaction is the over-potential, which is the potential difference of the solid phase potential and the electrolyte phase potential. Since there are two potential fields: Equation (2-1) accounts for the electron transport in the solid conductive material; and Equation (2-2) solves the protonic transport through the membrane.

$$\nabla \cdot (\sigma_{sol} \nabla \phi_{sol}) + i_{sol} = 0 \quad (2-1)$$

$$\nabla \cdot (\sigma_{mem} \nabla \phi_{mem}) + i_{mem} = 0 \quad (2-2)$$

Where  $\sigma_{sol}$  and  $\sigma_{mem}$  are the electrical conductivity (1/ohm-m) in the solid phase and the membrane phase,  $\phi_{sol}$  and  $\phi_{mem}$  is the electric potential (V), and  $i$  is the volumetric transfer current (A/m<sup>3</sup>). The membrane electric conductivity is not constant as other fuel cell parts. It depends on the water content and the temperature [50]:

$$\sigma_{mem} = \varepsilon (0.514\lambda - 0.326) e^{1268 \left( \frac{1}{303} - \frac{1}{T} \right)} \quad (2-3)$$

Where  $\lambda$  is the water content,  $\varepsilon$  is the membrane porosity and  $T$  is the absolute temperature of the membrane (K).

To solve these two field equations, the boundary conditions are specified as shown in Fig. 2.2. Electrons pass through the anode and cathode current collectors to the external electric circuit. At the anode side, the electrode voltage is usually set as 0V, while at the cathode side, the electrode voltage is set as the cell voltage. For the electric field, the boundary conditions are:

$$\phi_{sol} = 0 \quad (\text{anode}) \quad (2-4)$$

$$\phi_{sol} = V_{cell} \quad (\text{cathode}) \quad (2-5)$$

For the protonic field, there are no protons transferring through any current collector.

The boundary conditions are:

$$\frac{\partial \phi_{mem}}{\partial n} = 0 \quad (2-6)$$

Where  $n$  is the unit vector, pointing outward on the boundaries.

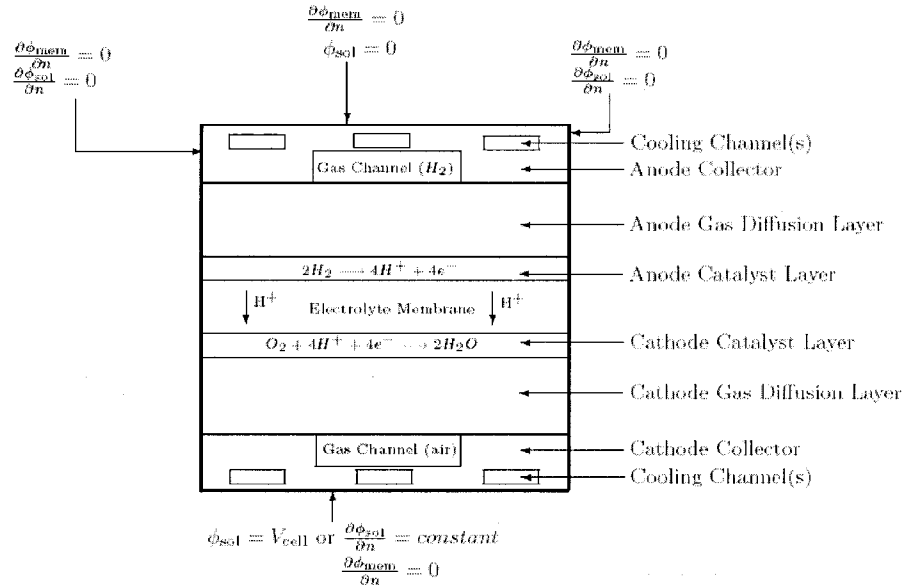


Fig. 2.2 Boundary conditions for  $\phi_{sol}$  and  $\phi_{mem}$  [49]

The source terms of Equations (2-1) and (2-2) are non-zero only at the anode and cathode catalyst layers. In the anode catalyst layer, protons and electrons are produced, while they are consumed in the cathode catalyst layer. The production and consumption rate depends on the electrochemical reaction rate, which is indicated by the current density.

$$\text{For the solid phase, } \begin{cases} i_{sol} = -i_{an} \\ i_{sol} = i_{cat} \end{cases}$$

$$\text{For the membrane phase, } \begin{cases} i_{mem} = i_{an} \\ i_{mem} = -i_{cat} \end{cases}$$

Where  $i_{an}$  and  $i_{cat}$  are the exchange current densities ( $A/m^3$ ). These exchange current densities can be described by the Butler-Volmer kinetic equations, which relate the over-potential  $\eta$  and current density  $i$  in electrochemical reactions [9]:

$$i_{an} = j_{an}^{ref} \left( \frac{[H_2]}{[H_2]_{ref}} \right)^{\gamma_{an}} \left( e^{\frac{\alpha_{an} F \eta_{an}}{RT}} - e^{-\frac{\alpha_{cat} F \eta_{an}}{RT}} \right) \quad (2-7)$$

$$i_{cat} = j_{cat}^{ref} \left( \frac{[O_2]}{[O_2]_{ref}} \right)^{\gamma_{cat}} \left( -e^{-\frac{\alpha_{an} F \eta_{cat}}{RT}} + e^{\frac{\alpha_{cat} F \eta_{cat}}{RT}} \right) \quad (2-8)$$

Where  $j^{ref}$  is volumetric reference exchange current density ( $A/m^3$ ), the symbols  $[ ]$  and  $[ ]^{ref}$  represent the local species concentration, and reference value ( $kg\text{-mol}/m^3$ ),  $\gamma$  is concentration dependence (dimensionless),  $\alpha$  is transfer coefficient (dimensionless), and  $F$  is the Faraday constant ( $96487\text{ C/g-mol}$ ).

During the chemical reaction, the driving force is the over-potential between the solid phase  $\phi_{sol}$  and the membrane phase  $\phi_{mem}$ , which is also known as the activation loss. The over-potentials  $\eta_{an}$  at the anode side and  $\eta_{cat}$  at the cathode catalyst side are calculated as:

$$\eta_{an} = \phi_{sol} - \phi_{mem} \quad (2-9)$$

$$\eta_{cat} = \phi_{sol} - \phi_{mem} - V_{oc} \quad (2-10)$$

Where,  $V_{oc}$  is the thermodynamic open circuit potential for the overall electrochemical reaction. It is governed by the Nernst equation [50]. For PEMFCs, it is calculated as:

$$V_{oc} = 1.229 - 0.9 \times 10^{-3}(T - 298) + 2.3 \frac{RT}{4F} \log(p_{H_2}^2 p_{O_2}) \quad (2-11)$$

Where R is the gas constant,  $T$  is the absolute temperature (K),  $p$  is the gas pressure (Pa), and F is the Faraday's constant.

The open circuit potential depends on the operating temperature and pressure. Different operating conditions will lead to different open circuit potential values.

### 2.1.2 Mass Conservation Equation

In this developed three-dimensional model, the mass conservation equation has different source terms in different cell zones. Generally, the mass conservation equation is expressed as:

$$\nabla \cdot (\rho_i U_i) = S_{mass} \quad (2-12)$$

Where,  $\rho_i$  is the density,  $U_i$  is the velocity vector, and  $S_{mass}$  is the source term. In the gas channel, as well as the gas diffusion layers and membrane, the source term  $S_{mass}$  is set to zero. In catalyst layer, there are hydrogen/oxygen consumption and water formation. The mass sink and source rates depend on the electrochemical reaction rates. Thus, they can be calculated by:

$$S_{H_2} = -\frac{M_{w,H_2}}{2F} i_{an} \quad (2-13)$$

$$S_{O_2} = -\frac{M_{w,H_2O}}{4F} i_{cat} \quad (2-14)$$

$$S_{H_2O} = \frac{M_{w,H_2O}}{2F} i_{cat} \quad (2-15)$$

Where,  $M_w$  is the molecule weight.

### 2.1.3 Momentum Conservation Equation

In the porous media regions, such as the gas diffusion layer and membrane, the momentum equation has to be modified as:

$$\frac{1}{\varepsilon(1-s)} \nabla \cdot (\rho_i U_i U_i) = -\nabla p_i + \frac{1}{\varepsilon(1-s)} \nabla \cdot (\mu_i \nabla U_i) + S_m \quad (2-16)$$

Where  $s$  is the liquid water saturation and  $\varepsilon$  is the porosity. The source term  $S_m$  is set to be zero at the gas channel and membrane zones. In the diffusion layer and the catalyst layer, it is calculated based on the absolute permeability  $K$  and relative permeability  $K_r$ , [50]:

$$S_m = -\frac{\mu_i}{K \cdot K_r} U_i \quad (2-17)$$

For the liquid,  $K_r$  is:

$$K_r = s^3 \quad (2-18)$$

For the gas phase,  $K_r$  is:

$$K_r = (1-s)^3 \quad (2-19)$$

### 2.1.4 Species Conservation

For the PEMFC, in order to model the multi-species transport, the Maxwell-Stefan equation is a proper one to analyze those kinds of phenomena [52]:

$$\nabla x_i = -\sum_{j=1}^N \frac{1}{cD_{ij}} (x_j N_i - x_i N_j) \quad (2-20)$$

Where  $c$  is the molar concentration (g-mole/cm<sup>3</sup>),  $N$  is the molar flux vector (g-mole/cm<sup>2</sup>-s),  $x_i$  and  $x_j$  are the mole fractions of components  $i$  and  $j$ . To determine the binary diffusivity  $D_{ij}$  (cm<sup>2</sup>/s), the reference diffusivity has been referred [53]:

$$D_{ij} = \varepsilon^{1.5} (1-s)^{2.5} D_{ij}^0 \left( \frac{p_0}{p} \right) \left( \frac{T}{T_0} \right)^{1.5} \quad (2-21)$$

Here the reference diffusivity  $D_{ij}^0$  is the property based on reference pressure  $p_0$  101325 Pa and reference temperature  $T_0$  300 K.

Fluid flow in porous media is model by Darcy's law since the gas diffusion layer and catalyst layer are assumed to be the homogeneous porous media.

$$U_i = -\frac{K_p}{\mu_i} \nabla p_i \quad (2-22)$$

Where  $K_p$  is permeability (m<sup>2</sup>) and  $\mu_i$  is gas viscosity (kg m<sup>-1</sup>s<sup>-1</sup>).

The species balance in the porous gas diffusion electrode can be solved by the following equation:

$$\nabla \cdot \left( -\rho w_i \sum \left( D_{ij} \nabla x_j + (x_j - w_j) \frac{\nabla p}{p} \right) + \rho w_i U \right) = 0 \quad (2-23)$$

Where  $w$  is the weight fraction,  $\rho$  is the mixture density (kg/m<sup>3</sup>), which can be calculated by:

$$\rho = \frac{\sum_i x_i M_{w,i}}{RT} p \quad (2-24)$$

Where,  $M_{w,i}$  is the molecular weight,  $R$  is the gas constant,  $T$  is the absolute temperature (K),  $x_i$  is the mole fraction of component  $i$ .

### 2.1.5 Energy Conservation

During the electrochemical reaction, the heat source includes the ohmic heat and reaction heat. In different zones, the heat source is different, such as in cathode catalyst, the reaction heat is the primary part; while in membrane, ohmic heat is the main heat source. The energy equation can be written as:

$$\nabla \cdot (\rho_i U_i T) = \nabla \cdot (k^{eff} \nabla T) + S_T \quad (2-25)$$

Where,  $S_T = I^2 R_{ohm} + h_{reaction} + \eta_{an} i_{an} + \eta_{cat} i_{cat}$ ,  $k^{eff}$  is the effective heat conductivity (W/m-K),  $I$  is the electric current (A),  $R$  is the electric resistance (ohm).

### 2.1.6 Water Model

PEMFC usually works under 100 °C, and the water is produced during the electrochemical reaction. In order to keep the membrane's high conductivity, the membrane should be hydrated in an appropriate level. Therefore, the inlet gas mixture humidity needs to be adjusted. It is critical to keep the membrane under the proper water content. Water flood can block the fuel diffusion and reduce the effective reacting surface area. On the other hand, dry membrane will cause the high electric resistance and increase the ohmic loss. A saturation model [54] can be used to model the water formation and transport:

$$\frac{\partial(\varepsilon \rho_l s)}{\partial t} + \nabla \cdot \left[ \rho_l \frac{K s^3}{\mu_l} \frac{dp_c}{ds} \nabla s \right] = r_w \quad (2-26)$$

Where  $\mu_l$  is the liquid water viscosity, the  $s$  is the liquid water saturation,  $K$  is the absolute permeability,  $p_c$  is the capillary pressure, the subscript  $l$  stands for liquid water, and  $r_w$  is the condensation rate:

$$r_w = c_\tau \max\left(\left[\left(1-s\right)\frac{p_{wv} - p_{sat}}{RT} M_{w,H_2O}\right], [-s\rho_l]\right) \quad (2-27)$$

Where  $M_{w,H_2O}$  is the water molecular weight,  $c_\tau = 100s^{-1}$ , and the capillary pressure  $p_c$  is computed as a function of  $s$  [55]:

$$p_c = \begin{cases} \frac{\sigma \cos \theta_c}{\left(\frac{K}{\varepsilon}\right)^{0.5}} (1.417(1-s) - 2.12(1-s)^2 + 1.263(1-s)^3) & \text{--- } \theta_c < 90^\circ \\ \frac{\sigma \cos \theta_c}{\left(\frac{K}{\varepsilon}\right)^{0.5}} (1.417s - 2.12s^2 + 1.263s^3) & \text{--- } \theta_c > 90^\circ \end{cases} \quad (2-28)$$

Here  $\varepsilon$  is the porosity,  $\sigma$  is the surface tension (N/m<sup>2</sup>) and  $\theta_c$  is the contact angle.

The water content  $\lambda$  is obtained by Springer et al's correlation [51]:

$$\lambda = 0.043 + 17.18a - 39.85a^2 + 36a^3 \quad \text{when } a < 1 \quad (2-29)$$

$$\lambda = 14 + 1.4(a-1) \quad \text{when } a > 1 \quad (2-30)$$

And the water activity  $a$  is defined as [56]:

$$a = \frac{p_{wv}}{p_{sat}} + 2s \quad (2-31)$$

Where the water vapor pressure is computed based on the vapor molar fraction and the local pressure  $p_{wv} = x_{H_2O}P$ .



## 2.2 Numerical Method

Finite volume method has been applied to simulate the transport phenomena in PEMFCs. In the finite volume method, the computational domain is discretized into a number of continuous finite volumes. The partial differential governing equations are integrated over each control volume into a set of discretized equations. In the current simulations, the commercial software Hypermesh® is used to generate the computational mesh. Then it is loaded into the CFD software Fluent ®.

### 2.2.1 Computational Domain

In order to validate the developed PEMFC numerical model, a single channel, three-dimensional numerical model has been created with nine zones, which are anode/cathode current collectors, anode/cathode gas channels, anode/cathode gas diffusion layers, anode/cathode catalyst layers and PEM membrane (see Fig. 2.1). The model dimensions are listed in Figure 2.3 and Table 2.1, which are chosen based on the work by Tao et al. [11], who has conducted a parametric study about single channel PEMFC performance. Similar single channel PEMFC problems have been adopted by other researchers [5]. Normally the top channel is set as the anode side and the bottom channels as the cathode side. The current collector contacts with the gas diffusion layer while the gas mixtures flow through the inner channels surrounded by the current collector. The MEA locates at the center of PEMFC with five layers.

Table 2.1 Dimensions of single channel PEMFC model

<i>Dimensions</i>	<i>Value</i>
Gas channel length	40 mm
Gas channel width	0.762 mm
Gas channel height	0.762 mm
Diffusion layer height	0.254 mm
Catalyst layer height	0.029 mm
Membrane height	0.23 mm
Current collector width	1.524 mm
<b>Current collector height</b>	<b>0.862 mm</b>

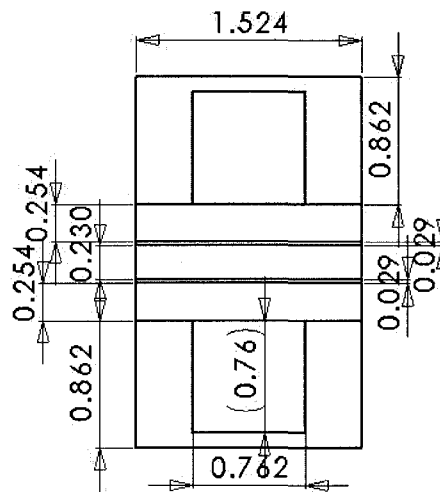


Fig. 2.3 Front view of single channel PEMFC (Unit: mm)

From Fig 2.3, the membrane electrode assembly, including the anode/cathode gas diffusion layers, the anode/cathode catalyst layers and the membrane, has a sandwich

structure. The catalyst layer is very thin and its thickness is only one tenth of the gas diffusion layer. The current collector contacts with the GDL's outer surfaces. Based on the assumption of the periodic conditions between each channels, it is reasonable to simulate only a single channel computational domain. In the real fuel cell active areas, there are thirty or more channels. Those channels are relatively long, compared to the channels' width and height. Usually the transport phenomenon is similar between those channels. Another reason is the computational power limitation of current research techniques. PEMFC model contains many transport equations and each of them is coupled with another, such as the energy equation coupled with the hydrodynamics equations, the species transport equation coupled with the electrochemical equation, etc. Many properties have been approximated based on velocity, temperature, pressure and other variables. Those require a huge amount of computing tasks. So that this single channel PEMFC model is reasonable and affordable. After the model validation for the single channel PEM fuel cell, it will be very straightforward to apply it to PEMFCs with other geometries and design cases.

Fig 2.4 shows the computational mesh with 772,500 cells and 773,832 nodes, which is created by using the Hypermesh® software. It includes the aforementioned nine zones. The hexahedral type mesh is applied, because the computational domain is rectangular. The mesh density is high at the channels' inlet and outlet sections along their flow direction, where significant changes in velocity, temperature and current density are expected. In the current collector zone, there are only the electric field and heat conduction, so the mesh size is larger here than in other zones. For gas channel zones, the gas mixture will develop the laminar inner duct velocity distribution and it has the

convection heat transfer. Then the middle size mesh is applied. In the gas diffusion layer, a porous material is used. The diffusion of the gas mixture, the heat transfer and the transport of electrons are simulated. Middle size mesh in GDL is necessary for accuracy requirement. For the catalyst layers, the mesh size is smallest, because the catalyst layer's thickness is one tenth of the gas diffusion layer or membrane. The electrochemical reactions happen including the electrons and protons transfer, water production, and phase change in the catalyst layers. For the proton exchange membrane, it is characterized by the water content and electric conductivity. Only protons and water transfer through it so that the mesh size is adopted between the gas diffusion layers' and catalyst layers'.

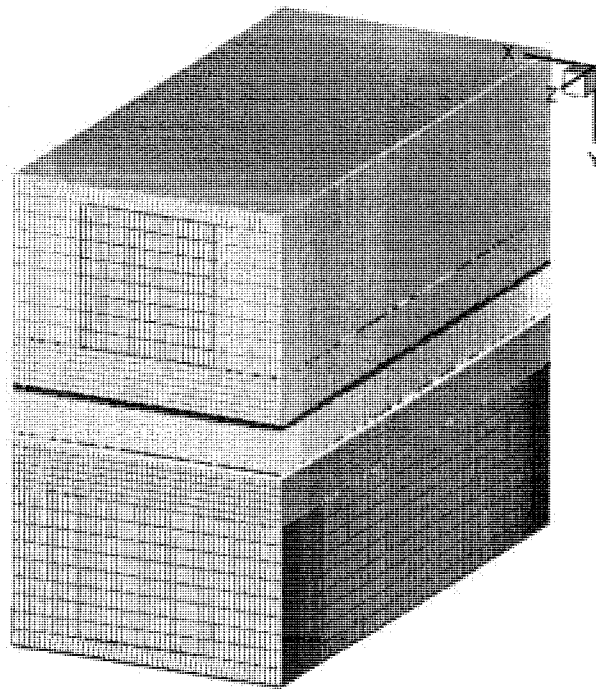


Fig. 2.4 Computational mesh

## 2.2.2 Boundary Conditions

### (1) Mass Inlet

In this single channel PEMFC model, there are two inlets: hydrogen mixture inlet (anode), air inlet (cathode). The mass inlet velocity is applied by the Equation (2-32) and (2-33) [11]:

$$u_a = \zeta_a \frac{I_{ref}}{2F} A_m \frac{RT_{a,in}}{p_{a,in}} \frac{1}{X_{h,in}} \frac{1}{A_{ch}} \quad (2-32)$$

$$u_c = \zeta_c \frac{I_{ref}}{4F} A_m \frac{RT_{c,in}}{p_{c,in}} \frac{1}{X_{o,in}} \frac{1}{A_{ch}} \quad (2-33)$$

Where  $\zeta_a$  and  $\zeta_c$  are the reactant stoichiometric flow ratio for the anode and cathode side. They are defined as the ratio of the amount of reactant supplied to the amount of reaction to generate the specified reference current density  $I_{ref}$  (A/m<sup>2</sup>) [22]. Usually the stoichiometric flow ratio is set in the range of 1 to 3, which means the inlet gas mixture provides 1 to 3 times the hydrogen or oxygen needs for the current reference current density  $I_{ref}$ .  $A_{ch}$  (m<sup>2</sup>) is the channel cross-sectional area of the gas channel;  $A_m$  (m<sup>2</sup>) is the geometrical area of the membrane.  $T_{a,in}$  (K) and  $T_{c,in}$  (K) are the inlet temperatures.  $X$  is the molar fraction of the hydrogen or oxygen, and  $p_{in}$  (Pa) is the inlet pressure.

The inlet fluid in the PEMFC is the gas mixture. At the anode side, the gas components are hydrogen and water vapor, while in the cathode side, it contains the oxygen, water vapor and nitrogen. The different molar fractions of water vapor lead to different inlet humidity. In this validation model, it is set at the normal conditions, around 30% relative humidity. The mass fraction is set as 0.8 for hydrogen and 0.2 for water vapor in anode fuel mixture, 0.2 for oxygen and 0.1 for water vapor in cathode air.

## (2) Thermal Boundary Conditions

The energy equation is solved to obtain the temperature distribution within the PEM fuel cell. Heat is generated by the electrochemical reaction in the catalyst layers and the current flow in the MEA. The “coupled” heat transfer is solved between the fluid zones (fluid in gas channels, gas diffusion layers, catalyst layers and membrane) and the solid zone (the current collectors). The inlet fuel and air temperature is set as 323K, which is the operating condition used by Ticinalli et al. [58]. The side walls of the fuel cell are considered as adiabatic since it is assumed as the periodic conditions of parallel channels. There is convection heat transfer between the anode/cathode current collectors and the ambient air. According to the Costamagna’s work [57], the heat transfer coefficient is estimated as  $20 \text{ W/m}^2\text{-K}$  and the ambient temperature is 323K.

## (3) Fluid Flow

The gas mixture is assumed as incompressible fluid. At the wall boundary, a non-slip boundary condition is assumed. The inlet mass flow rate of the gas mixture is set according to Equations (2-32) and (2-33). The outlet boundary condition is the pressure outlet with 0 Pa gauge pressure.

## (4) Fluid and Solid Zones

The current collector is the solid zone, while the others are different types of fluid zones. The gas diffusion layers, catalyst layers and membrane are also porous zones, the gas channels are the normal fluid zone. In the current collector zones, for the energy equation, the source term is the ohmic heat source. For the catalyst layers, they are fluid zones and the gas mixture will diffuse through them. The catalyst layers have three source terms for different equations: electric potential field Equation (2-1), protonic

potential field Equation (2-2) and mass conservation Equation (2-12). In the catalyst layers, the source term of the energy equation needs the additional term, which accounts for the chemical reaction heat generation. In gas diffusion layers, there are only two source terms: one is used in energy equation and the other used in electric potential field equation. The membrane is the fluid porous zone. The ohmic heat generation is used in the energy equation.

### 2.2.3 PEM Model

The interpreted PEM module is loaded into Fluent® with predefined user-defined function (UDF). To set up a PEMFC module, functions of Joule heating, reaction heating, Bultler-Volmer rate and membrane water transport are used. There are many parameters to be set properly. In the published literature, different research groups have used different sets of parameters based on the materials, temperatures and the fuel cell operating conditions. In order to validate the PEMFC model, the parameters are carefully set according to the physical properties in the experimental work by Ticianelli et al. [58], other physical properties reported from Tao et al. [11] and Bernadi et al. [16] for the missing parameters in Ticianelli's report. The total PEMFC parameters are listed in Table 2.2, which include the electrochemical reaction, species transport and heat transfer parameters. They are properly approximated to match Ticianelli's PEMFC experiment [58]. The electrochemical boundary conditions are set by assigning the user-defined scalars (UDS) value at the two terminal walls, which are located at outside of the anode/cathode current collectors.

Table 2.2 PEMFC parameters

<i>Parameter</i>	<i>Value</i>	<i>Reference</i>
<i>Anode ref current density</i>	$5 \times 10^7 \text{ A/m}^3$	[11]
<i>Anode ref concentration</i>	$0.0564 \text{ kmol/m}^3$	[60]
<i>Anode concentration exponent</i>	0.5	
<i>Anode exchange coefficient</i>	2	
<i>Cathode ref current density</i>	$120 \text{ A/m}^3$	[11]
<i>Cathode ref concentration</i>	$3.39 \times 10^{-3} \text{ kmol/m}^3$	[60]
<i>Cathode concentration exponent</i>	1	
<i>Exchange coefficient</i>	1	
<i>Open-circuit voltage</i>	1.15 V	
<i>Reference diffusivity hydrogen</i>	$9.15 \times 10^{-5} \text{ m}^2/\text{s}$	[22]
<i>Reference diffusivity oxygen</i>	$2.2 \times 10^{-5} \text{ m}^2/\text{s}$	[22]
<i>Reference diffusivity water</i>	$2.56 \times 10^{-5} \text{ m}^2/\text{s}$	[22]
<i>Reference diffusivity other species</i>	$3 \times 10^{-5} \text{ m}^2/\text{s}$	
<i>Diffusion layer porosity</i>	0.3	[61]
<i>Diffusion layer viscous resistance</i>	$5.68 \times 10^{12} \text{ 1/m}^2$	[19]
<i>Catalyst layer porosity</i>	0.28	[62]
<i>Catalyst layer viscous resistance</i>	$5.68 \times 10^{12} \text{ 1/m}^2$	



<i>Catalyst layer surface-to-volume ratio</i>	<i>200000 1/m</i>	
<i>Membrane equivalent weight</i>	<i>1100 kg/kmol</i>	
<i>MEA projected area</i>	<i><math>6.096 \times 10^{-5} m^2</math></i>	
<i>Absolute permeability K</i>	<i><math>1.76 \times 10^{-11} m^2</math></i>	<i>[19]</i>
<i>Current collector/GDL/catalyst conductivity</i>	<i>120 s/m</i>	<i>[59]</i>
<i>Membrane conductivity</i>	<i>17 s/m</i>	<i>[59]</i>
<i>Current collector/GDL/catalyst thermal conductivity</i>	<i>150 W/m-K</i>	<i>[19]</i>
<i>Membrane thermal conductivity</i>	<i>0.95 W/m-K</i>	<i>[19]</i>
<i>Fuel/air stoichiometric flow ratio</i>	<i>3</i>	<i>[22]</i>

#### 2.2.4 Numerical Techniques

There are several coupled equations, such as the electrochemical, electric and protonic equations, so that the under-relaxation factors are adjusted to ensure the convergence of the numerical simulation. In Fluent®, the default under-relaxation parameters are set to values that are near the optional largest possible number. The higher the under-relaxation factor, the faster the calculation reaches the convergence. Usually low under-relaxation factors can provide stable iteration process. For this PEMFC model, the factor for the pressure correction equation is set as 0.7, and 0.3 for the momentum

equation. The protonic potential and water content are set as 0.95. The others use the default value 1.0 to obtain the possible fast converged solutions.

The implicit formulation is applied while the solver is set as pressure based. The SIMPLE (Semi-Implicit Method for Pressure-Linked Equations) scheme is selected to treat the pressure-velocity coupling, and the discretization scheme is chosen as the “standard” for the pressure and “second order upwind” for the others: density, momentum, energy, species and potential fields. The “first order upwind” scheme cannot provide the converged solution under this model. There are 4 user-defined scalars (UDS): electric potential, protonic potential, water saturation and water content and 15 user-defined memories (UDM): the current flux density, ohmic heat source, reaction heat, overpotential, liquid water activity, etc. They are coupled with the governing equations to solve for the velocity, temperature, voltage and current density.

A grid independent study is performed by increasing the mesh density for the single channel case. The results are shown in Fig. 2.5. In this case, the PEMFC works under 0.8V cell voltage. While the mesh density increases, the numerical results of current density approach to converged value. Based on the results of this grid independent study, the element size of the third case is selected for further mesh generation for other cases.

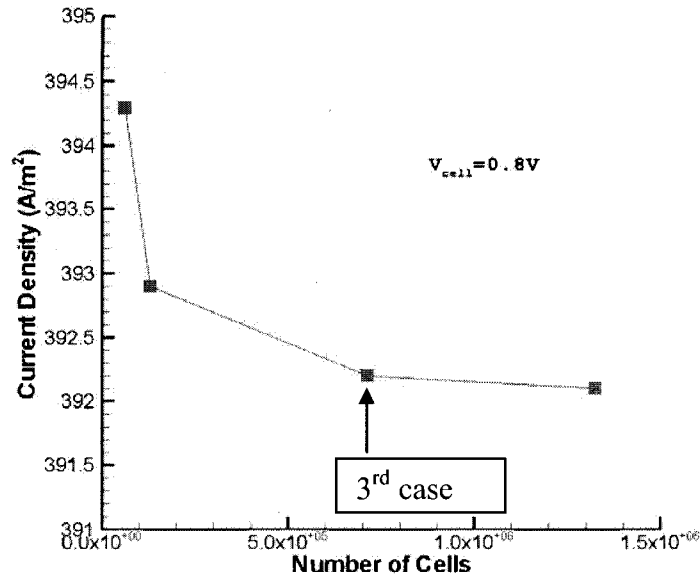


Fig. 2.5 Grid independent Study

## 2.3 PEMFC Model Validation

### 2.3.1 Available Published Experimental Work

Ticianelli et al. [58] have conducted the experimental optimization work by using only one-tenth of previous platinum loading ( $4 \text{ mg/cm}^2$ ). They prepared the experiment basically by (1) brushing a 5% Nafion solution (Nafion® 117) onto the Prototech gas diffusion electrodes ( $0.35 \text{ mg Pt/cm}^2$ ); (2) evaporation of the solvent from the Nafion solution in the electrode under ambient conditions, followed by vacuum drying at  $70 \text{ }^\circ\text{C}$  for 1 hour; (3) hot-pressing a pair of these electrodes on both sides of a Nafion® membrane.

The experimental work was carried out in the fuel cell made with carbon end plates. The fuel cell is equipped with a reversible hydrogen reference electrode. The graphite end plates contain gas feed inlets and outlets, ribbed channels for gas flow behind the porous gas diffusion electrodes, and holes for cartridge heaters and for a thermocouple. After

positioning the MEA between two gaskets and graphite plates, the latter is clamped between stainless steel plates that are insulated from the cell body with polytetrafluorethylene (PTFE) sheets. The active electrode area in this cell is  $5 \text{ cm}^2$ . Humidification of reactant gases is carried out by passing the gases through stainless steel bottles containing water at about  $5\text{-}15 \text{ }^\circ\text{C}$  above the cell temperature. The schematic of a single cell is shown in Fig 2.6 [58].

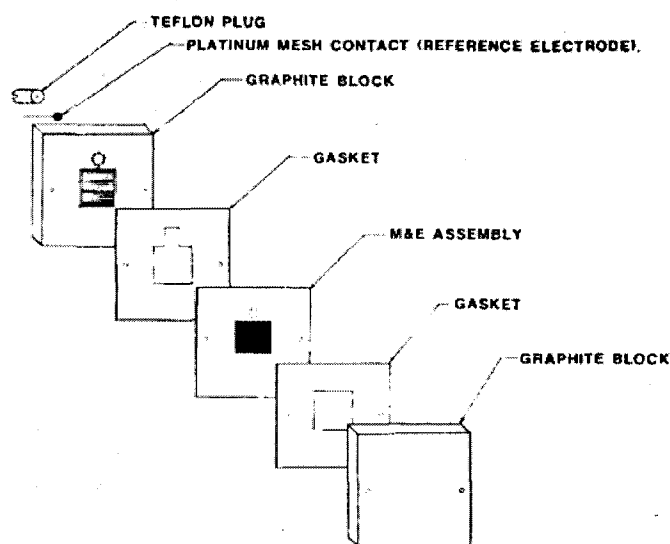


Fig. 2.6 Schematic of single cell [58]

The experiment result data are shown in Fig. 2.7. These are the V-I curves under  $50 \text{ }^\circ\text{C}$  and 1 atmospheric pressure operation conditions. The A and C cases use Nafion-impregnated and as received Prototech electrodes and B case uses GE/HS-UTC membrane and electrode assembly ( $4 \text{ mg Pt/cm}^2$ ). The solid lines are curve fitting plots and the Xs are is the experimental points.

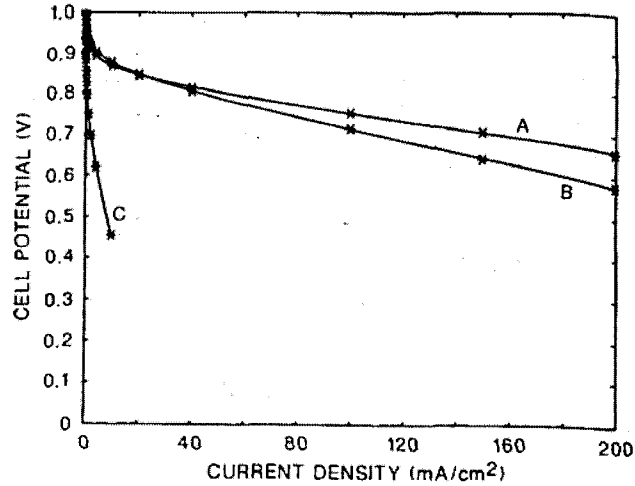


Fig. 2.7 Cell V-I curves for PEMFC at 50 °C, 1 atm: A and C cells with Nafion-impregnated and asreceived Prototech electrodes (0.35 mg Pt/cm<sup>2</sup>, respectively; B cell with GE/HS-UTC membrane and electrode assembly (4 mg Pt/cm<sup>2</sup>) [58]

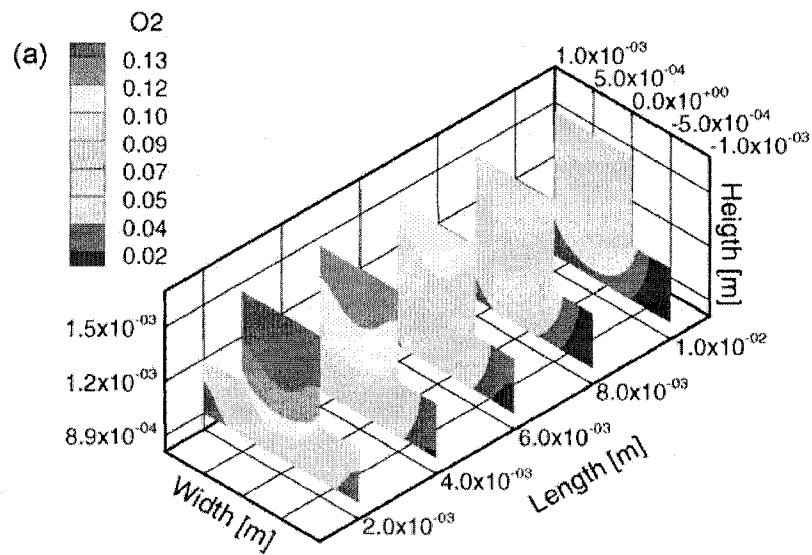
The result shows that the activation loss is significant when cell works with current densities from 0 to 40 mA/cm<sup>2</sup>. Since there is only the data under 200 mA/cm<sup>2</sup>, the mass concentration polarization loss is not shown in Fig. 2.7.

### 2.3.2 CFD Data from Other Research Groups

A comprehensive, three-dimensional analysis of a PEMFC has been developed by Baca et al. [63] to study the performance of a PEMFC under different operating conditions. This steady-state analysis is single-phase and non-isothermal. Their model includes the conservation equations for species, energy, charge, mass and momentum. Different boundary conditions were applied to a computational domain to simulate a single channel PEM fuel cell.

Figs. 2.8 (a) and (b) show the oxygen and hydrogen mass fraction at the 0.37 V cell voltages. In each cutting plane, it includes the channels and gas diffusion layers for both

anode and cathode side. The oxygen and hydrogen consumptions along the flow direction can be found. The low oxygen mass fraction appears at the shoulder area of the gas diffusion layer. Because the oxygen has to pass by the center area in gas diffusion layer then diffuse into the shoulder area. Most of the oxygen is consumed at the center area where has the high current density. On the other hand, the hydrogen concentration experiences little change in a single plane of the anode side, which indicates that the hydrogen has the higher diffusivity than oxygen. Another reason is that, on anode side, there is rarely flooding problem at the high current density operating conditions.



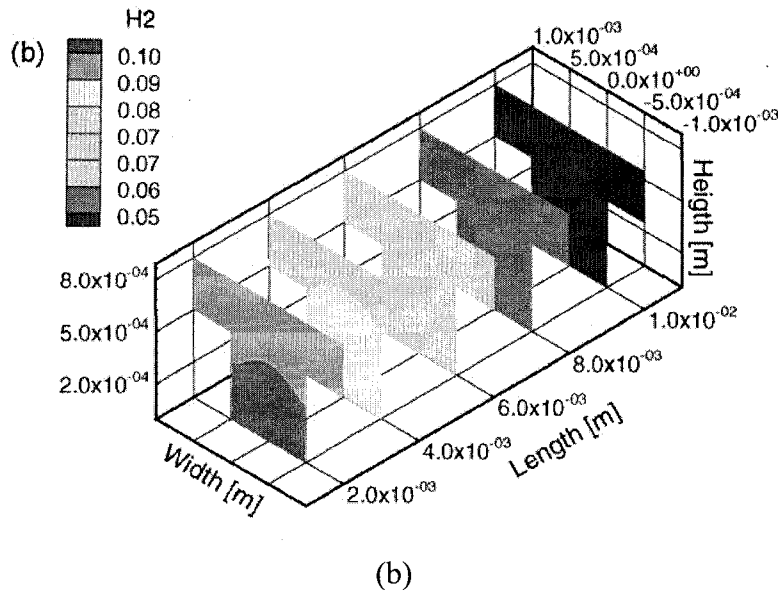


Fig. 2.8 Oxygen (a) and hydrogen (b) mass fraction at a 0.37 cell voltage [63]

### 2.3.3 PEMFC Model Validation

Numerical simulations of the single channel PEMFC have been conducted under several cases with different cell voltages, ranging from 0.9 to 0.6 V. Each simulation has obtained the converged solution with the iteration residue of energy less than  $1 \times 10^{-6}$ . After the converged solution is achieved, the current density based on the projected membrane area is calculated. The V-I curve is one of the PEMFC's important characteristics, which shows the fuel cell's performance under certain operating conditions. Ticianelli's report [58] does not provide the detail geometry data and each single material property. However, the parameters, which are used in this model, are set according to the published data from other related research work, and those parameters provide reasonable approximation to the Ticianelli's fuel cell experiment. Comparisons of the computed polarization curve with Ticianelli et al.'s measurements [58] are shown in Fig. 2.9. It can be seen that, the simulated V-I curve shows a good agreement with the

compared experimental data. This good agreement indicates that the current PEMFC model has been validated by Ticianelli et al.'s experimental work [58].

By comparing Fig 2.8 and Fig. 2.10, a similar oxygen concentration distribution is observed. Fig. 2.10 shows the simulated result from the present PEMFC model. Similar to Baca's result [63], along the air flow direction the oxygen mass fraction decreases in the similar pattern from gas channel to GDL. On each single plane shown in Fig. 2.10, oxygen diffuses through the gas diffusion layer and the low oxygen concentration appears at the shoulder area.

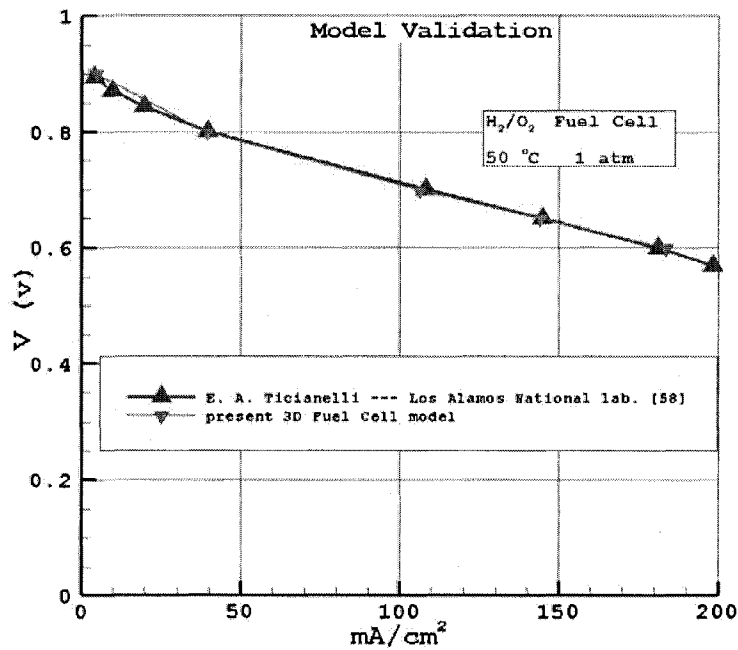


Fig. 2.9 Comparison of the V-I curves with experiment data



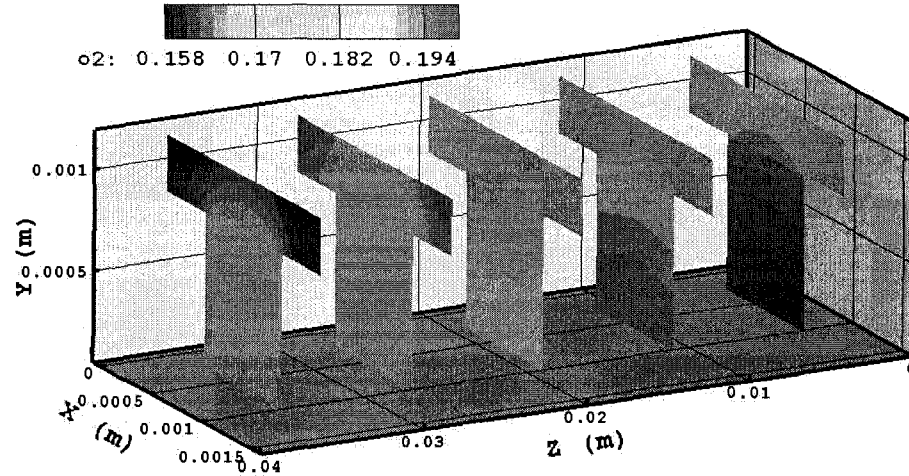


Fig. 2.10 Oxygen mass fraction in gas channel and GDL

In summary, a PEMFC model was developed and a set of coupled governing equations are solved. The developed PEMFC model has been validated in a single channel case, and the simulated numerical data are compared with Ticianelli et al.'s experimental work [58]. The numerical result shows (Fig. 2.9) a good agreement in a reasonable range. This numerical result is also similar to Baca's [63] by comparing the oxygen mass fraction distribution in PEMFC cathode side. These prove that developed numerical PEMFC model in this thesis works well under this type of PEMFC with the specific materials and operating conditions.

## CHAPTER 3

### BASELINE DESIGN OF PEMFC

In this chapter, the baseline design of the bipolar plate has been implemented and studied in the proposed PEMFC model. The three-dimensional simulation has been performed. Numerical results are discussed to evaluate the performance of this kind of PEM design. The velocity distribution along channels and temperature distribution have also been studied. The electrochemical performance is investigated by considering the current density distribution within the catalyst layers and hydrogen/oxygen mass fraction and water content in membrane.

#### 3.1 Design Description

A three-dimensional PEMFC model has been developed and implemented into the single fuel cell stack which is different from the single channel PEMFC design. This model contains the whole size bipolar plates (also recognized as the current collectors), the gas channels and the membrane electrode assembly. A schematic view of this single fuel cell pack model is illustrated in Fig 3.1. From the top to the bottom those are anode current collector, anode gas channel, anode gas diffusion layer, anode catalyst layer (very thin), membrane, cathode catalyst layer, cathode gas diffusion layer, cathode gas channel, and cathode current collector. In bipolar plates, the traditional parallel channel layout is

implemented in order to investigate the PEMFC system performance. The bipolar plate top view is shown in Fig 3.2 (a) with fourteen channels at the center area and small sized cubes at the two side header areas which are designed for supporting the bipolar plate in fuel cell stack.

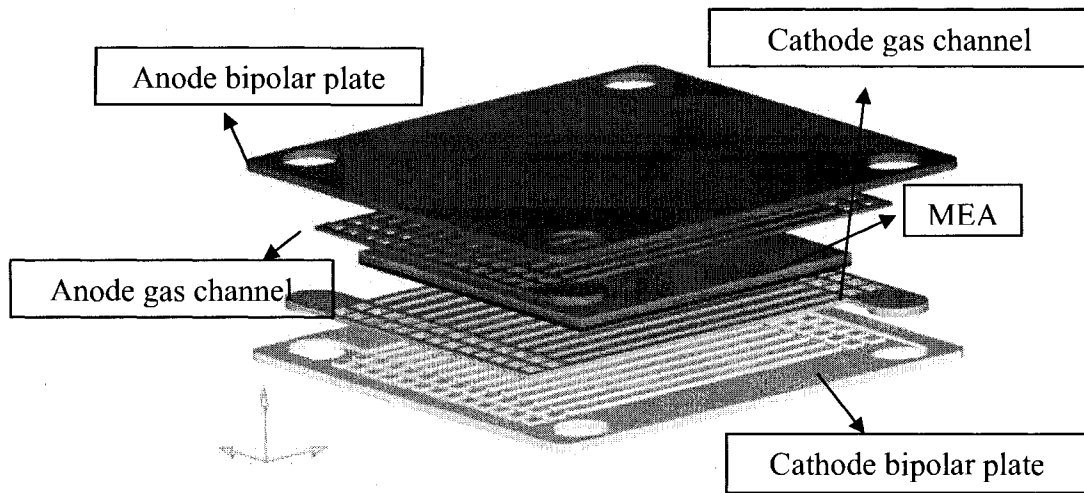


Fig. 3.1 Schematic view of single pack PEMFC

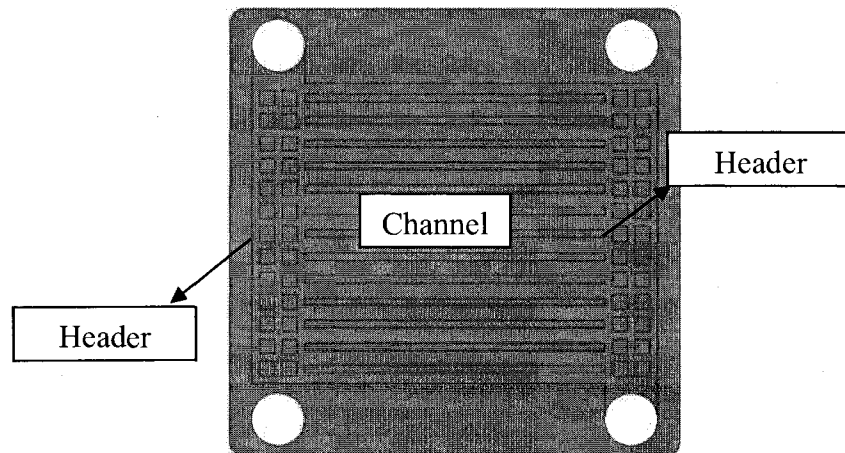


Fig. 3.2 (a) Top view of bipolar plate

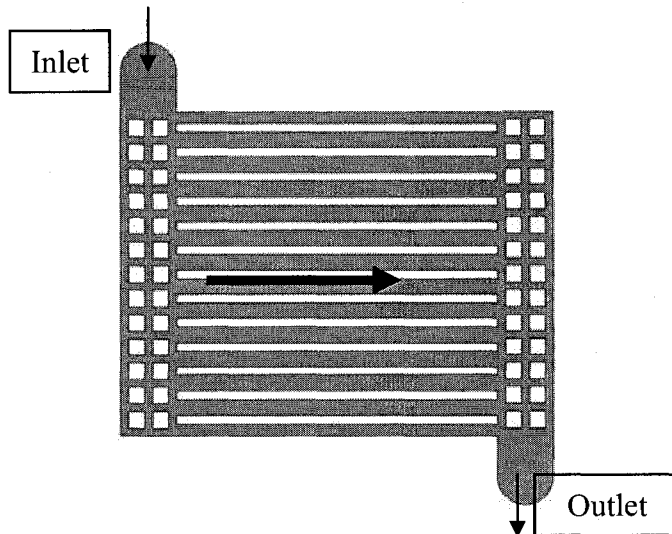


Fig. 3.2 (b) Top view of gas channel

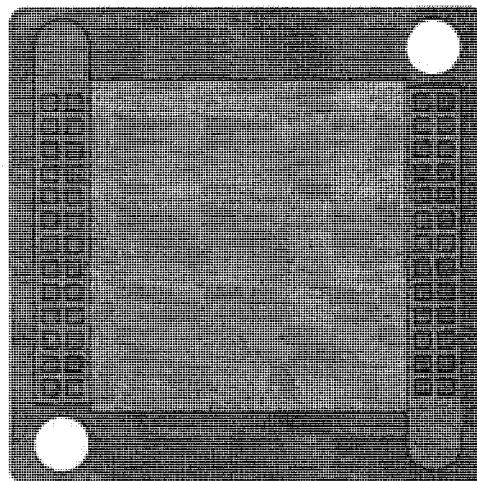


Fig. 3.2 (c) Assembly view of bipolar plate, gas channel and membrane

Fig. 3.2 (b) is the top view of the gas channel which corresponds to the bipolar plate in Fig.3.2 (a). The gas mixture flows into channels from the inlet then spreads to the header area. After passing through the fourteen channels, it leaves in the direction as shown in Fig. 3.2 (b). Fig. 3.2 (c) is the assembly view of the bipolar plate and membrane. The membrane is placed at the center of the gas channels and it has dimensions of 4 in  $\times$  5 in, located at the center position of the bipolar plate. Dimensions

of the designed bipolar plate are shown in Fig. 3.3, where the unit is inch. The bipolar plate thickness is 0.1 in with 6 in  $\times$  6 in width and length. The channel width is 0.2 in and the channel rib is 0.2 in wide and 0.05 in height. The cube in the header area is 0.2 in  $\times$  0.2 in  $\times$  0.05 in. The inlet diameter is 0.7 in. The gas diffusion layer height, catalyst height and membrane thickness are used based on the validated case, the single channel PEMFC in Chapter 2.

A three-dimensional computational mesh has been generated with 735,050 cells and 427,859 nodes, which is shown in Fig 3.4. At the edge of the bipolar plates, shown in Fig. 3.4 (a), there is only heat conduction and electron transfer, therefore a coarse mesh with the large elements is used in order to save computational cost. For the header area and channel area, the denser mesh with small elements is necessary, where there are the heat transfer and fluid flow and diffusion and high gradations are expected to exist. The electrochemical reactions occur inside MEA. The finest mesh is chosen to ensure the accuracy of numerical computation. Fig. 3.4 (a) shows the computational mesh of the bipolar plate and its gas channels. Fig. 3.4 (b) shows that the MEA is placed on the top gas channel and in the center of the domain. Fig. 3.4 (c) shows the whole domain mesh of the single pack PEMFC. The anode gas channel and the cathode gas channel are parallel with counter flow configuration.

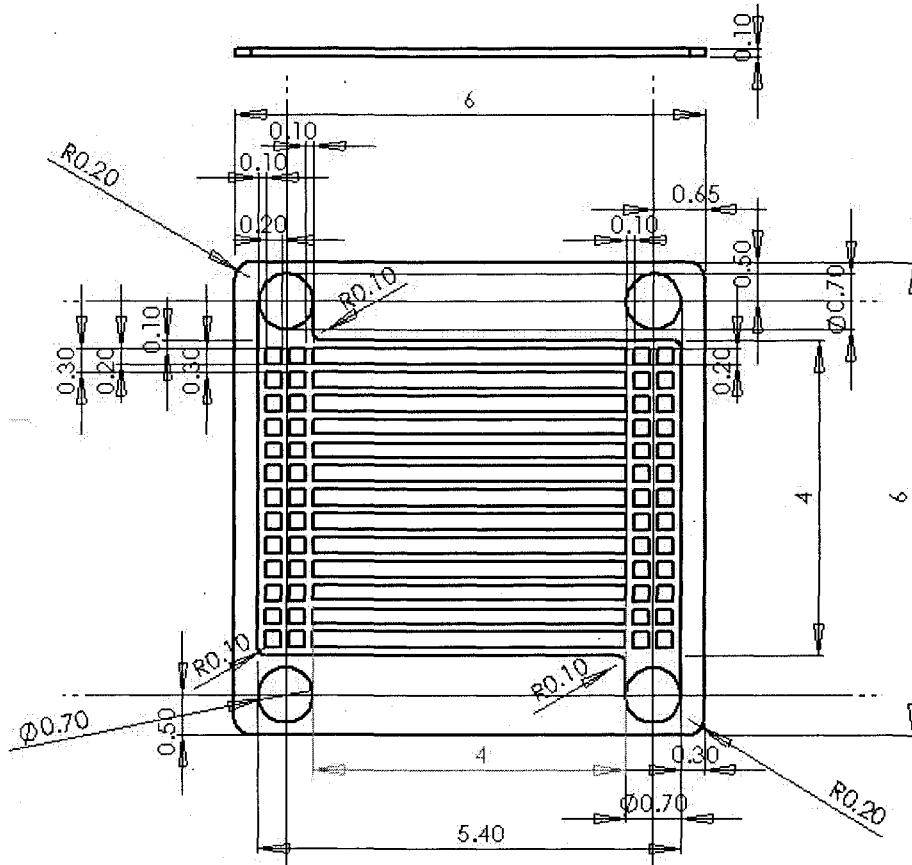


Fig. 3.3 Dimensions of bipolar plate design (unit: in)

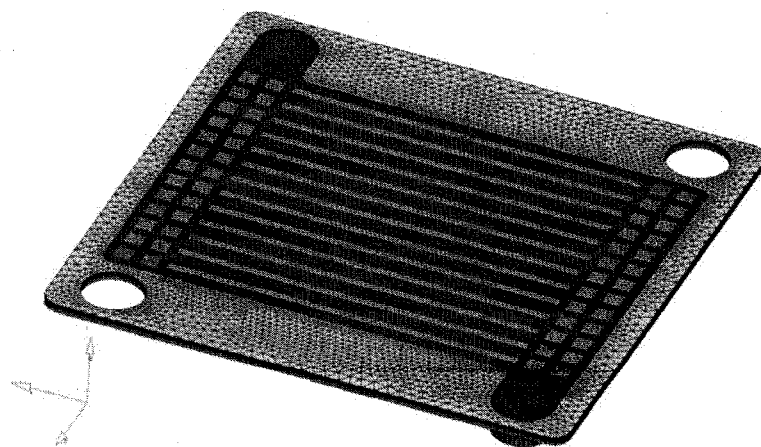


Fig. 3.4 (a) Computational mesh of bipolar plate and gas channel

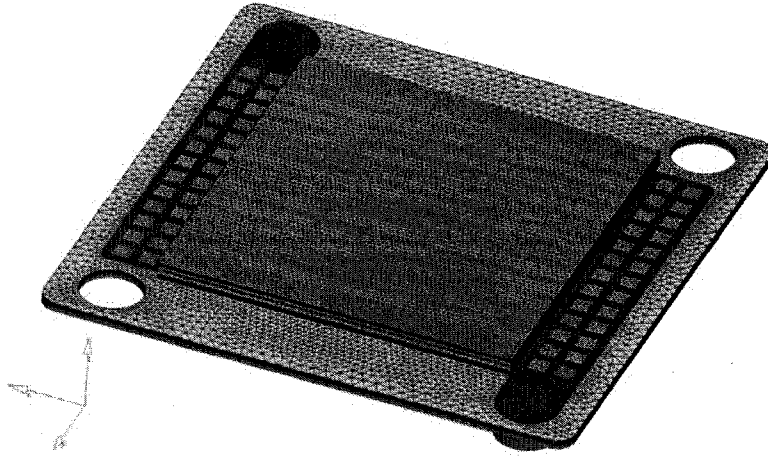


Fig. 3.4 (b) Computational meshes of bipolar plate, gas channel and MEA



Fig. 3.4 (c) Computational mesh of the whole single pack fuel cell

### 3.2 Boundary Conditions

The commercial CFD software Fluent® is used as the computational tool. The PEMFC model is loaded with the user-defined functions in order to model the physical and electrochemical processes within PEMFCs. All the electrochemical parameters are specified as the same as the validated PEMFC model. The PEMFC operates at 50 °C

ambient air with convection heat transfer, which boundary conditions are specified the same as the validation model.

(1) Mass inlet

The inlet boundary conditions are mass flow rates, which are defined in Chapter 2 by:

$$u_a = \zeta_a \frac{I_{ref}}{2F} A_m \frac{RT_{a,in}}{P_{a,in}} \frac{1}{X_{h,in}} \frac{1}{A_{ch}} \quad (2-32)$$

$$u_c = \zeta_c \frac{I_{ref}}{4F} A_m \frac{RT_{c,in}}{P_{c,in}} \frac{1}{X_{o,in}} \frac{1}{A_{ch}} \quad (2-33)$$

Where the  $I_{ref}$  is set as 400 mA/cm<sup>2</sup>. The parametric study will be conducted by varying the stoichiometric flow ratios  $\zeta_a$  and  $\zeta_c$  from 1 to 25. This represents the flow rate change in gas channel.

(2) Cell voltage

The PEMFC normally works between the 0.4V and 0.8V. When it's at 0.8V, the current density is low and the hydrogen and oxygen consumption rate is also low. While the PEMFC operates at 0.4V, the fuel cell has the high loading and its current density is high. Under this high current density condition, the electrochemical reaction rate can not increase by increasing the fuel supply due to the mass transport limitation in GDL. The 0.8V and 0.4V operating conditions have been simulated to study the PEMFC performance based on different cell voltage conditions.



### 3.3 Results and Discussion

The converged numerical results of this baseline design simulation are obtained. The velocity distribution and temperature distribution are investigated. The electrochemical phenomena are also examined by hydrogen/oxygen mass fraction, water content and current density distribution.

#### 3.3.1 Velocity Distribution

The velocity distribution at the middle length of the channels is investigated. The distribution between the channels is non-uniform, which is the same as the results reported by Martin et al. in 2007 [64]. Basically the high velocity appears at the beginning and ending channels, the relatively low velocity is at the middle channels. The bar chart of the velocity distributions are illustrated in Fig. 3.5 (a) (b) for the  $\zeta = 1$  and  $\zeta = 25$ . Since the velocity inlet is different in these two cases, Fig. 3.5 shows the normalized velocity by dividing its own inlet velocity. By comparing the velocity distribution, it is found that the high flow rate can increase the velocity in lateral channels. The velocity at center channels is decreased. That leads to the worse non-uniform velocity distribution.

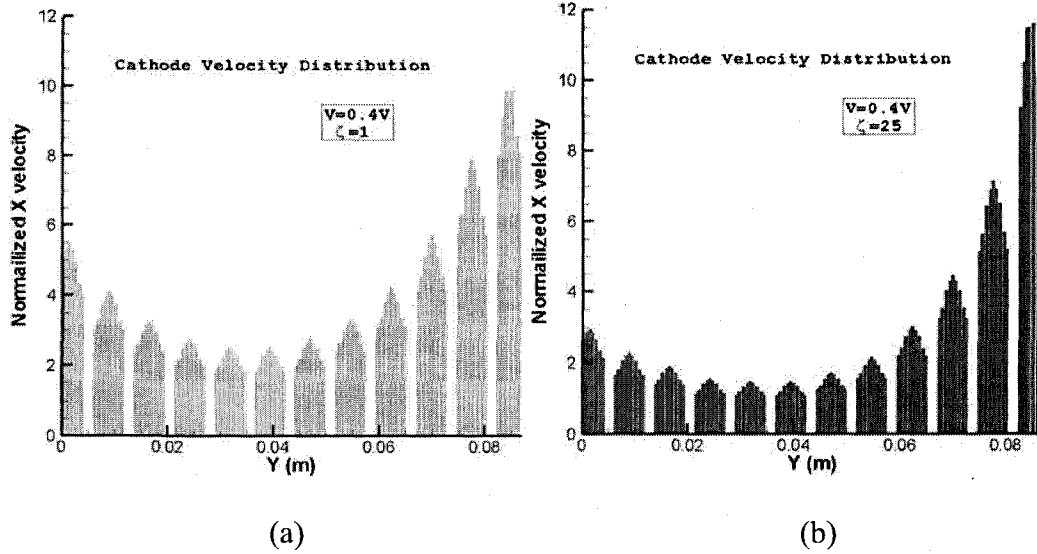


Fig. 3.5 Velocity distribution between channels

### 3.3.2 Temperature Distribution

The temperature distribution is analyzed in bipolar plate, gas channel and catalyst layers. The heat source is the reaction heat and ohmic heat. The parametric study is performed to study relationship between the flow rate and fuel cell temperature. In this model, there are no specific cooling channels, so that the heat is transferred into outside by the convection from the bipolar plate into the ambient and the convection from gas channel into the exhaust gas.

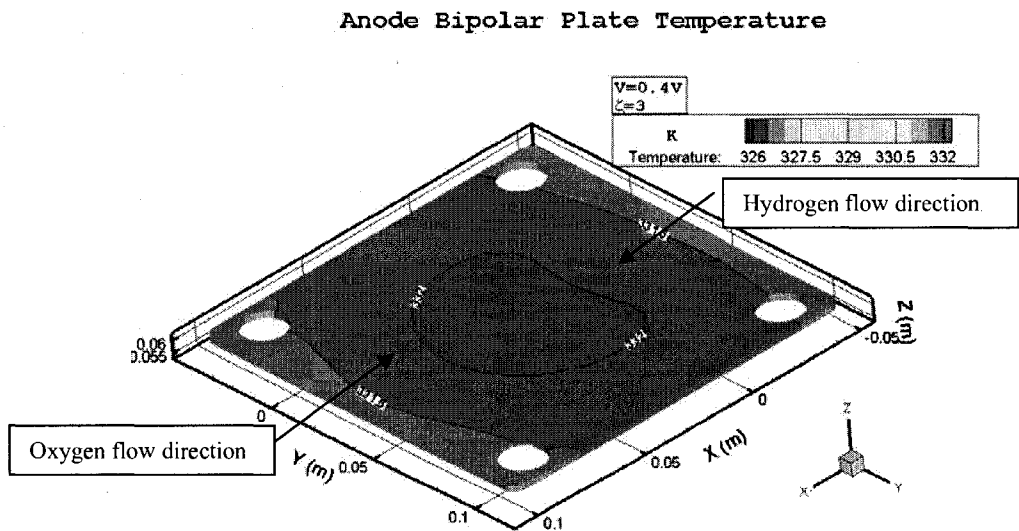
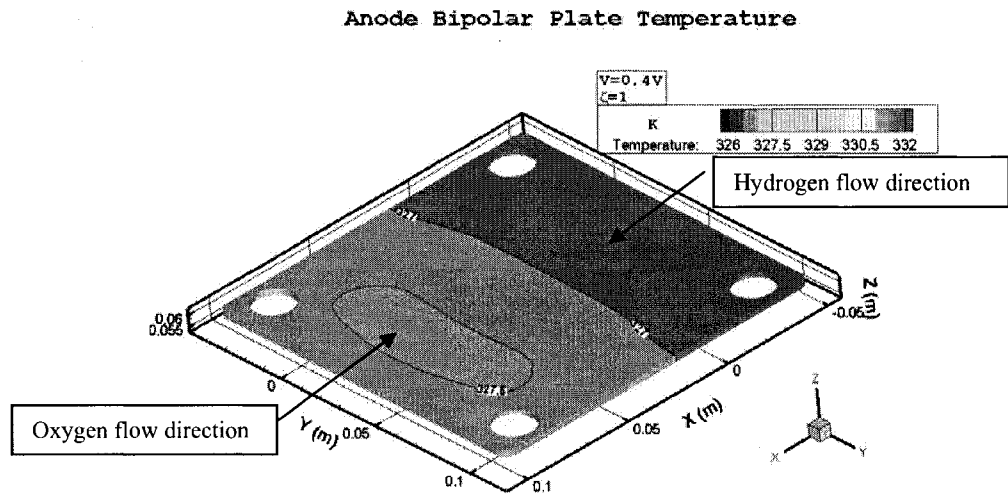
#### 3.3.2.1 Bipolar Plate

The temperature of bipolar plate has increased by 2-10K above the ambient temperature (323K). Due to the high conductivity of the bipolar plate, the temperature different is within 1K throughout the whole plate. In the operating condition of 0.4V, the cell current density is at a high level. A large amount of reaction heat and ohmic heat is generated. It is transferred to the bipolar plate by conduction through the GDL. The

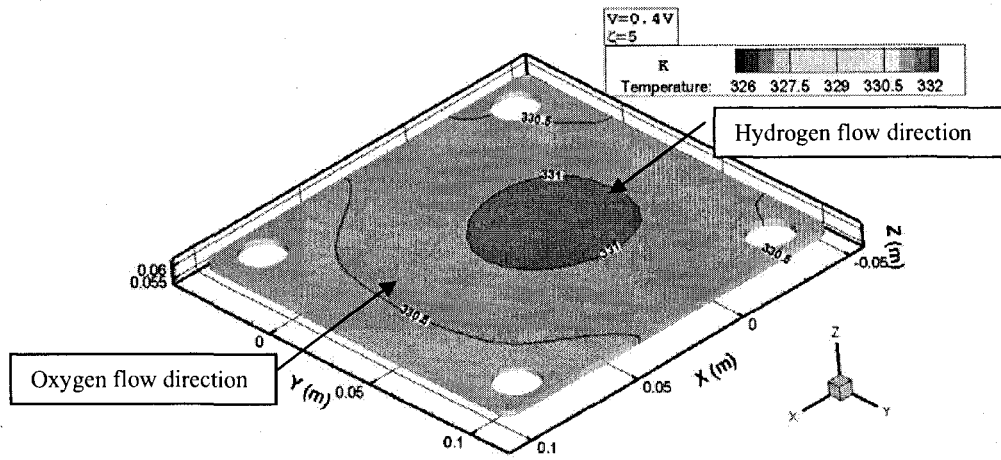
convection heat transfer from bipolar plate to the ambient air is noticeably large. The inlet gas mixture's temperature is 323K (the ambient temperature). The hot bipolar plate can also heat up the gas mixture. When the flow rate is high, heat transfer between the bipolar plate and gas mixtures becomes significant. On the other hand, when the flow rate is low, the gas mixture temperature is close to the temperature of bipolar plate and the inside channel convection heat transfer can be ignored. Fig. 3.6 shows the anode bipolar plate temperature contour for the operating condition of 0.4V cell voltage. The hydrogen mixture flows along the negative  $x$ -axis, from  $x = 0.07$  to  $x = -0.03$ m. When  $\zeta = 1$ , in Fig. 3.6 (a), the highest temperature appears at  $x = 0.07$ m, which is the beginning of the hydrogen channel position. For this condition ( $\zeta = 1$ ,  $V_{cell} = 0.4V$ ), the hydrogen flow does not provide enough fuel. Most of the hydrogen is consumed at the channels' upstream. Increasing  $\zeta$  from 1 to 3, which is shown in Fig. 3.6 (b), results in the noticeable increase in the bipolar plate's temperature. The highest temperature moves from the upstream to the center region. While  $\zeta$  is further increased to a value higher than 5, the temperature starts to decrease and the relative low temperature appears at the two sides of the plate ( $y = \pm 0.07$  m). It is important to know that the hydrogen velocity distribution is non-uniform and the velocity in the two side channels is very high. The heat transfer from plate into exhaust gas mixture becomes significant. This "gas flow cooling" effect causes the decreasing of the bipolar plate's temperature. In Fig. 3.6 (d), the 328K contour line is not symmetric. The temperature at  $y = 0.08$ m is lower than other places. This is the because of the high velocity at this region.

When the fuel cell is at  $V_{cell} = 0.8V$ , the oxygen consumption rates become low and the current density is small. The heat generation is in low level. In Fig. 3.7 (a), the whole

plate's temperature only increased by 1.6K. From the temperature contour, it indicates that the oxygen supply is more than demanding. As  $\zeta$  increases, the increased oxygen supply is wasted in the exhaust gas mixture. Due to the "gas flow cooling" effect, the bipolar plate's temperature starts to decrease, as is shown in Fig. 3.7 (b) (c).

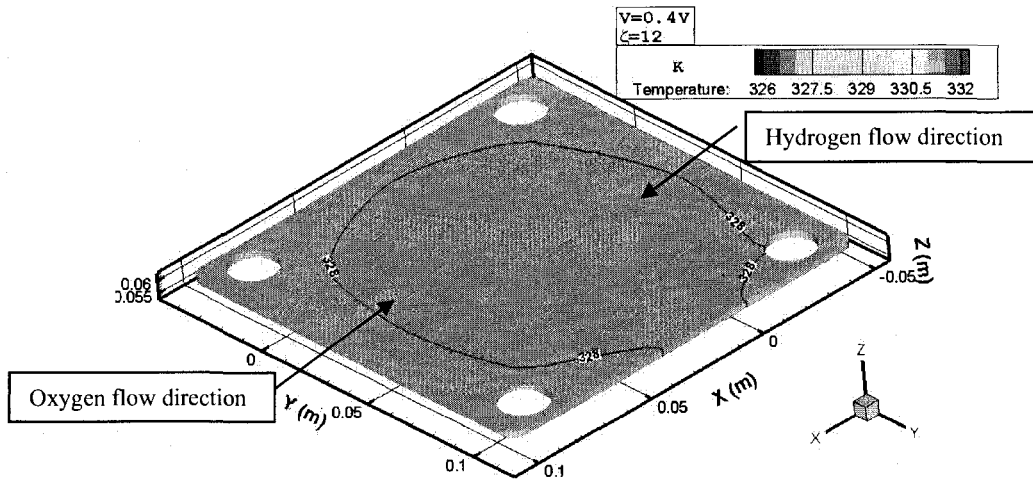


Anode Bipolar Plate Temperature



(c)

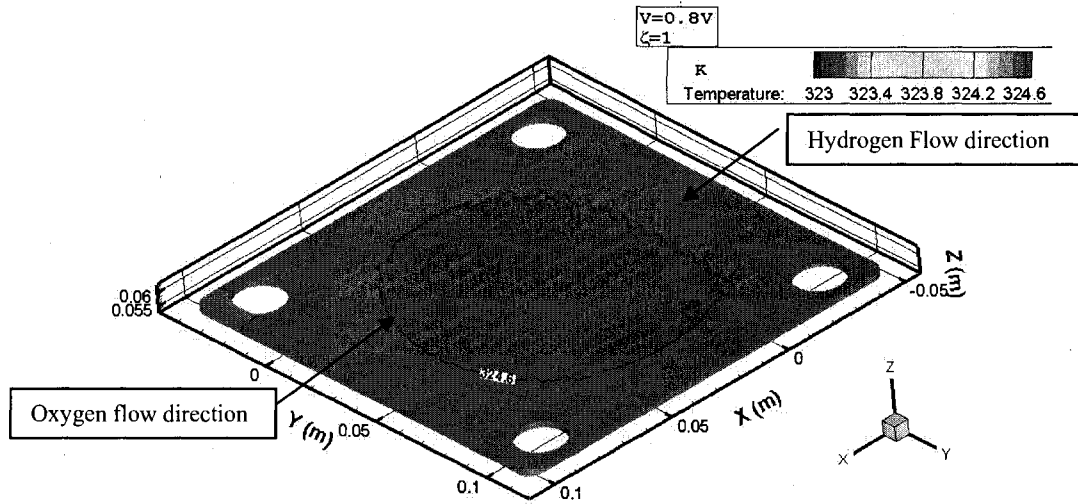
Anode Bipolar Plate Temperature



(d)

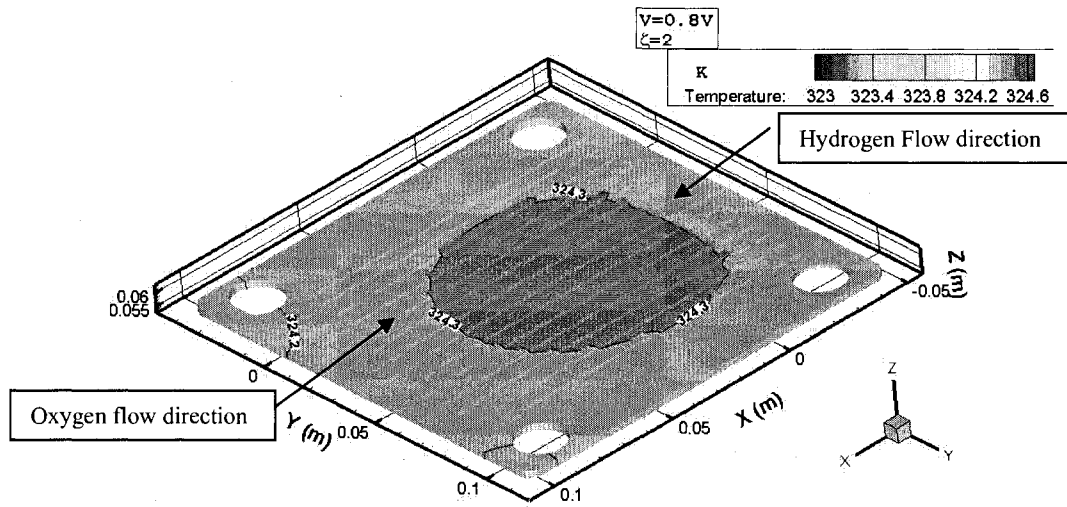
Fig. 3.6 Anode bipolar plate temperature at 0.4V

### Cathode Bipolar Plate Temperature



(a)

### Cathode Bipolar Plate Temperature



(b)

### Cathode Bipolar Plate Temperature

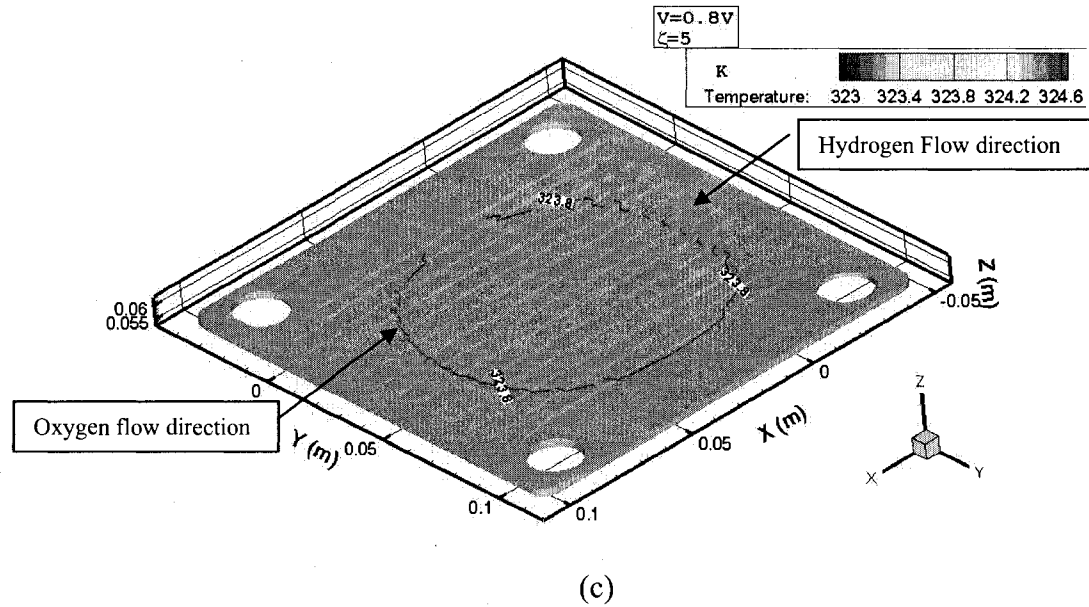


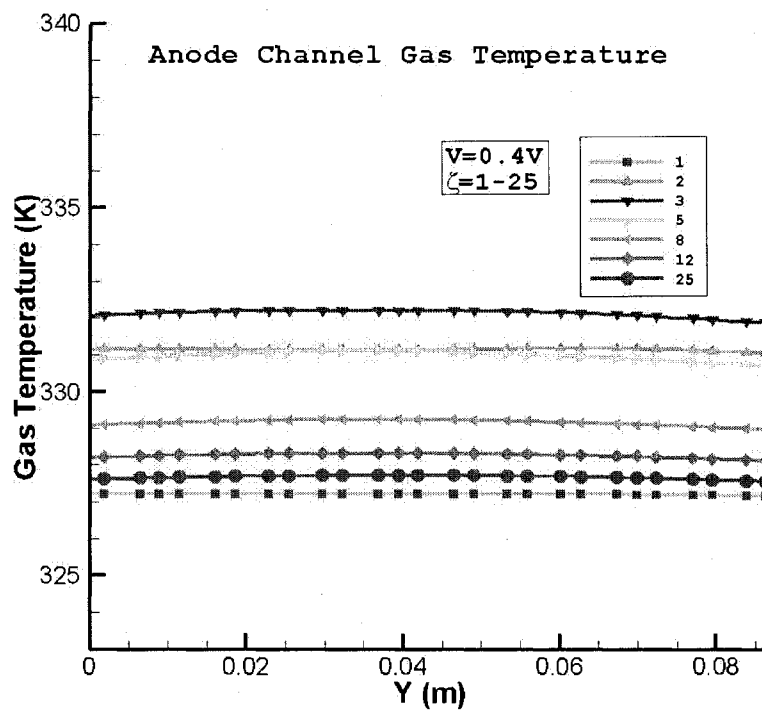
Fig. 3.7 Cathode bipolar plate temperature at 0.8V

#### 3.3.2.2 Gas Channel Temperature

A parametric study about the gas mixture temperature inside the channels is performed by varying flow rates under low/high current density conditions. The gas temperature is mainly related to the electrochemical reaction. The heat is transferred from the bipolar plate and the GDL. Fig. 3.8 shows the gas mixture temperature at all channels' middle length. In Fig. 3.8 (a), the fuel cell operates at  $V_{cell} = 0.4V$  condition. The temperature difference between the channels is small compared to the velocity distribution. When  $\zeta$  increases from 1 to 2, temperature increases by 4K, which means electrochemical reaction rate increases significantly. When  $\zeta$  is greater than 3, the heat generation in the fuel cell reaches its limitation due to the electrochemical reaction mechanism. The hydrogen mixture temperature starts to decrease until it approaches

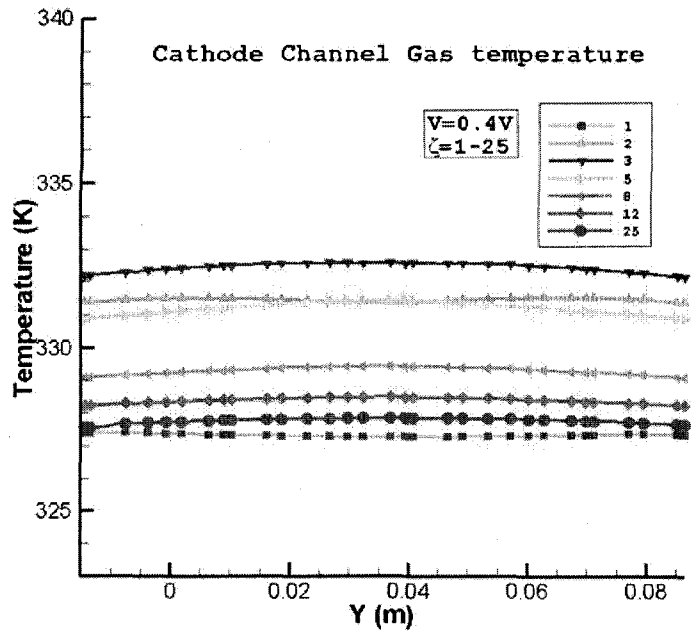
327K. There is an optimum flow rate according to the fuel cell operating voltage. By comparing Fig. 3.8 (a) and Fig. 3.8 (b), the anode channel temperature distributions are similar to the cathode's under the same operating cell voltage.

At low current density condition,  $V_{cell} = 0.8V$ , the heat generation is small. The “gas flow cooling” effect dominates the heat transfer. Increasing flow rate leads to the temperature decreasing of the oxygen gas mixture. Increasing flow rate further, the temperature decreases to 323.6K value. This trend is shown in Fig. 3.8 (c) and Fig. 3.8 (d).

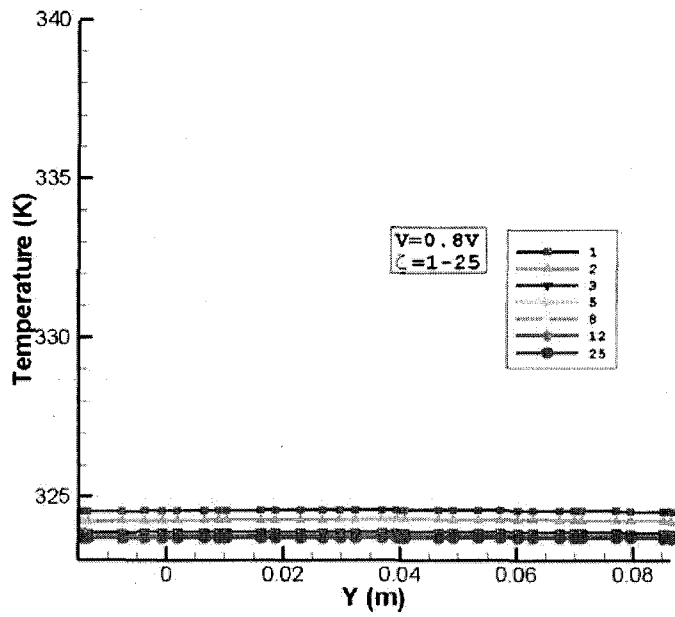


(a)

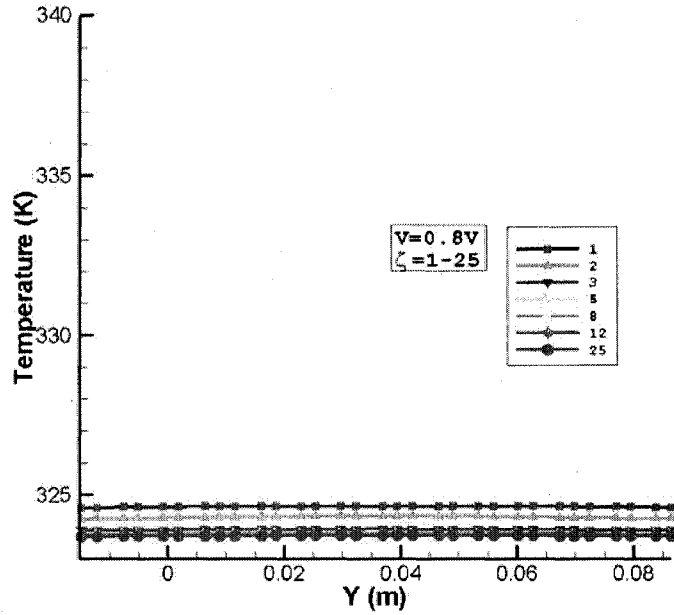




(b)



(c)



(d)

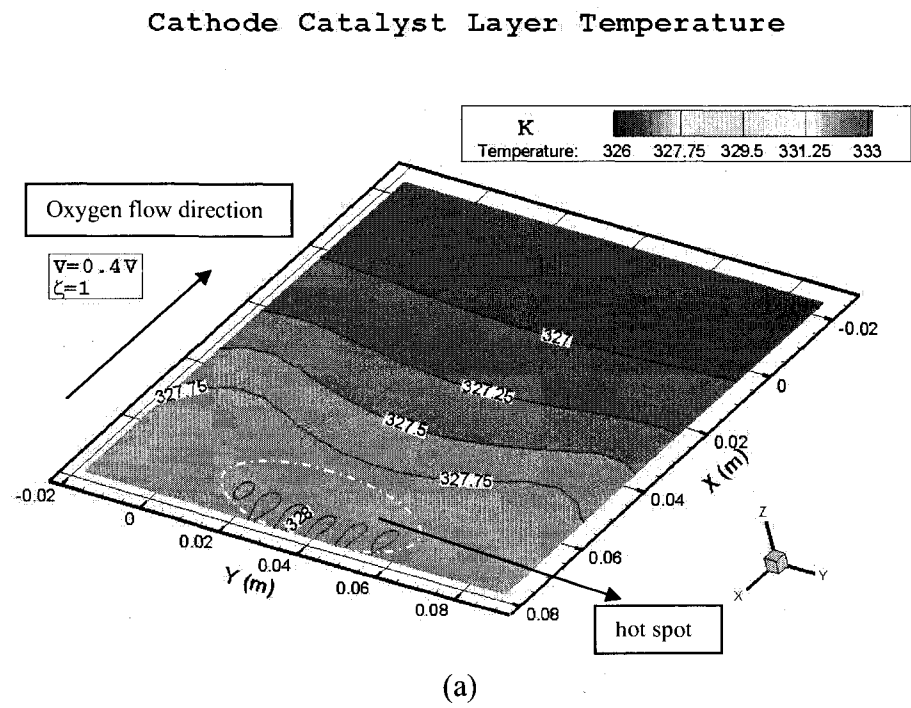
Fig. 3.8 Gas channel temperature

### 3.3.2.3 Catalyst Temperature

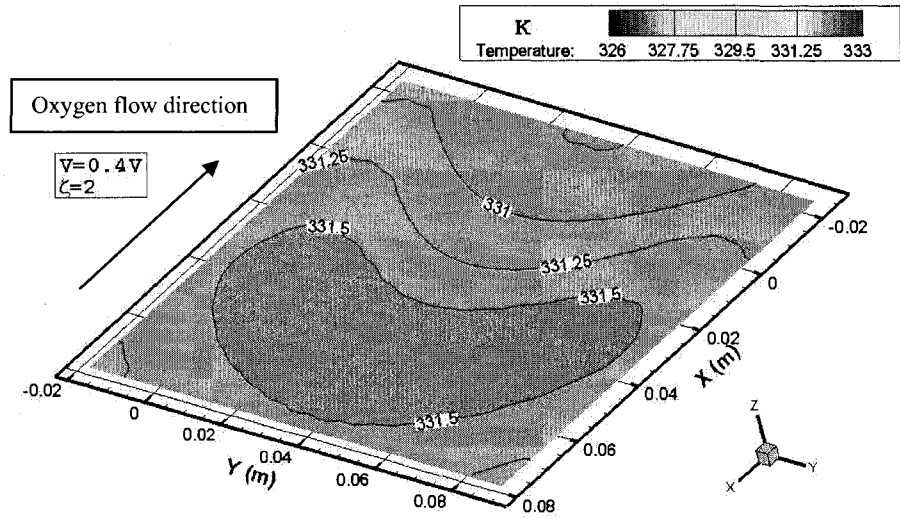
The catalyst temperature is directly related to the electrochemical reaction. At the high current density condition,  $V_{cell} = 0.4V$ , the oxygen demanding is high. When the flow rate  $\zeta = 1$ , high temperature spots appear at the upper stream of the catalyst layer ( $x = 0.07m$ ), which is shown in Fig. 3.9 (a). At the end of the catalyst ( $x = -0.02m$ ), the temperature is uniform along the  $y$ -axis direction, which means the oxygen concentration is at low level in all gas channels. The hot spots pattern at the upper stream is the result of the parallel channel layout design. The temperature difference in catalyst is around 1K. The highest temperature is 328K at the spot region as shown in Fig. 3.9 (a). By increasing the flow rates, the catalyst temperature increases when  $\zeta \leq 3$  and decreases when  $\zeta > 3$ . The relative low temperature appears at the two sides of the catalyst layer ( $y = -0.01 m$

and  $y = 0.08$  m), where the channel velocity is high. This is the effect of “gas flow cooling”. On the other hand, by investigating the water content in the catalyst layer, it is found that the low relative humidity (30%) gas flow can take water vapor out of fuel cell. This “channel flow drying” effect becomes strong when  $\zeta$  is high. The dehydrated membrane leads to the high proton resistance, low current density and heat generation.

Fig. 3.10 shows the catalyst layer temperature at low current density ( $V_{cell} = 0.8V$ ). The temperature only increased 1.5K when  $\zeta = 1$ . The temperature distribution pattern shows that the fuel supply under this operating condition is already sufficient at the point. When  $\zeta$  increases from 1 to 25, the catalyst temperature keeps decreasing. It is only 0.7K above the ambient temperature when  $\zeta = 25$ .

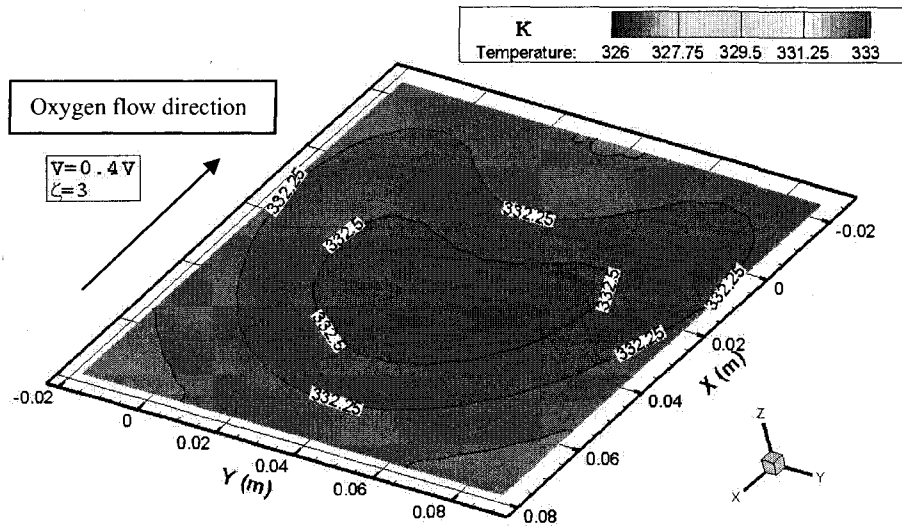


### Cathode Catalyst Layer Temperature



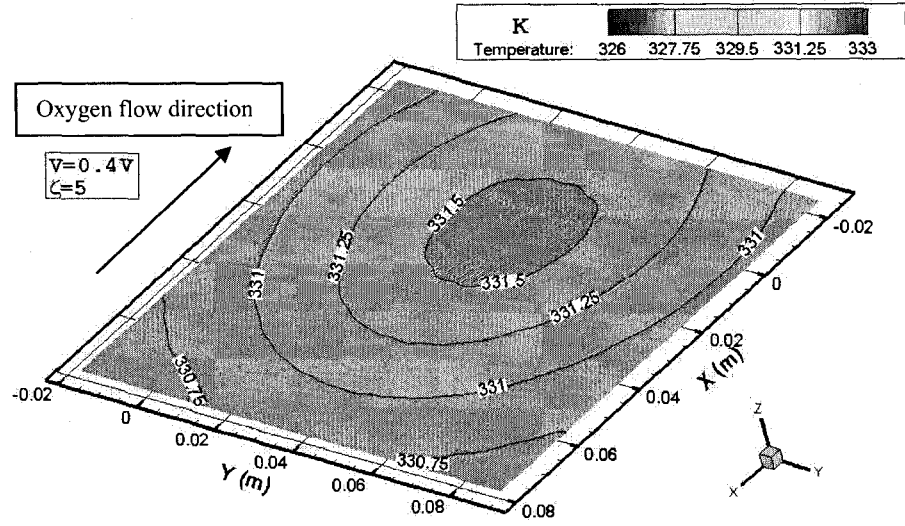
(b)

### Cathode Catalyst Layer Temperature



(c)

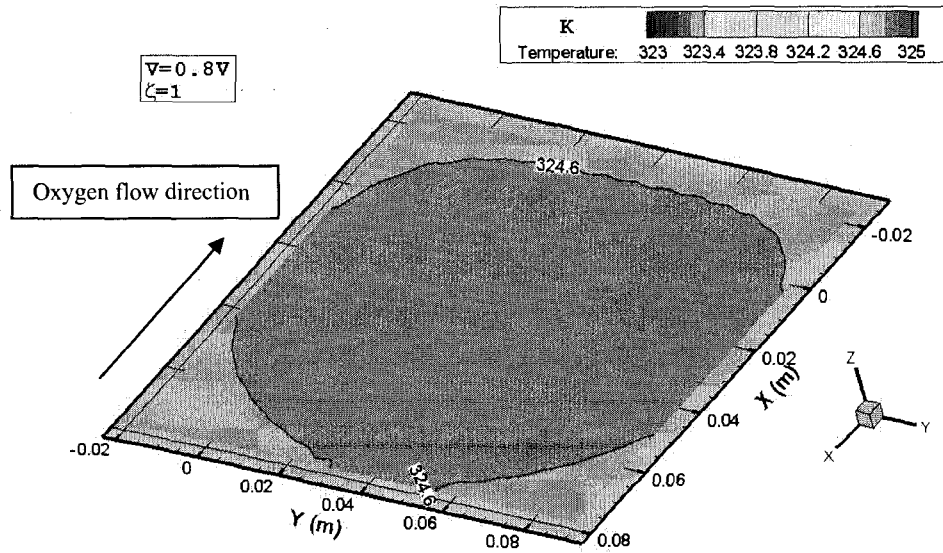
### Cathode Catalyst Layer Temperature



(d)

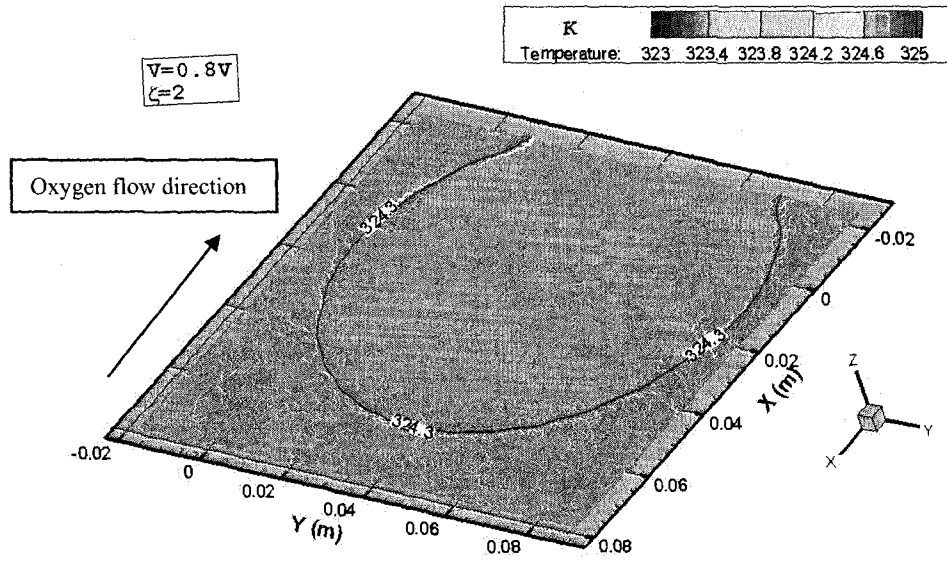
Fig. 3.9 Cathode catalyst layer temperature at 0.4V

### Cathode Catalyst Temperature



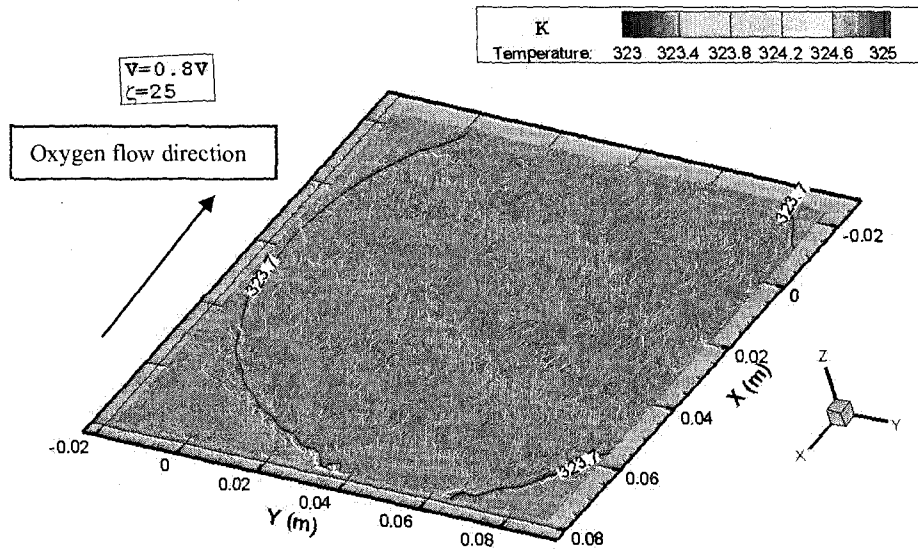
(a)

### Cathode Catalyst Temperature



(b)

### Cathode Catalyst Temperature



(c)

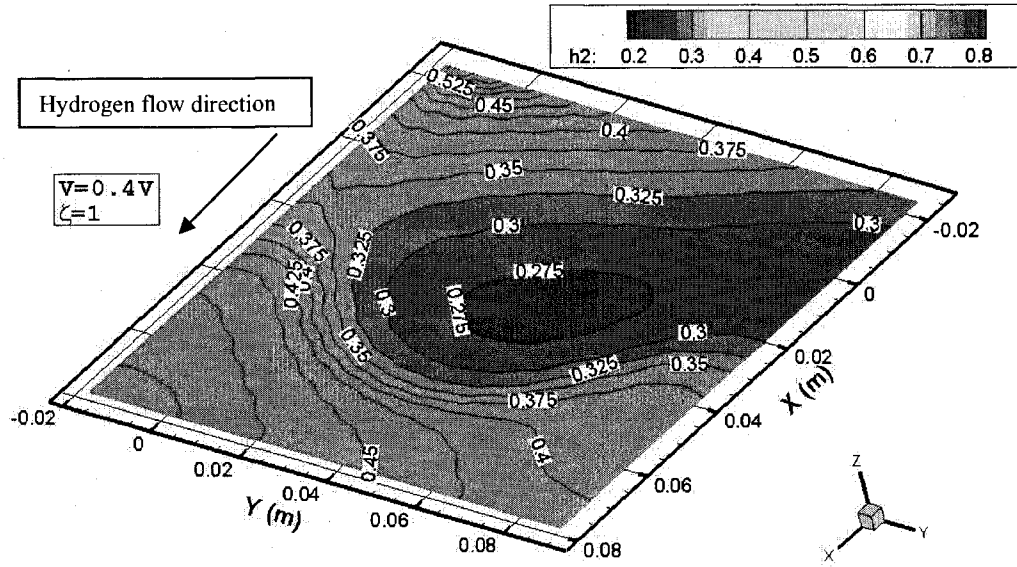
Fig. 3.10 Cathode catalyst temperature at 0.8V

### 3.3.3 Hydrogen Mass Fraction

Hydrogen mass fraction at the anode catalyst layer reflects the hydrogen supply and the relative humidity level. The hydrogen stream flows along the positive X-axis direction from  $x = -0.02\text{m}$  to  $x = 0.08\text{m}$ . Fig. 3.11 shows the hydrogen mass fraction at anode catalyst layer when PEMFC works under high current density  $V_{cell} = 0.4V$ . When  $\zeta = 1$ , the hydrogen mass fraction ranges from 0.275 to 0.525, which indicates that hydrogen supply is not enough. The water, which is produced in cathode catalyst layer, diffuses to the anode catalyst layer under the concentration gradient. The irregular hydrogen mass fraction contour is the result of non-uniform hydrogen supply and water diffusion at the catalyst layers. When the  $\zeta$  increases to 8, the hydrogen mass fraction contour is near elliptic shape, as is shown in Fig. 3.11 (c). High hydrogen mass fraction at lateral region ( $y = 0.08\text{ m}$  and  $y = -0.01\text{m}$ ) reflects the high velocity in lateral channels.

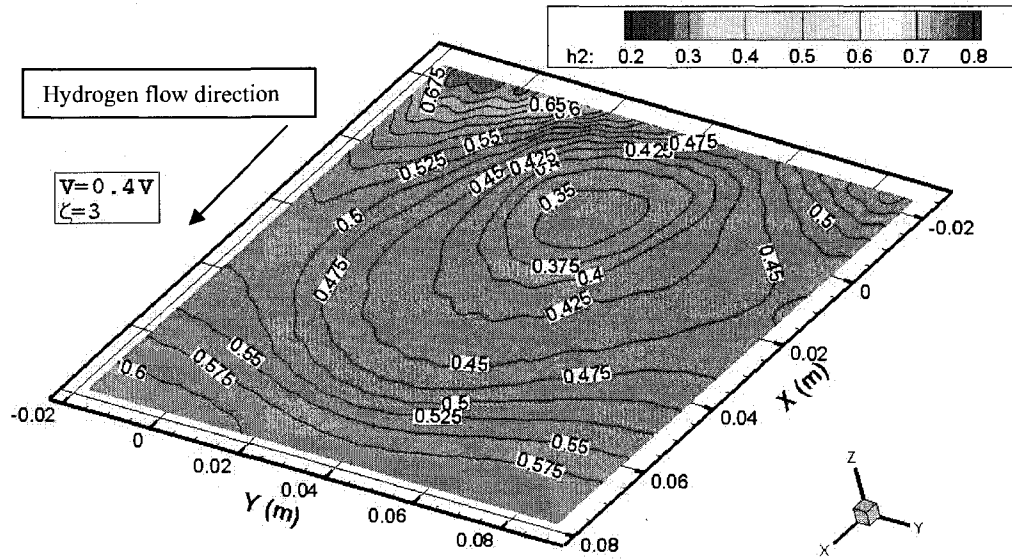
The anode side channel hydrogen mass fraction is shown in Fig. 3.12 (a). As the  $\zeta$  increases from 1 to 25, the hydrogen mass fraction increases to near 0.8. Due to the non-uniform velocity distribution as discussed before, it is reasonable that the hydrogen mass fractions are lower in center channels than as in the lateral channels. However, when  $\zeta$  is less than 3, the hydrogen mass fraction is almost uniformly distributed between those channels. This indicates that when  $\zeta \leq 3$ , the hydrogen supply is not enough under  $V_{cell} = 0.4V$  operating condition. Similar patterns are shown in Fig. 3.12 (b) for fuel cell operating under  $V_{cell} = 0.8V$ . The pattern in Fig. 3.12 (b) indicates that the hydrogen supply is enough when  $\zeta \geq 2$ .

# Anode Catalyst Layer Hydrogen Fraction



(a)

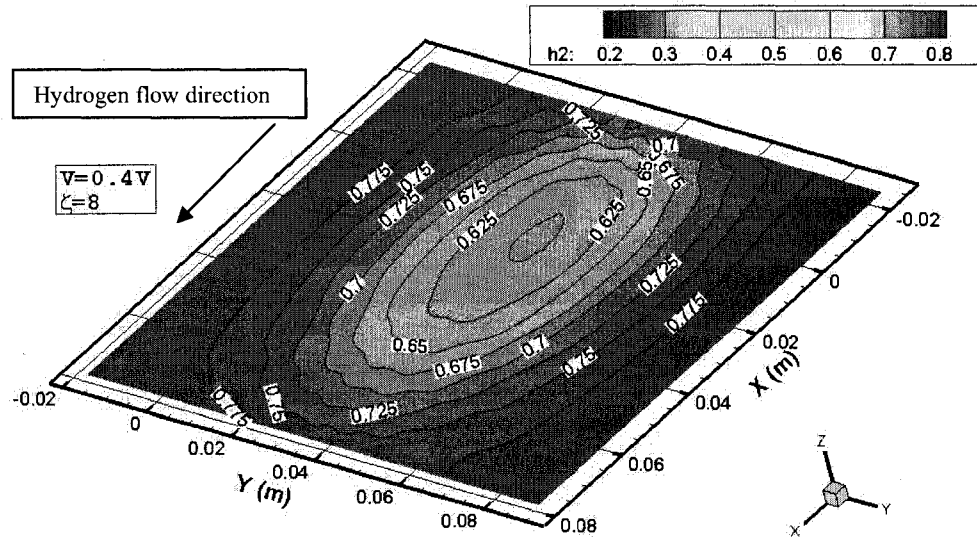
# Anode Catalyst Layer Hydrogen Fraction



(b)

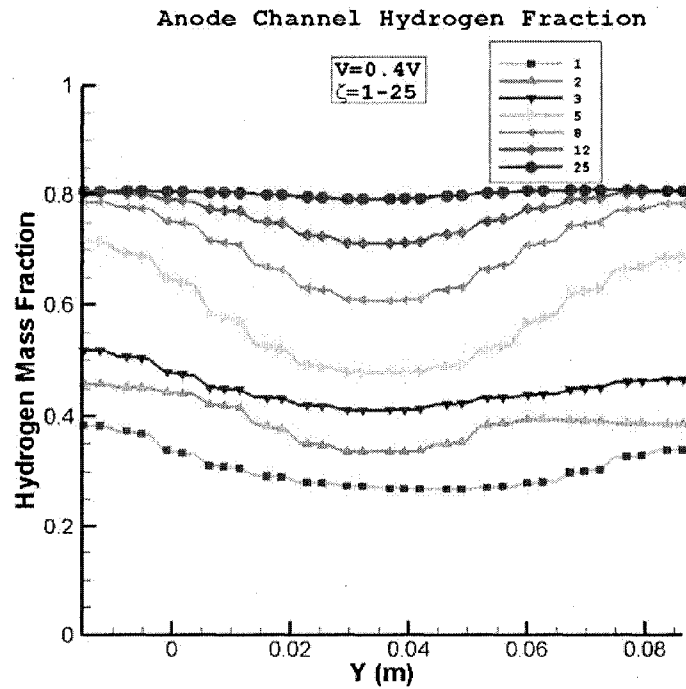


### Anode Catalyst Layer Hydrogen Fraction

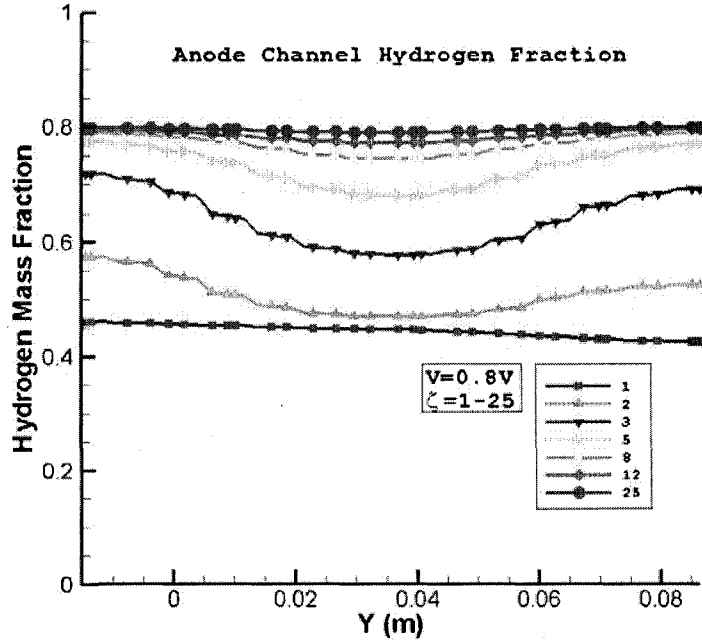


(c)

Fig. 3.11 Anode catalyst hydrogen mass fraction at 0.4V



(a)



(b)

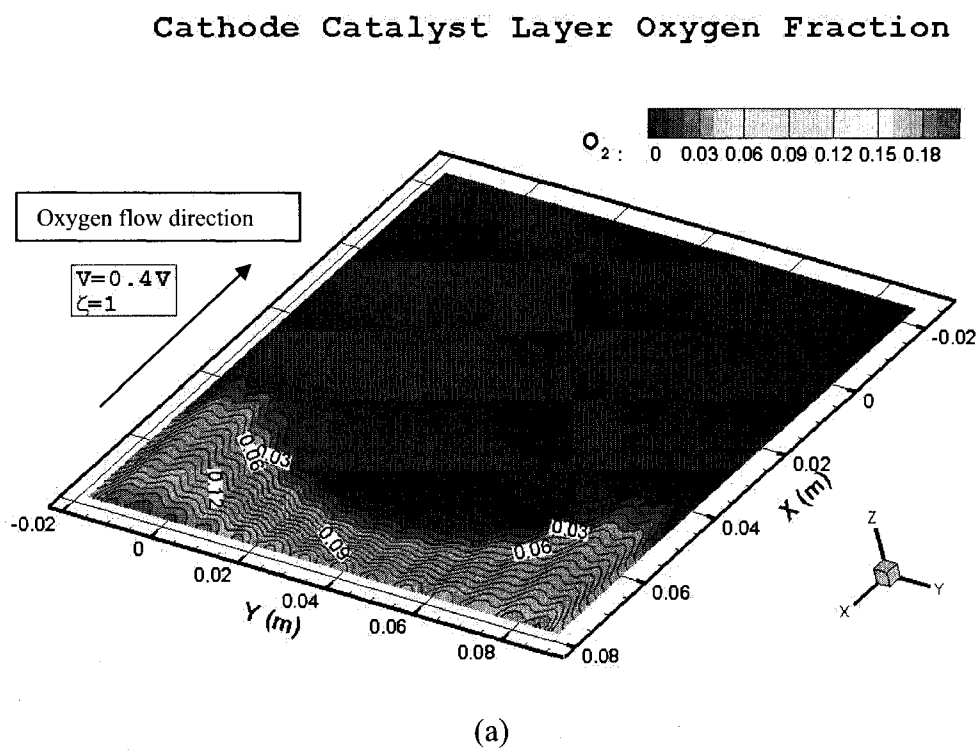
Fig. 3.12 Anode gas channel hydrogen mass fraction

### 3.3.4 Oxygen Mass Fraction

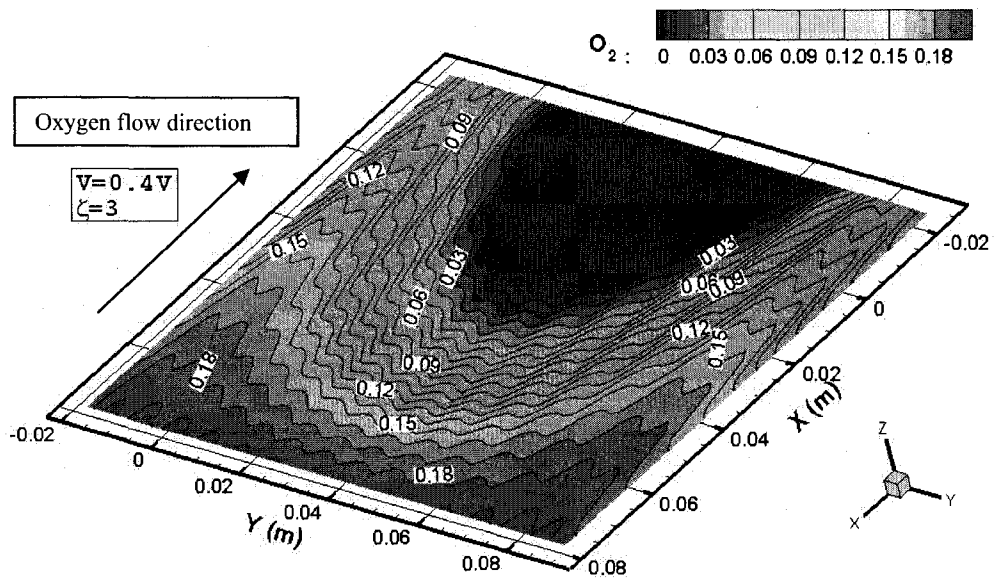
The oxygen mass fraction at cathode catalyst layer directly influences the electrochemical reaction rate. Fig. 3.13 shows the oxygen mass fraction in cathode catalyst layer operating under  $V_{cell} = 0.4V$ . The inlet oxygen mass fraction is 0.2. As discussed above, the oxygen supply is not enough when  $\zeta$  is less than 3. Under  $\zeta=1$ , oxygen mass fraction drops from 0.2 to 0.03 sharply at the upper stream area. After  $\zeta$  increases from 1 to 3, as is shown in Fig. 3.13 (b), the oxygen mass fraction at two sides increases more than the center area. This is the result of the non-uniform velocity distribution.

Fig. 3.14 shows the oxygen mass fraction in the cathode side channels, under two operating conditions  $V_{cell} = 0.4V$  and  $V_{cell} = 0.8V$ . It is similar to the hydrogen mass

fraction in anode channels. The oxygen fraction is low in the center channels and high in the lateral channels. The desired  $\zeta$  values range from 3 to 8 for  $V_{cell} = 0.4V$  and from 1 to 3 for  $V_{cell} = 0.8V$  because in these ranges the oxygen supply and consumption is almost in the equilibrium state.

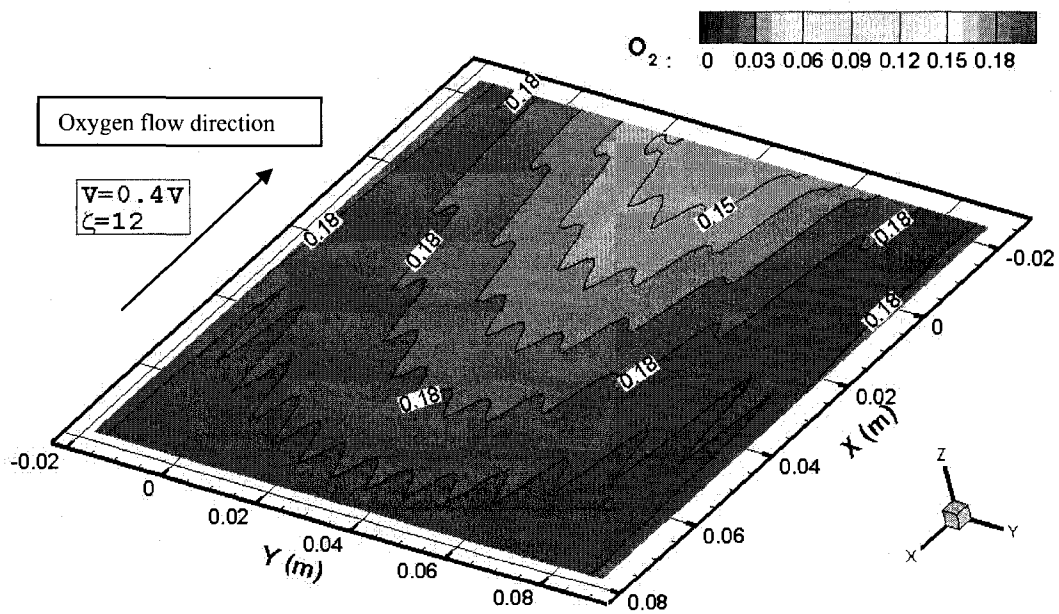


### Cathode Catalyst Layer Oxygen Fraction



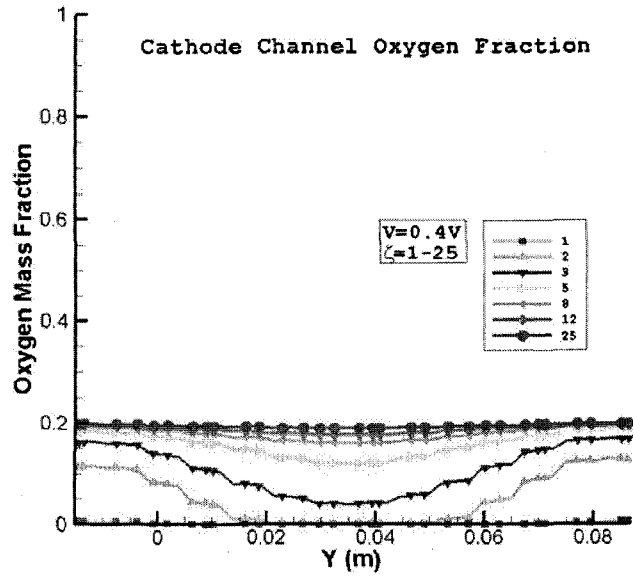
(b)

### Cathode Catalyst Layer Oxygen Fraction

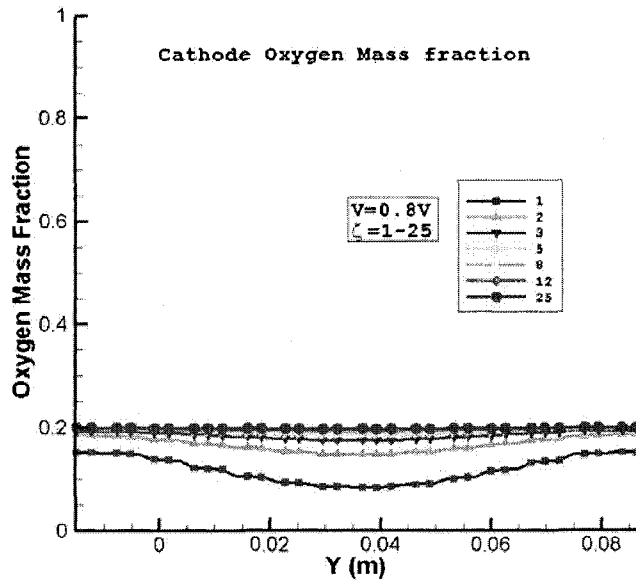


(c)

Fig. 3.13 Cathode oxygen mass fraction at 0.4V



(a)



(b)

Fig. 3.14 Cathode gas channel oxygen mass fraction

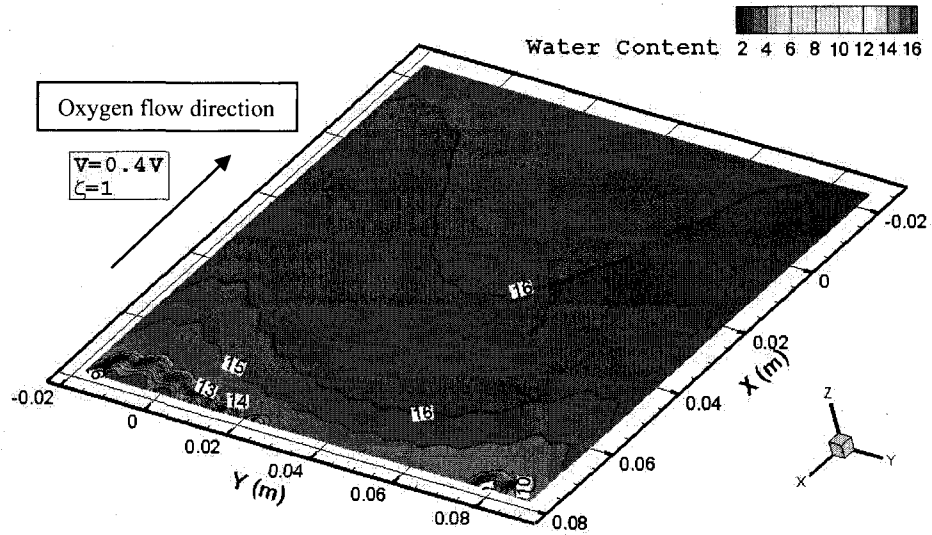
### 3.3.5 Water Content

In PEMFCs, the water content is very important. The membrane needs to be hydrated in order to get the high protonic conductivity. Fig. 3.15 illustrates the catalyst water content when fuel cell operated under  $V_{cell} = 0.4V$ . By comparing Fig. 3.15 (a), (b) and (c), it is found that the high flow rate can dehydrate the catalyst layer. In other words, the water content decreases as flow rate increases. As discussed above, the electrochemical reaction rate cannot keep increasing by increasing the inlet flow rate due to the operating conditions and the mass transport limitation. The water production is limited under each operating conditions. The high flow rate in channels will then lead to the low relative humidity. This will create a large water concentration gradient between the catalyst layers and gas channels. Extremely high flow rate will cause the high resistance of MEA with low water content and low current density even with high fuel and oxygen supply. This can significantly lower the fuel cell performance.

Fig. 3.16 shows the water mass fraction in the cathode gas channels. As discussed above, the high velocity comes with the low relative humidity. It is found in Fig. 3.16 that the center channels have the higher water content than the lateral channels. This reflects the non-uniform velocity distribution in cathode gas channels. The “gas channel drying” effect becomes strong when  $\zeta$  reaches 8. This “gas channel drying” effect is observed by investigating the gas mixture relative humidity at the inlet and outlet which is shown in Table 3.1. The inlet relative humidity is 32.5% for the anode gas mixture and 22.5% for the cathode air. When  $\zeta = 1$  the water is produced at the cathode catalyst layer then it is evaporated and transported to the gas channels. The relative humidity increases to 277%

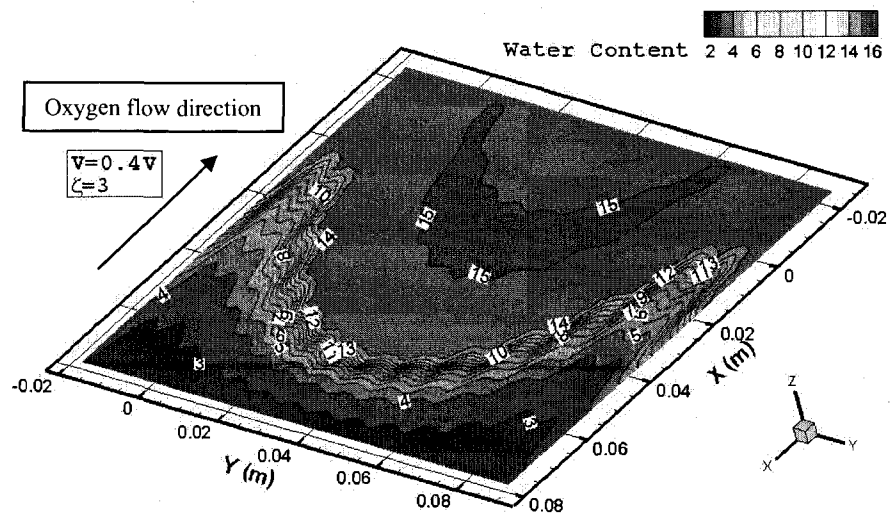
for anode side outlet and 61.6% for cathode side. When  $\zeta$  further increases to 25, the relative humidity decreases to the value which is near the inlet relative humidity.

### Cathode Catalyst Layer Water Fraction



(a)

### Cathode Catalyst Layer Water Fraction



(b)

### Cathode Catalyst Layer Water Fraction

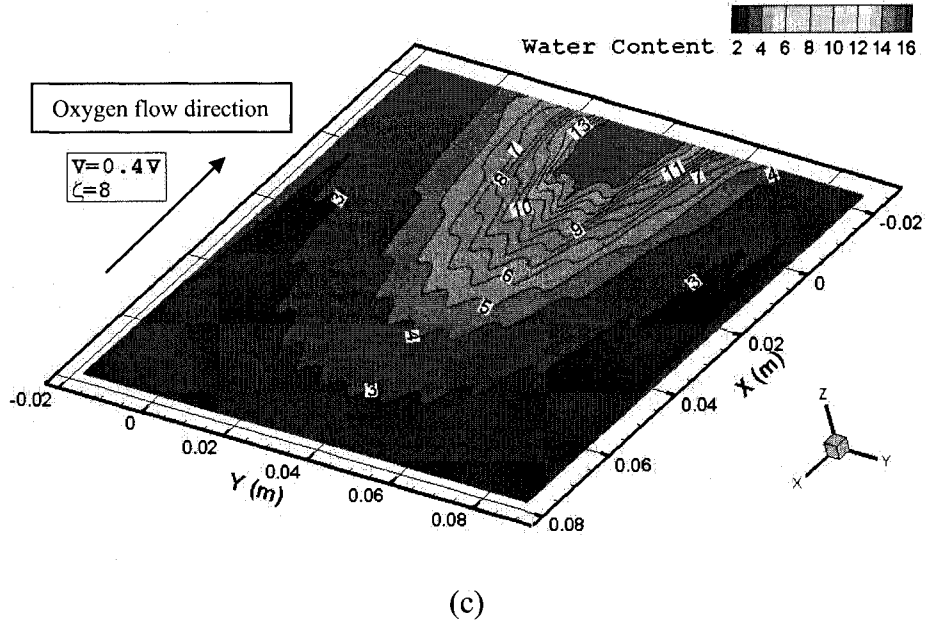


Fig. 3.15 Cathode catalyst water at 0.4V

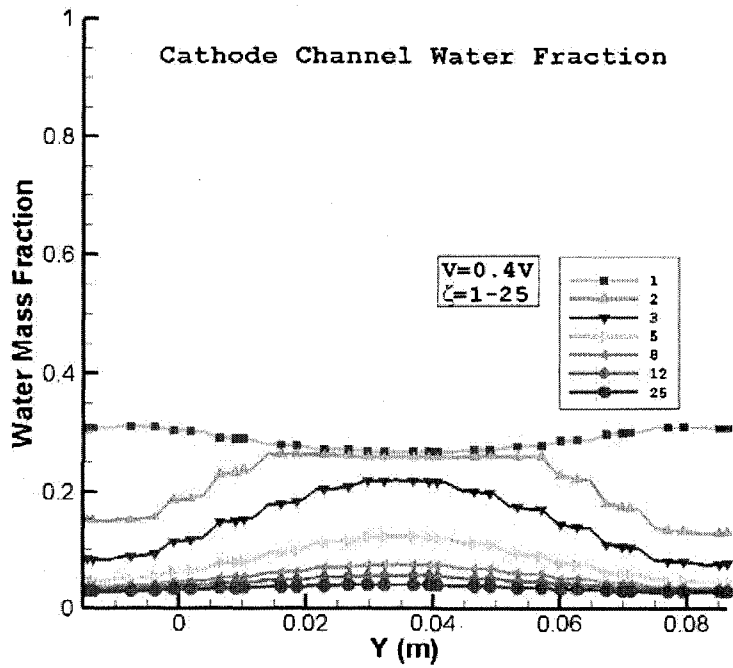


Fig. 3.16 Cathode gas channel water mass fraction at 0.4V



Table 3.1 Inlet and outlet humidity at anode/cathode gas mixtures

$\zeta$		Inlet	Outlet
1	cathode	32.5%	277.2%
	anode	22.5%	61.6%
5	cathode	32.5%	164.9%
	anode	22.5%	35.01%
25	cathode	32.5%	35.49%
	anode	22.5%	23.3%

### 3.3.6 Current Density

The current density of PEMFC reflects the fuel cell performance and how much power it provides to the outside circuit. A parametric study is performed by varying the inlet flow rates to find its effect on current density at both low ( $V_{cell} = 0.4V$ ) and high ( $V_{cell} = 0.8V$ ) cell voltage operating conditions.

Fig. 3.17 shows the relation between the flow rate and normalized fuel cell current density. Under  $V_{cell} = 0.4V$ , the current density will increase significantly with increasing flow rate. However, further increasing of flow rate leads to the current density decreasing. Because when  $\zeta$  is larger than 5, the “gas channel drying” effect becomes significant, which downgrades the membrane and causes the high proton resistance. The fuel demanding is low under high cell voltage operating condition ( $V_{cell} = 0.8V$ ), so that the increasing flow rate only brings the poor performance.

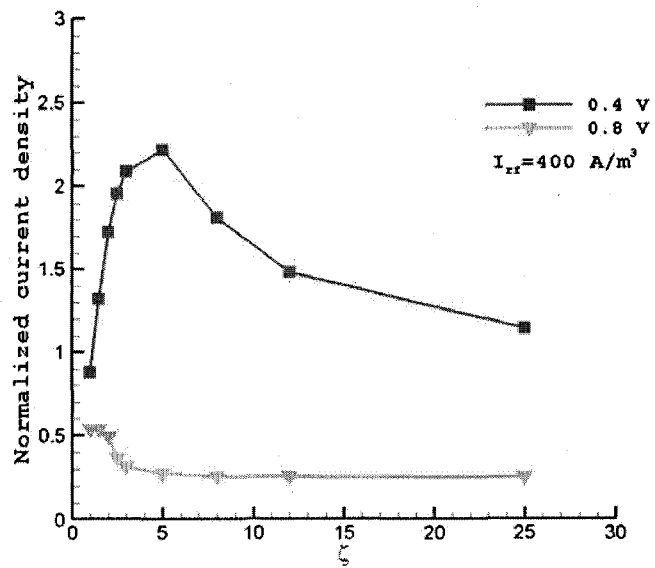


Fig. 3.17 Current density flow rate curves at 0.4V and 0.8V

## CHAPTER 4

### AN IMPROVED DESIGN OF PEMFC

In this chapter, an improved design is presented. The three-dimensional PEMFC simulation is performed. From the results of the velocity, temperature and current density distribution, it is found that the fuel cell performance has been improved significantly compared to the baseline design. The parametric study of the flow rate is also performed to study the effects of channel flow rate to the temperature, water content and current density.

#### 4.1 Design Description

The new design of PEMFC is similar to the baseline design with the same size active electrochemical area. The difference is that the new design has the improved bipolar plate design with four inlets instead of one inlet in baseline design. This design aims to improve the channel flow distribution. The schematic view of the bipolar plate is shown in Fig. 4.1. The dimensions of drawing are in inches. The inlet diameter is 0.5 in and they are separated from each other with 0.5 in distance. The header area contains the 0.2 in diameter cylinders instead of the cubes found in the baseline design. In the channel region, the channel width, height and rim width are applied as the same as in the baseline design. The MEA dimensions including the thickness are all the same. With the newly

designed header area and four inlets, the new bipolar plate is a little longer than the baseline one, which dimensions are 8 in long and 5 in wide. Fig. 4.2 shows the 3-D configuration of the new design, which includes the anode channel fluid, MEA and cathode bipolar plate from the top to the bottom.

The three-dimensional computation meshes are generated in Hypermesh® by tetrahedral meshes with 2,311,626 cells and 1,265,365 nodes. The meshes of anode channel fluid, MEA and cathode bipolar plate are shown in Fig. 4.3. The boundary conditions for the hydrodynamic, heat transfer and electrochemical simulation are the same as the baseline design.

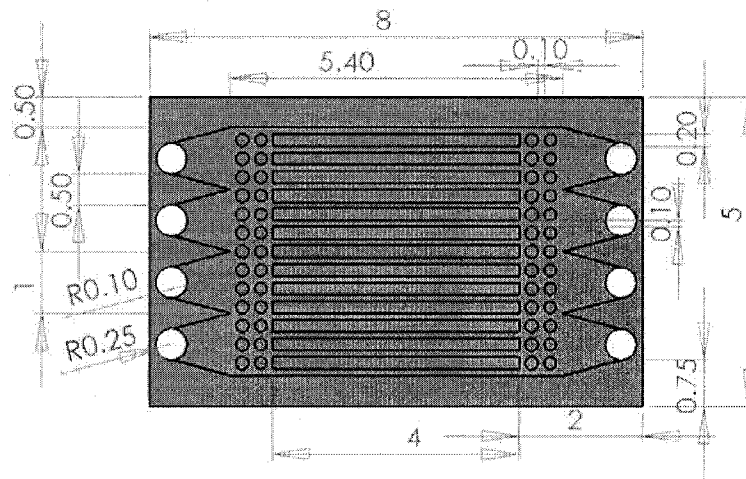


Fig. 4.1 Schematic view of bipolar plate design

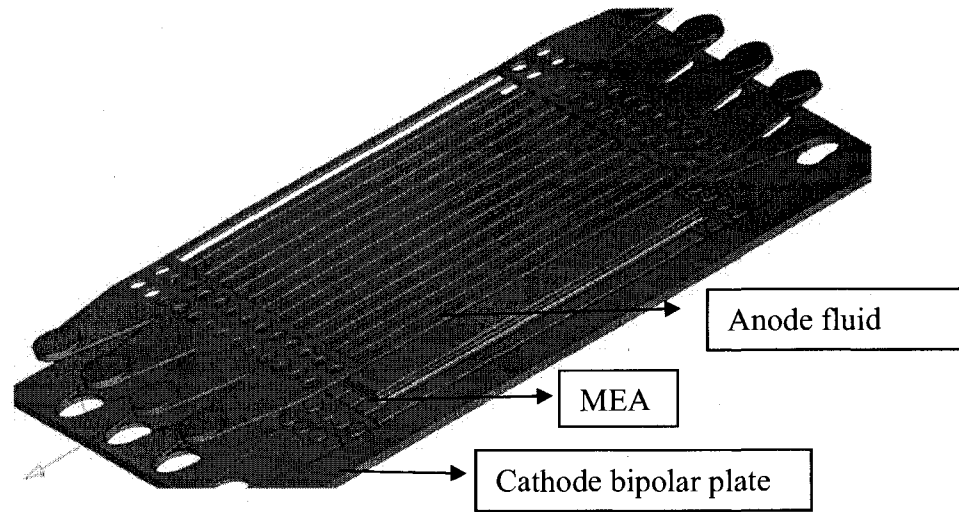


Fig. 4.2 Improved design of PEMFC

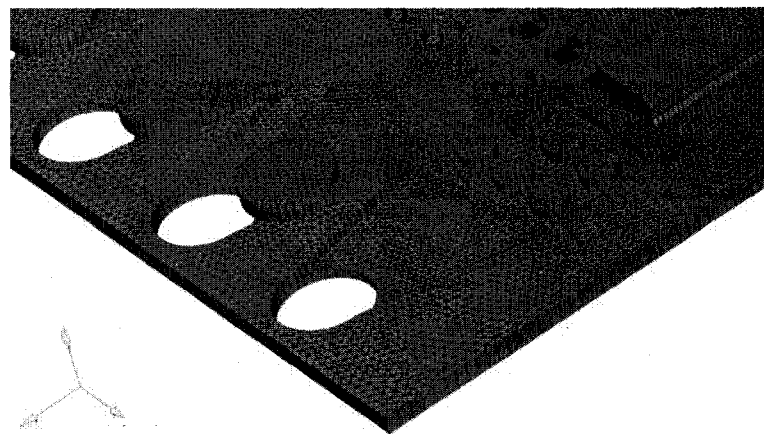


Fig. 4.3 Computational mesh-part view

## 4.2 Results and Discussion

### 4.2.1 Velocity Distributions

Fig. 4.4 shows the velocity distribution of the anode side at the middle length of the channel where the velocity profile is already fully developed. The velocity distribution between channels is much better than the base design result, as shown in Fig. 3.5. It gives an almost uniform velocity distribution in each channel. When the inlet flow rate

increases, the velocity in these channels will increase in the same ratio and the same amount. This uniform velocity distribution is true for the investigated flow rate range. Due to the non-symmetric header area design, the velocity in lateral channels is slightly lower than the middle ones. This kind of velocity distribution is favorable to the fuel cell performance because the flow rate adjustment will not bring extremely high velocity in the lateral channels. A uniform-velocity distribution can provide a better adjustment of fuel supply which will lead to the fuel cell's high efficiency. On the other hand, it also brings the uniform temperature distribution, uniform electrochemical reaction rate in catalyst layers and efficient usage of expensive catalyst.

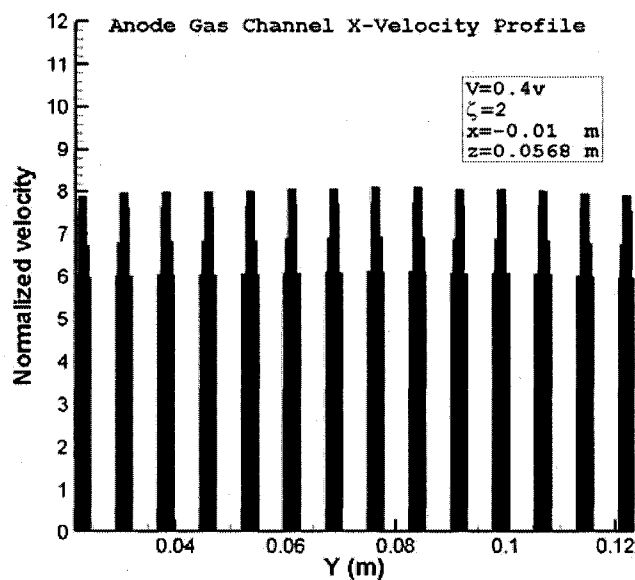


Fig. 4.4 Velocity distribution between channels

#### 4.2.2 Temperature distributions

Temperature distributions in the bipolar plate, gas channel and catalyst are also investigated. The temperature difference within single bipolar plate is less than 1.5K. The

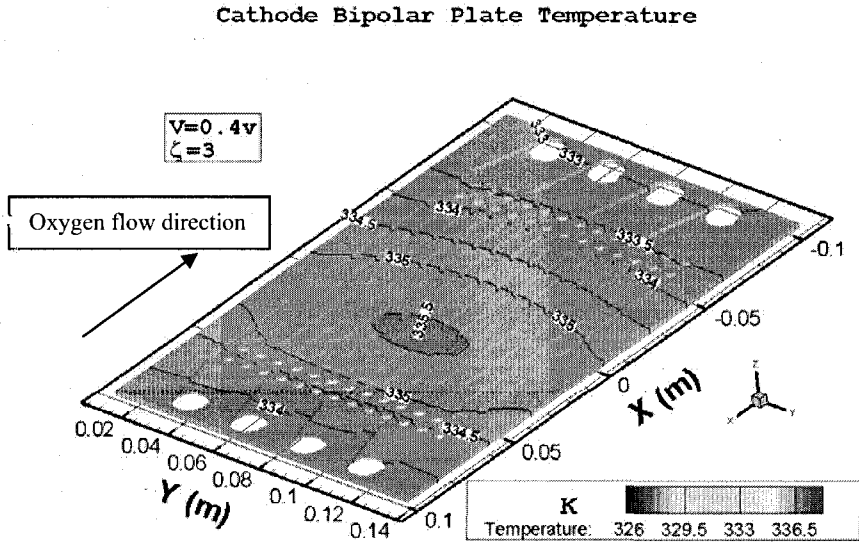
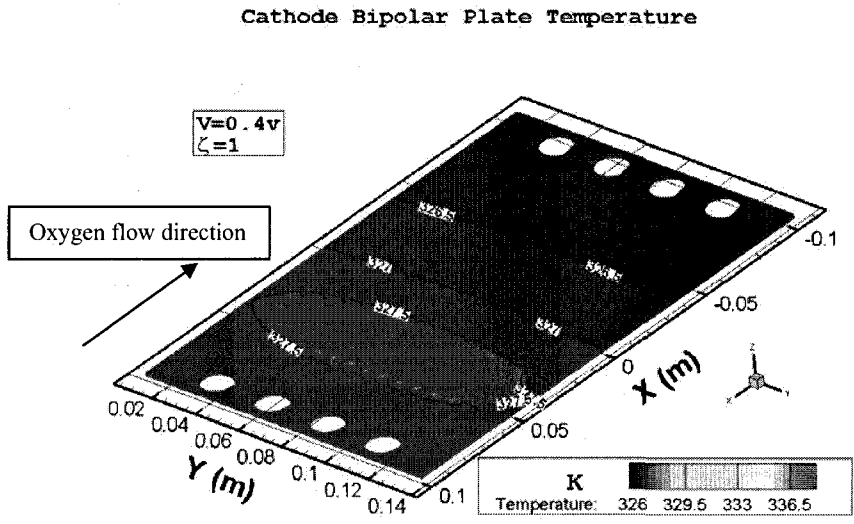
temperature varies along the  $x$ -axis and the temperature difference is small along the  $y$ -axis. The high temperature appears at the oxygen inlet side when flow rate is small. While flow rate increases, the high temperature area moves to the MEA center part. The “gas channel cooling” still exists in this new design. However its impact on the fuel cell performance is not as significant as on the baseline design.

#### 4.2.2.1 Bipolar Plate

The bipolar plate temperature is examined. At the high current density situation ( $V_{cell} = 0.4V$ ), the temperature of bipolar plate is 4.5K higher than the ambient temperature when the  $\zeta = 1$ , as is shown in Fig. 4.5 (a). Similar to the baseline design, the increased flow rate leads to a higher bipolar plate temperature while further increasing will decrease its temperature. After the  $\zeta$  increases to 5, the average temperature of bipolar plate is around 7K higher than the baseline design case which means the new design use the fuel more efficiently under the same flow rate value  $\zeta$ . The high temperature area moves from the upper stream to the channel center when  $\zeta$  is 5 which is shown in Fig. 4.5 (a) to (d). When  $\zeta = 1$ , the oxygen supply is not enough, so that a high electrochemical reaction rate happens at the upper stream area where the oxygen concentration is high. After flow rate increases, the “gas flow cooling” effect becomes significant. The temperature at two sides ( $y=0.02m$ ,  $y=0.12m$ ) are lower than as at the channel center.

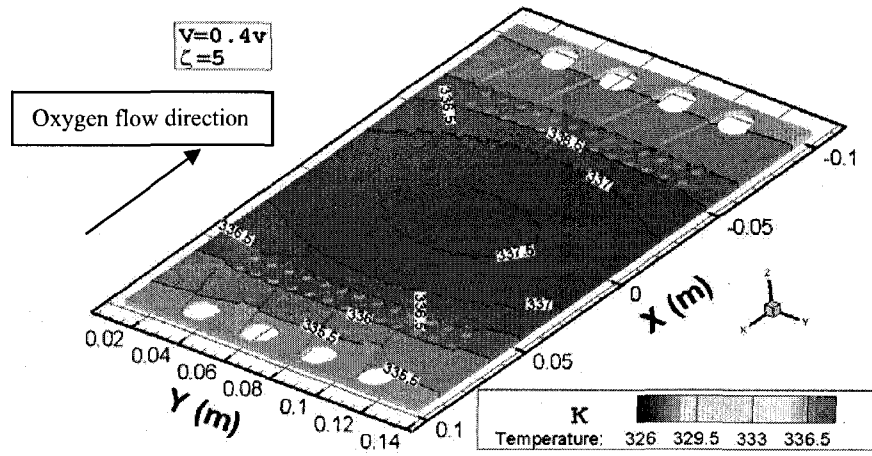
Fig. 4.6 shows the anode bipolar plate temperature under the low current density condition ( $V_{cell} = 0.8V$ ). Similarly to the high current density condition, temperature increases with increasing  $\zeta$ . When  $\zeta = 5$ , the temperature is 1.2K higher than the baseline design case. The temperature at the center( $y=0.08$ ) is slightly higher than that at two side

sides( $y=0.02, y=0.12$ ). This is not caused by the “gas flow cooling” effect because the velocity distribution is uniform. The MEA is smaller than the bipolar plate so that there is no heat source at the two sides ( $y=0.02, y=0.12$ ). However, the heat is still transferred to the ambient air by convection. That is the reason why the temperature at two sides is lower than the temperature at center area.



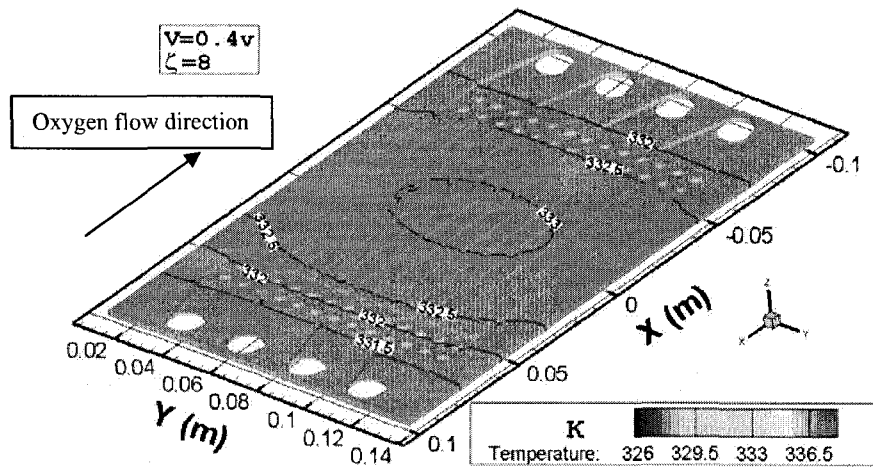


Cathode Bipolar Plate Temperature



(c)

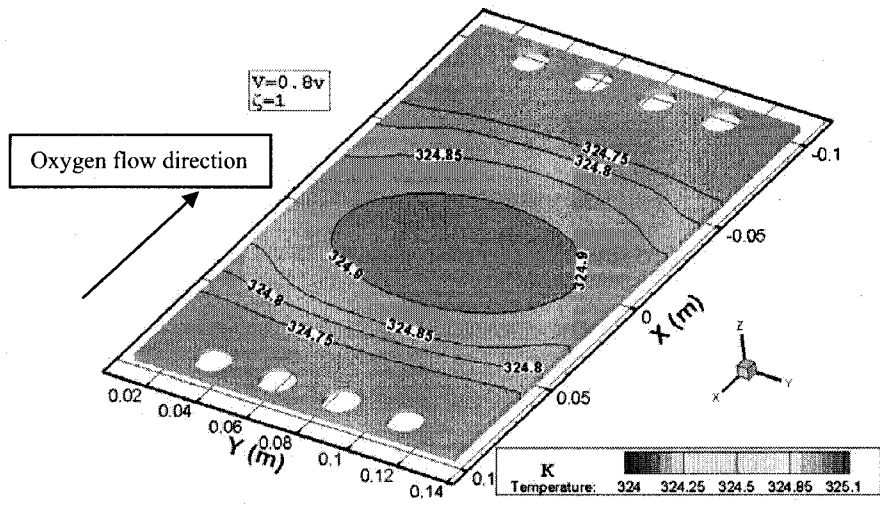
Cathode Bipolar Plate Temperature



(d)

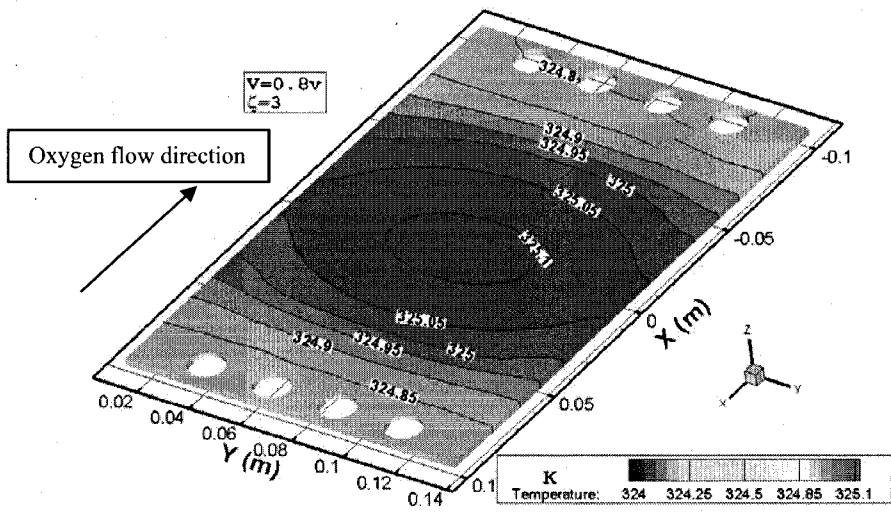
Fig. 4.5 Cathode bipolar plate temperature at 0.4V

### Anode Bipolar Plate Temperature



(a)

### Anode Bipolar Plate Temperature



(b)

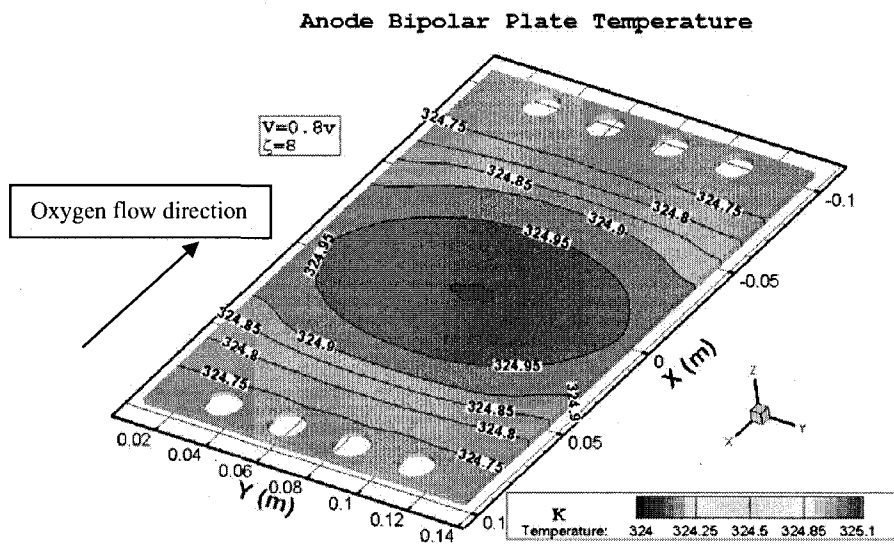
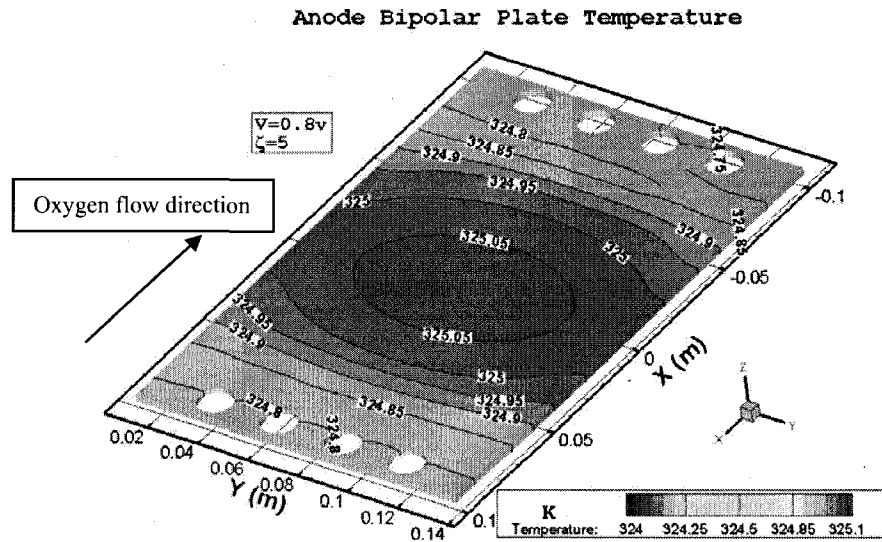
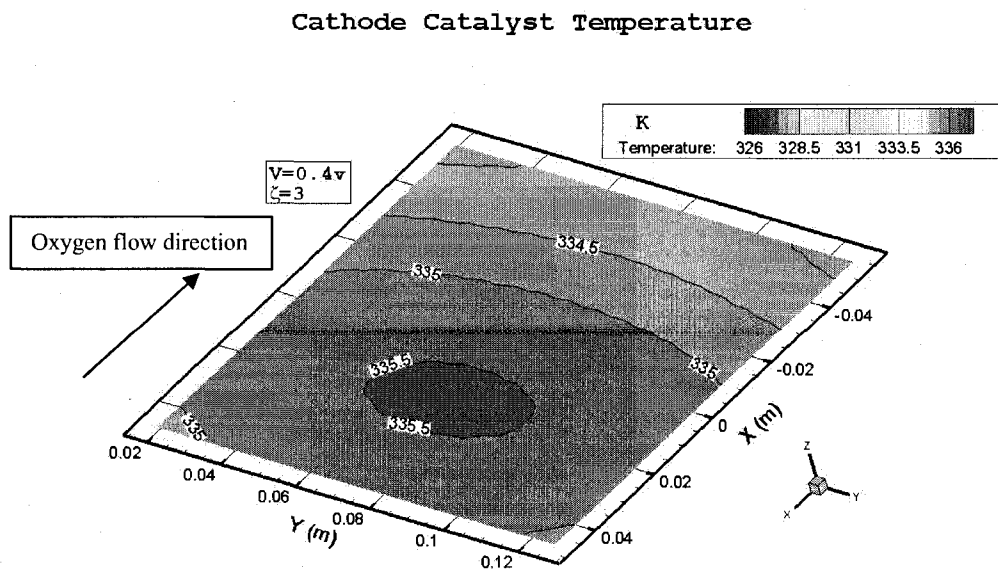
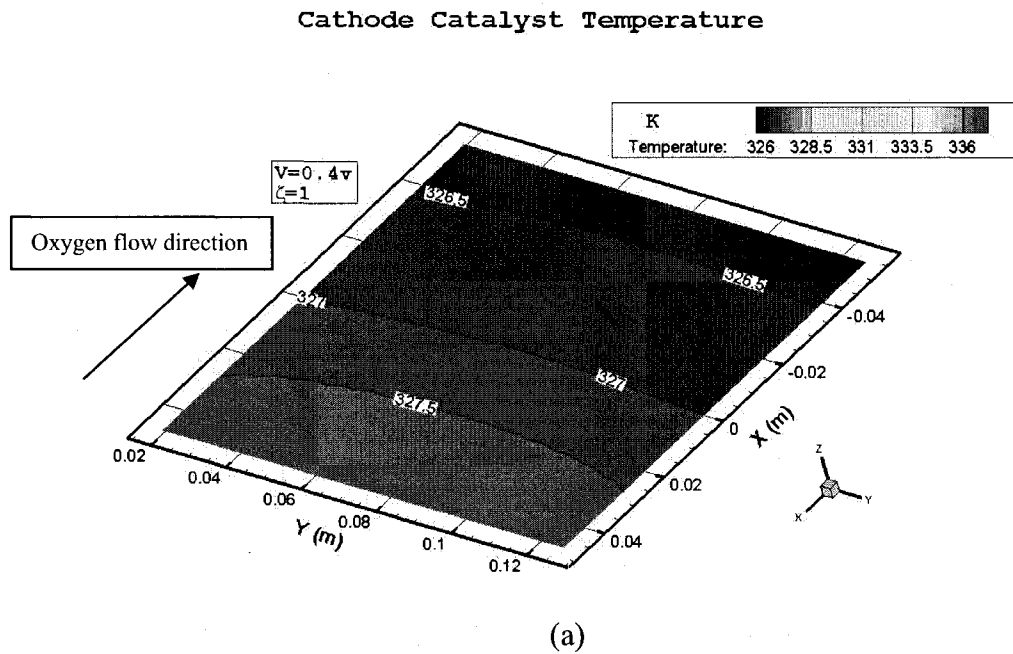


Fig. 4.6 Anode bipolar plate temperature at 0.8V

#### 4.2.2.2 Catalyst Temperature

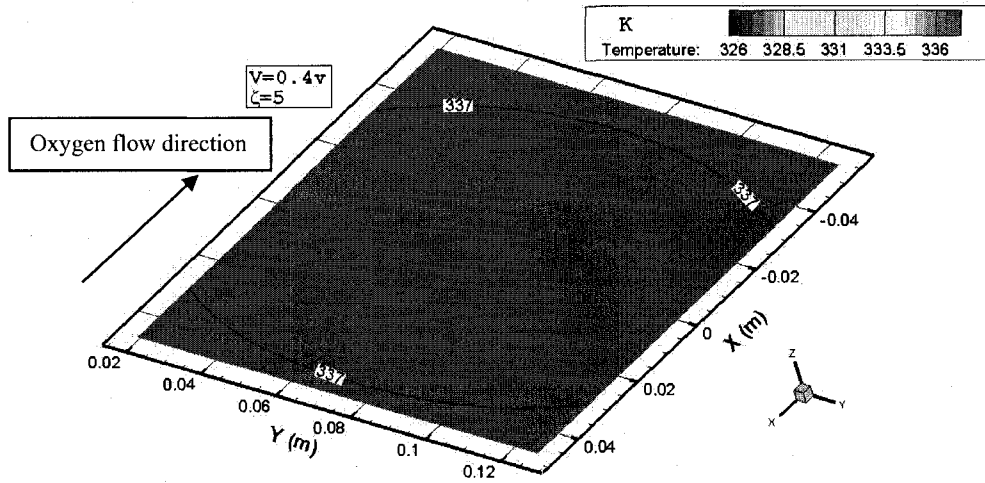
The temperature distribution in the catalyst layer is almost uniform while a big temperature difference appears at the baseline design along the  $y$ -axis which is shown in Fig. 3.9 (a) and Fig. 4.7 (a). Generally, the catalyst temperature at the new design case is

2 to 3 K higher than the baseline case. For the high flow rate, the temperature variation within the catalyst layer in the new design case as shown in Fig. 4.7 (c) is even smaller than in the baseline design case as illustrated in Fig. 3.9 (d). When it is under the low current density condition ( $V_{cell} = 0.8V$ ), the “gas flow cooling” effect becomes weak. Fig. 4.8 shows that the temperature has only slight decrease when flow rate increases.



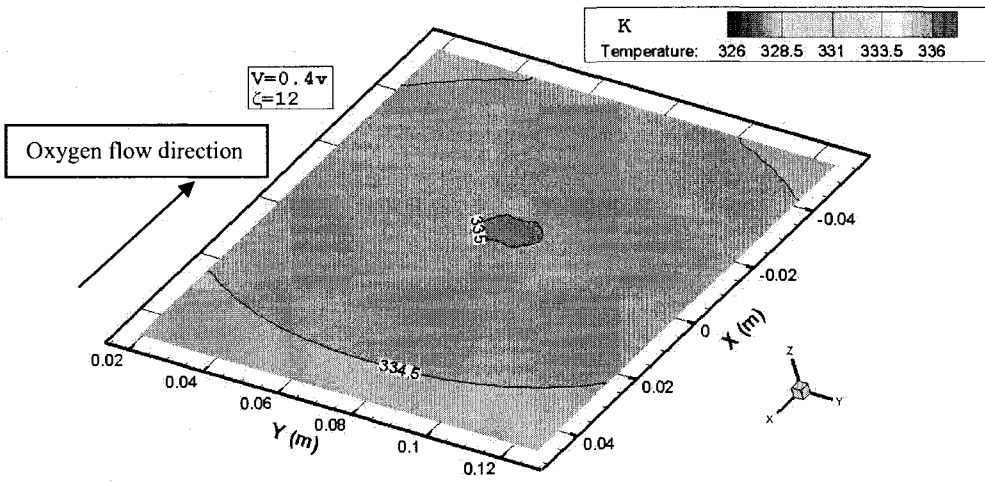
(b)

Cathode Catalyst Temperature



(c)

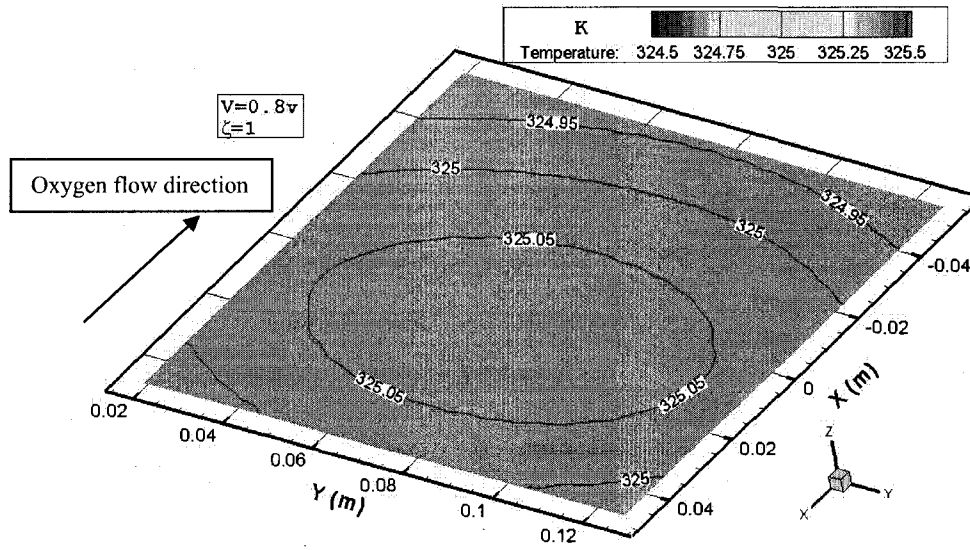
Cathode Catalyst Temperature



(d)

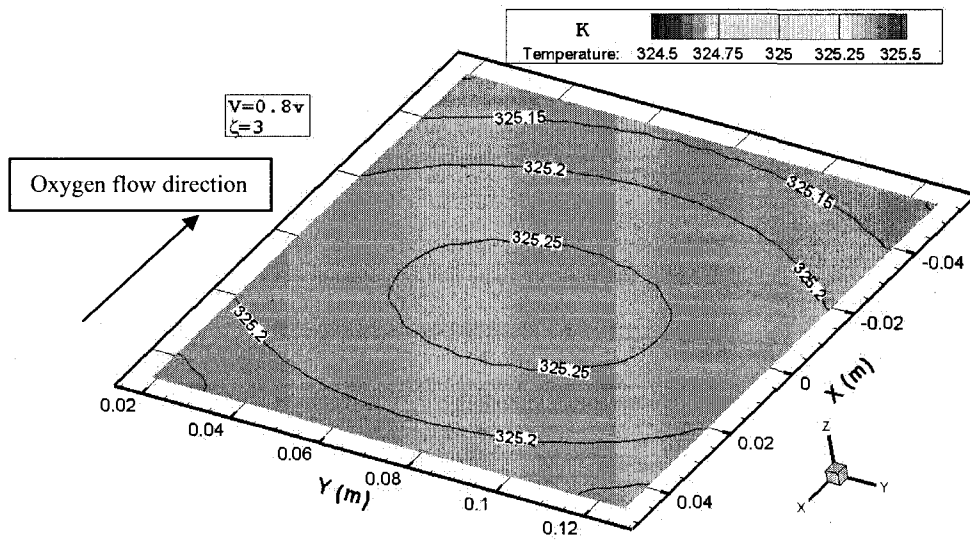
Fig. 4.7 Cathode catalyst temperature at 0.4V

### Cathode Catalyst Temperature



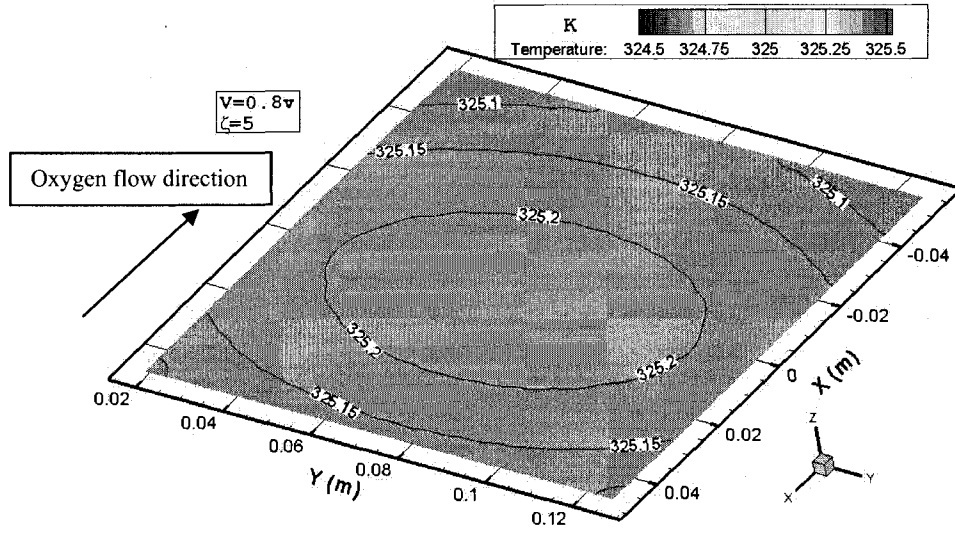
(a)

### Cathode Catalyst Temperature



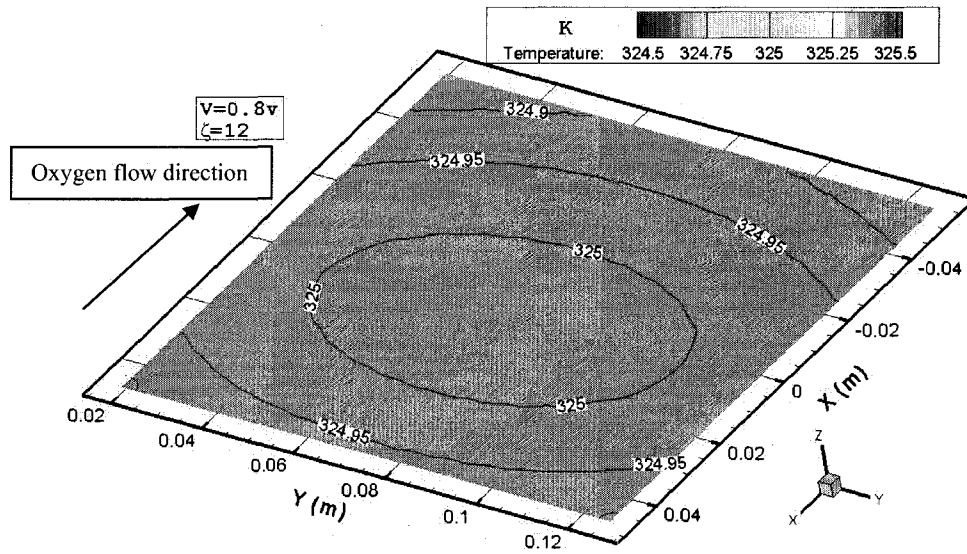
(b)

### Cathode Catalyst Temperature



(c)

### Cathode Catalyst Temperature

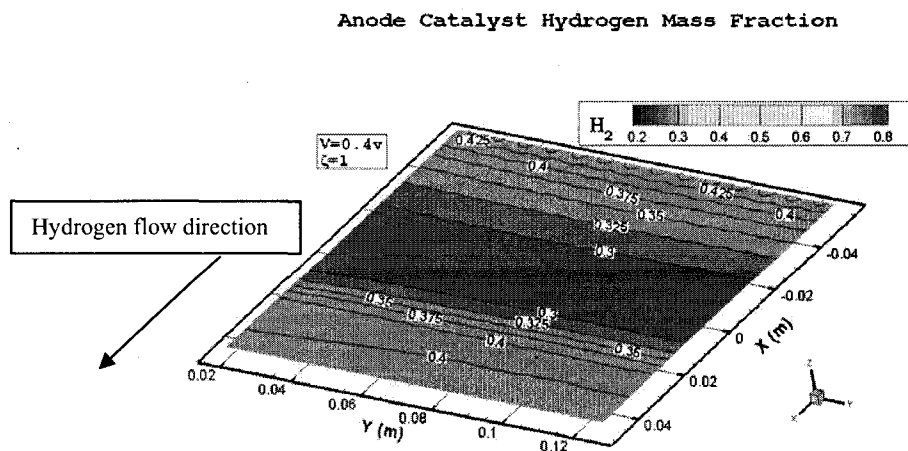


(d)

Fig. 4.8 Cathode catalyst temperature at 0.8V

### 4.2.3 Hydrogen Mass Fraction

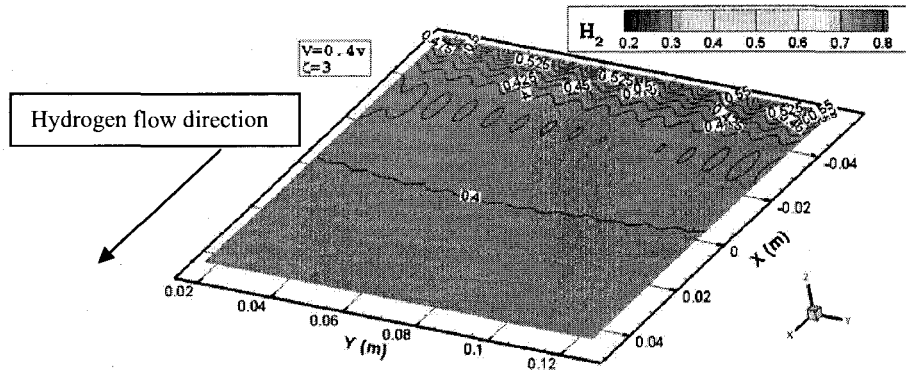
From Fig. 3.11(a) and Fig. 4.9 (a), it can be seen that the hydrogen mass fraction distribution is uniform along the y-axis direction, which is better than the complicated distribution shown in the baseline design case. The contour line has the wave-like shape which is the effect of the channel and rim configuration. The mass fraction is relatively large under the channels while it is small under the rims. It is noticed that the hydrogen mass fraction decreases and then increases along the gas flow direction (positive X) at  $\zeta=1$ . And it keeps decreasing along flow direction at  $\zeta=8$ . From Fig. 4.10, the water content level changes with flow rate in the catalyst layer. The water content is high at the upper stream and center area ( $x=-0.04\text{m}$  and  $x=0\text{m}$ ) for  $\zeta=1$ . This causes the low mass fraction of hydrogen at upper stream and center area. As  $\zeta=8$ , the “gas flow drying” effect strongly removes the water from catalyst layer into the gas channels. The water content of catalyst layer becomes low and its effect on the hydrogen mass fraction decreases. Generally, the hydrogen distribution in the new design is better than the complicated distribution in the baseline design.



(a)

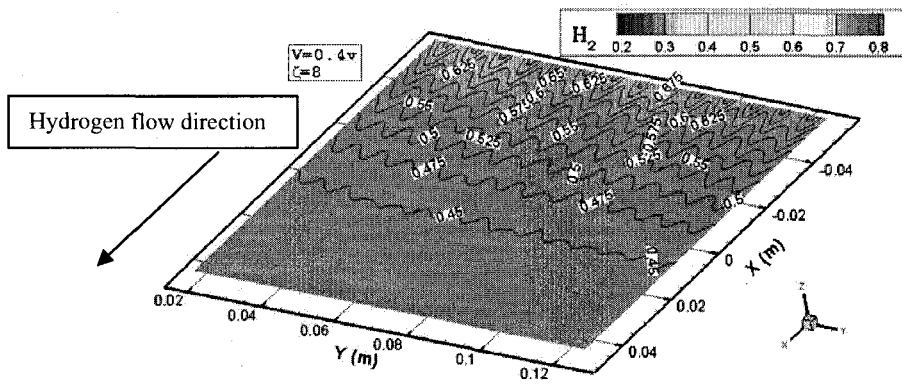


Anode Catalyst Hydrogen Mass Fraction



(b)

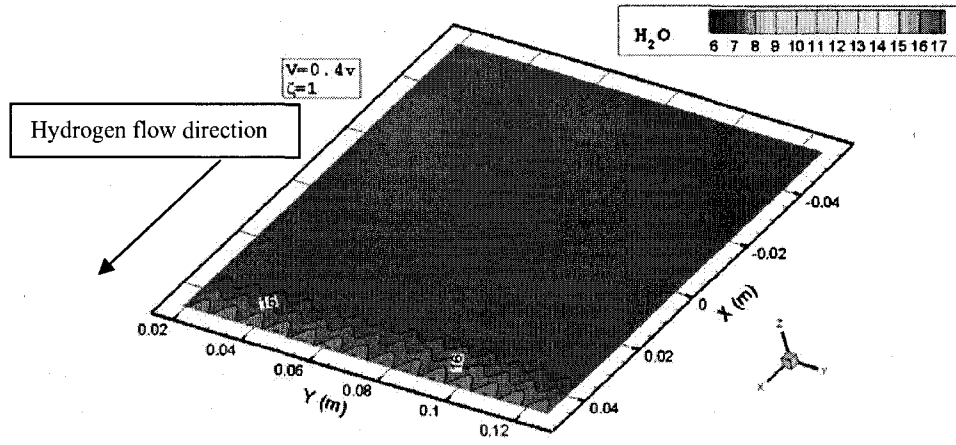
Anode Catalyst Hydrogen Mass Fraction



(c)

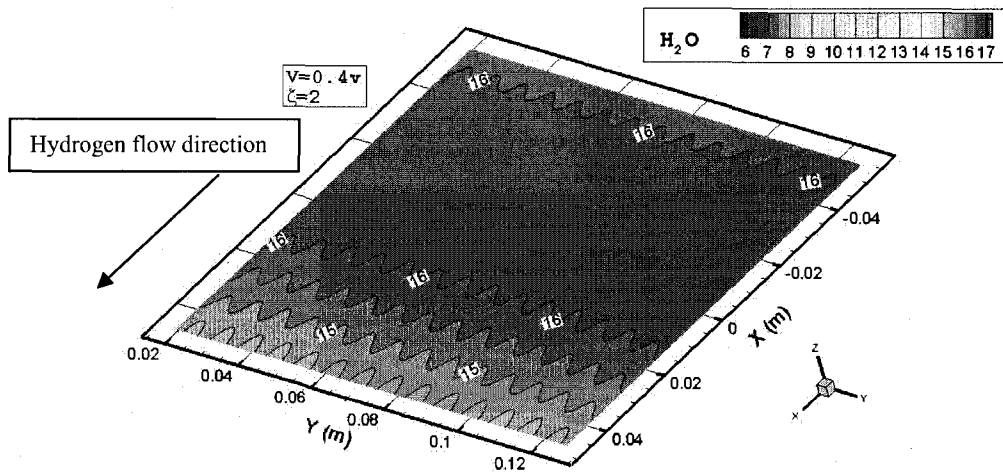
Fig. 4.9 Anode catalyst hydrogen mass fraction at 0.4V

### Cathode Catalyst Water Mass Fraction



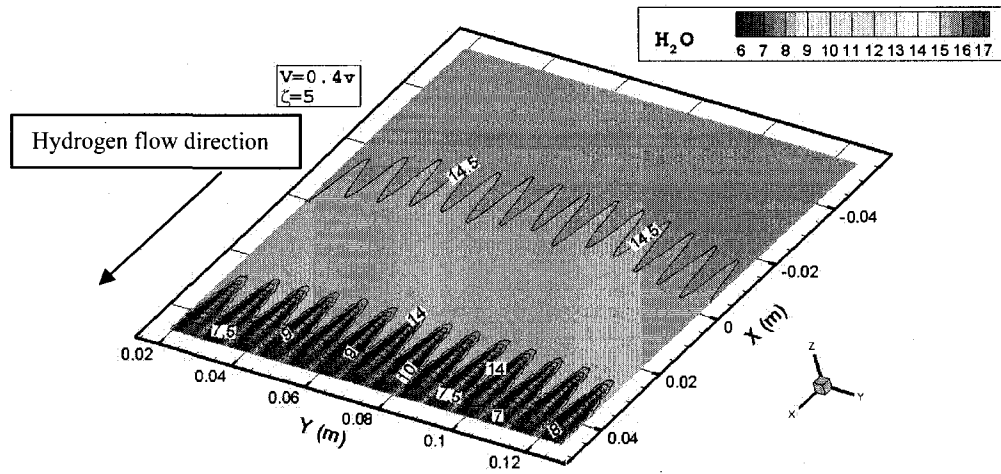
(a)

### Cathode Catalyst Water Mass Fraction



(b)

### Cathode Catalyst Water Mass Fraction



(c)

Fig. 4.10 Cathode catalyst water mass fraction at 0.4V

#### 4.2.4 Current Density

The most important improvement for the new design, compared with the base design, is the increased current density, i.e. power, under the same fuel cell operating conditions. Fig. 4.11 shows the normalized current density under different  $\zeta$  values. When fuel cell operates under high current density condition ( $V_{cell} = 0.4V$ ), the current density will increase by increasing the flow rate  $\zeta$ . However, further increase in  $\zeta$  will decrease the current density because of the “gas flow drying” effect which downgrades the membrane. The new design case has up to 60% higher current density under the same flow rate. Even when flow rate is high, the amount of current density decreasing is less than that in the baseline design. When the fuel cell operates under low current density condition ( $V_{cell} = 0.8V$ ), the new design case also has higher current density. When the flow rate is high, the current density only decreases within 10% compared to around 50% decreasing

in baseline design. Based on the above analysis, the uniform velocity can significantly improve the PEMFC performance with higher power output. The improved new design of PEMFC has better performance compared to baseline design for the different gas flow rates.

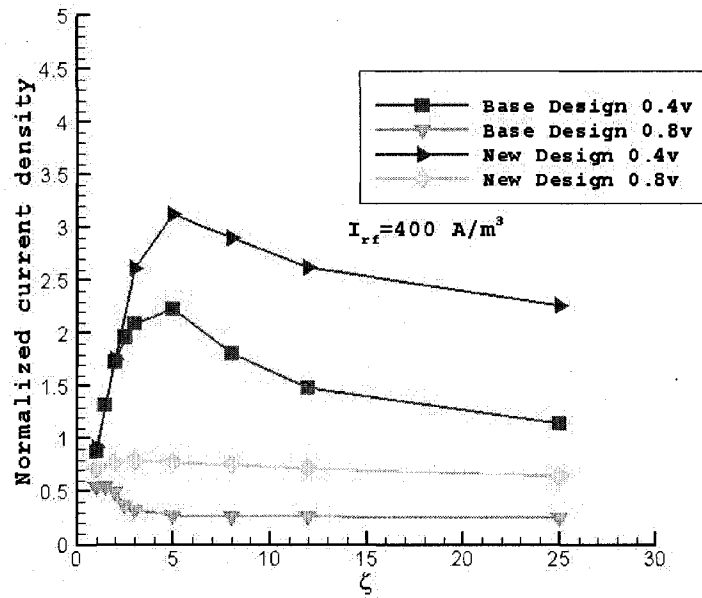


Fig. 4.11 Normalized current density under different  $\zeta$

## CHAPTER 5

### CONCLUSIONS AND RECOMMENDATIONS

#### 5.1 Conclusions

A three-dimensional PEMFC model has been studied and numerical methods have been applied to solve this model. This PEMFC model includes the current collectors, gas channels, gas diffusion layers, catalyst layers and proton exchange membrane. The single unit PEM fuel cell is modeled for the simultaneously occurring hydrodynamics, heat transfer, multi-species diffusion, and electrochemical reaction within it.

This model is validated in the single channel fuel cell case by comparing the numerical results of current density, mass fraction distribution with the published experimental data in the literature. The obtained numerical results are in good agreement with the available experimental data. All the validated parameters are then applied to the single unit PEM fuel cell. A baseline design and an improved design are both studied and simulated, and it is found a great improvement of the fuel cell performance is achieved under the same operating conditions. A parametric study is conducted by varying the gas flow rates at the anode and cathode inlets. The fuel cell performance is investigated under both high and low current density conditions.

PEMFC is a very complicated energy conversion device. The fuel cell performance can be affected by flow rate, water content level, temperature, and geometric design etc.

It is found that the improved design has the better performance than the baseline design case:

- A uniform velocity distribution is obtained in the improved design for the parallel channel layout. The baseline design has a very non-uniform velocity distribution: high at the lateral channels and low at the center channels.

- When flow rate increases, the non-uniform velocity distribution becomes worse in the baseline design case. The velocity in lateral channels reaches extremely high value. However, in the improved new design case, the velocity between channels keeps the uniform distribution as the flow rate increases.

- The fuel cell temperature change is based on the heat generation, and heat loss. When the gas flow rate increases, more fuel supply leads to the higher current density and heat generation. Then the fuel cell temperature increases. However, when the gas flow rate reaches certain high value the electrochemical reaction rate will not increase due to the mass transport limitation. In this situation, the convection heat transfer from the fuel cell to the gas mixture becomes significant. The temperature will decrease.

- The fuel cell water content will increase then decrease as the inlet flow rate increases from  $\zeta=1$  to  $\zeta=25$ . The relative humidity in gas channel is lower than in the MEA. The increased flow rate can lead to the “gas flow drying” effect to the MEA which can significantly increase the membrane protonic resistance.

- The improved design case has a much better velocity and temperature distribution compared with the baseline design. Its performance is more robust to the disturbance of the flow rate changes. When flow rate is high, it can have the higher current density than baseline design under the same operating conditions.

To sum up, in the improved design, the current density has increased by 60%-80% under the same operating conditions compared to the baseline design. Its uniform velocity distribution provides the better performance under both high and low flow rate operating conditions.

## 5.2 Recommendations

Many fuel cell designs and operating parameters are directly influencing the fuel cell performance. Most of them are coupled and related to each other, such as the flow rate and fuel cell temperature, the water content and inlet relative humidity, the operating pressure and diffusivity, etc. Further parametric study is needed in order to obtain the optimized fuel cell performance such as the study about the channels geometric design, the purity of fuel with the GDL porosity and thickness, membrane conductivity, and the inlet relative humidity with fuel cell current density. The single stack performance can not be simply applied to the fuel cell stack performance because the fuel cell stack has more complicated fuel and temperature distributions and water management issues. The three-dimensional fuel cell stack simulation in the system level is also important for the future research to achieve the high performance fuel cell stack.

## REFERENCES

- [1] L. Carrette, K.A. Freidrich, U. Stimming, "Fuel Cells Fundamentals and Applications, Fuel Cells," 1 (2001) 5-39.
- [2] T.V. Nguyen, M.W. Knobbe, "A liquid water management strategy for PEM fuel cell stacks," *Journal of Power Sources* 114 (2003) 70-79.
- [3] EG&G Technical Services, Inc., Fuel Cell Handbook, 6<sup>th</sup> ed., DOE NETL, 2002.
- [4] C. Stone, A.E. Morrison, "From curiosity to 'power to change the world'," *Solid State Ionics* 2002, 152:1-13.
- [5] T. Berning, "Three-Dimensional Computational Analysis of Transport Phenomena in a PEM Fuel Cell," Ph.D., Thesis, 2002.
- [6] J.A. Kolde, B. Bahar, M.S. Wilson, T.A. Zawodzinski, and S. Gottesfeld, "Advanced Composite Polymer Electrolyte Fuel Cell Membranes," *Proc. Electrochem. Society*, 23:193-201, 1995.
- [7] N. Djilali, "Computational modeling of polymer electrolyte membrane (PEM) fuel cells: Challenges and opportunities," *Energy* 32 (2007) 269-280.
- [8] P.W. Atkins, *Physical Chemistry*, fifth edition, Oxford University Press, Oxford, 1994.
- [9] A.J. Bard, L.R. Faulkner, *Electrochemical Methods*, Wiley New York, p86-116, 1980.
- [10] Weber & Newman, *Chem. Rev.*, 104, pp. 4679-4726, 2004.
- [11] W.Q. Tao, C.H. Min, X.L. Liu, Y.L. He, B.H. Yin, W. Jiang, "Parameter sensitivity examination and discussion of PEM fuel cell simulation model validation Part I. Current status of modeling research and model development," *Journal of Power Sources* 160 (2006) 359-373.
- [12] C. Marr, X. Li, "Composition and performance modeling of catalyst layer in a proton exchange membrane fuel cell," *Journal of Power Sources* 77 (1999) 17-27.



- [13] F. Jaouen, G. Lindbergh, G. Sundholm, "Investigation of mass-transport limitations in the solid polymer fuel cell cathode," *Journal of the Electrochemical Society*, v 149, n 4, April, 2002, p A437-A447.
- [14] K.V. Zhukovsky, "Three dimensional model of oxygen transport in a porous diffuser of a PEM fuel cell," *AIChE Journal*, v 49, n 12, 2003, p 3029-3036.
- [15] H. Zhu, R.J. Kee, "A general mathematical model for analyzing the performance of fuel-cell membrane-electrode assemblies," *Journal of Power Sources* 117(2003) 61-74.
- [16] D.M. Bernardi, M.W. Verbrugge, "A mathematical model of the solidpolymer-electrolyte fuel cell," *Journal of Electrochemical Society* 139 (9) (1992) 2477-2491.
- [17] T.E. Springer, M.S. Wilson, S. Gottesfeld, "Modeling and experimental diagnostics in polymer electrolyte fuel cell," *Journal of Electrochemical Society*, 140 (12) (1993) 3513-3526.
- [18] A. Kazim, H.T. Liu, P. Forges, "Modeling of performance of PEM fuel cells with conventional and interdigitated flow fields," *Journal of Applied Electrochemistry*, v 29, n 12, Dec, 1999, p 1409-1416.
- [19] V. Gurau, H.T. Liu, S. Kakac, "Two-dimensional model for proton exchange membrane fuel cells," *AIChE Journal* 44 (11) (1998) 2410-2422.
- [20] W.S. He, J.S. Yi, T.V. Nguyen, "Two-phase flow model of the cathode of PEM fuel cells using interdigitated flow fields," *AIChE Journal* 46 (10) (2000) 2053-2064.
- [21] S. Dutta, S. Shimpalee, J.W. Van Zee, "Three-dimensional numerical simulation of straight channel PEM fuel cells," *Journal of Applied Electrochemistry*. 30 (2000) 135-146.
- [22] T. Berning, D.M. Lu, N. Djilali, "Three-dimensional computational analysis of transport phenomena in a PEM fuel cell," *Journal of Power Source* 106 (2002) 284-294.
- [23] T.C. Jen, T. Yan, S.H. Chan, "Chemical reacting transport phenomena in a PEM fuel cell," *Int. Journal of Heat Transfer* 46 (22) (2003) 4157-4168.
- [24] J. Ramousse, J. Deseure, O. Lottin, S. Didierjean, D. Maillet, "Modelling of heat, mass and charge transfer in a PEMFC single cell," *Journal of Power Sources*, 145 (2), pp. 416-427, 2005.

- [25] H. Meng, "A three-dimensional PEM fuel cell model with consistent treatment of water transport in MEA," *Journal of Power Sources*, 162, pp. 426- 435, 2006.
- [26] R.F. Mann, J.C. Amphlett, M.A.I. H.M. Hooper, Jensen, B.A. Peppley, P.R. Roberge, "Development and application of a generalized steady-state electrochemical model for a PEM fuel cell," *Journal of Power Sources*, 86, pp. 173-180, 2000.
- [27] P.T. Nguyen, T. Berning, Djilali, "Computational model of a PEM fuel cell with serpentine gas flow channels," *Journal of Power Sources*, 130, pp. 149-157, 2004.
- [28] J. Park and X. Li, "An experimental and numerical investigation on the cross flow through gas diffusion layer in a PEM fuel cell with a serpentine flow channel," *Journal of Power Sources*, 163, pp. 853- 863, 2007.
- [29] S.A. Grigoriev, A.A. Kalinnikov, V.N. Fateev, A.A. Wragg, "Numerical optimization of bipolar plates and gas diffusion layers for PEM fuel cells," *Journal of Applied electrochemistry*, 36, pp. 991-996, 2006.
- [30] A. Kumar, R.G. Reddy, "Effect of gas flow field-design in the bipolar/end plates on the study and transient state performance of polymer electrolyte membrane fuel cells," *Journal of Power Sources*, 155, pp. 264-271, 2006.
- [31] J.K. Kuo, C.K. Chen, "A novel Nylon-6-S316L fiber compound material for injection molded PEM fuel cell bipolar plates," *Journal of Power Sources*, 162 (1), pp. 207-214, 2006.
- [32] S. Joseph, J.C. McClure, R. Chianelli, P. Pich, P.J. Sebastian, "Conducting polymer-coated stainless steel bipolar plates for proton exchange membrane fuel cells (PEMFC)," *International Journal of Hydrogen Energy*, 30 (12), pp. 1339-1344 SEP 2005.
- [33] E.A. Cho, U.S. Jeon, H.Y. Ha, S.A. Hong, I.H. Oh, "Characteristics of composite bipolar plates for polymer electrolyte membrane fuel cells," *Journal of Power Sources*, 125, pp. 178-182, 2004.
- [34] U. Beuscher, S.J.C. Cleghorn, W.B. Johnson, "Challenges for PEM fuel cell membranes", *International Journal of Energy Research*, 29 (12), pp. 1103-1112, 2005.
- [35] Jalani, H. Nikhil, C. Pyoungho, D. Ravindra, "Design of high temperature membranes for PEMFC," 205th Meeting of The Electrochemical Society, MA 2004 01, 2004, p 29.

- [36] B. Carnes, , N. Djilali, "Analysis of coupled proton and water transport in a PEM fuel cell using the binary friction membrane model," *Electrochimica Acta*, v 52, n 3, Nov 12, 2006, p 1038-1052.
- [37] J. T. Gostick, M.W. Fowler, M.D. Pritzker, M.A. Ioannidis and L.M. Behra, "In-plane and through-plane gas permeability of carbon fiber electrode backing layers," *Journal of Power Sources*, 162, pp. 228- 238, 2006.
- [38] H.X. Zhong, H.M. Zhang, Y.M. Liang, J.L. Zhang, M.R. Wang, X.L Wang, "A novel non-noble electrocatalyst for oxygen reduction in proton exchange membrane fuel cells," *Journal Of Power Sources*, 164 (2), pp. 572-577, 2007.
- [39] C.H. Cheng, H.H. Lin, G.J. Lai, "Numerical prediction of the effect of catalyst layer Nafion loading on the performance of PEM fuel cells," *Journal of Power Sources*, 164 (2), pp. 730-741, 2007.
- [40] R.L. Borup, J.R. Davey, F.H. Garzon, D.L. Wood, M.A. Inbody, A. Michael, "PEM fuel cell electro catalyst durability measurements," *Journal of Power Sources*, 163 (1), pp. 76-81, 2006.
- [41] P. Yong, M. Paterson-Beedle, I. P. Mikheenko, L. E. Macaskie, "From biomineralisation to fuel cells: biomanufacture of Pt and Pd nanocrystals for fuel cell electrode catalyst," *Biotechnol Lett* (2007) 29:539–544.
- [42] D. J. Ludlow, C. M. Calebrese, S. H. Yu., Dannehy, D.L. Jacobson, D.S. Hussey, Arif, M. K. Jensen, G. A. Eisman, "PEM fuel cell membrane hydration measurement by neutron imaging," *Jouranal of Power Sources*, 162, pp. 271-278, 2006.
- [43] Z. Zhan, J. Xiao, D. Li, M. Pan and R. Yuan, "Effects of porosity distribution variation on the liquid water flux through gas diffusion layers of PEM fuel cells," *Journal of Power Sources*, 160, pp. 1041- 1048, 2006.
- [44] K. Jiao, B. Zhou, P. Quan, "Liquid water transport in straight micro-parallel-channels with manifolds for PEM fuel cell cathode," *Journal of Power Sources* 157 (2006) 226–243.
- [45] D.L. Wood, J.S. Yi and T.V. Nguyen, "Effect of direct liquid water injection and interdigitated flow field on the performance of proton exchange membrane fuel cells," *Electrochimica Acta*, Vol. 43, No. 24, pp. 3795-3809, 1998.
- [46] J.H. Jang, W.M Yan, H.Y Li, Y.C Chou, "Humidity of reactant fuel on the cell performance of PEM fuel cell with baffle-blocked flow field designs," *Journal of Power Sources* 159 (2006) 468–477.

- [47] W.M Yan, H.S Chu, J.Y Chen, C.Y. Soong, F. Chen, "Transient analysis of water transport in PEM fuel cells," *Journal of Power Sources* 162 (2006) 1147–1156.
- [48] K.H. Choi, D.H Peck, C.S Kim, D.R Shin, T.H Lee, "Water transport in polymer membranes for PEMFC," *Journal of Power Sources* 86 (2000) 197-201.
- [49] FLUENT, Inc., FLUENT 6.2. User's Guide, Lebanon, NH, 2005.
- [50] T.A. Zawodzinski, T.E. Springer, S. Gottesfeld, "Polymer electrolyte fuel cell model," *Journal of the Electrochemical Society*, v 138, n 8, Aug, 1991, p 2334-2342.
- [51] Z.H. Wang, C.Y. Wang, K.S. Chen, "Two-phase flow and transport in the air cathode of proton exchange membrane fuel cells," *J. Power Sources* 94 (2001) 40–50.
- [52] R.B. Bird, W.E. Stewart, and E.N. Lightfoot, *Transport Phenomena*, 2<sup>nd</sup> Edition John Wiley & Sons, Inc., 2002.
- [53] C.Y. Wang, S. Um and K.S. Chen, "Computational fluid dynamics modeling of proton exchange membrane fuel cells," *Journal of Electrochemical Society*, 147(12):4485-4493, 2000.
- [54] T. V. Nguyen, *Electrochemical Soc. Proceedings*, 99(14):222-241.
- [55] J.H. Nam and M. Karviany, "Effective Diffusivity and Water-Saturation Distribution in Single and Two-layer PEMFC Diffusion Medium," *Int. Journal of Heat Mass Transfer*, 2003.
- [56] B.M. Eaton, "One dimensional Transient Model of Heat, Mass, and Charge Transfer in a Proton Exchange Membrane," M.S. Thesis, 2001.
- [57] P. Costamagna, "Transport Phenomena in Polymeric Membrane Fuel Cells," *Chemical Engineering Science*, vol 56 (2001), pp. 323-332.
- [58] E.A. Ticianelli, C.R. Derouin, A. Redondo and S. Srinivasan, "Methods to Advance Technology of Proton Exchange Membrane Fuel Cells," *J. Electrochem. Soc.* 135 (9) (1988) 2209–2214.
- [59] D.M. Bernardi, "Water-balance calculations for solid polymer-electrolyte fuel cell," *J. Electrochem. Soc.* 137 (8) (1990) 3344–3350.
- [60] D.M. Bernardi, M.W. Verbrugge, "A mathematical model of the solid polymer-electrolyte fuel cell," *J. Electrochem. Soc.* 139 (9) (1992) 2477–2491.

- [61] G. Lin, W. He, T.V. Nguyen, "Modeling liquid water effects in the gas diffusion and catalyst layers of the cathode of a PEM fuel cell," *J. Electrochem. Soc.* 151 (2) (2004) A1999–A2006.
- [62] S. Mazumder, J.V. Cole, "Rigorous 3-D mathematical modeling of PEM fuel cells. I. Model predictions without liquid water transport," *J. Electrochim. Soc.* 150 (11) (2003) A1503–A1509.
- [63] C.M. Baca, R. Travis and M. Bang, "Three-dimensional, single-phase, non-isothermal CFD model of a PEM fuel cell," *Journal of Power Sources* 178 (2008) 269–281.
- [64] D. Martin, D.M. Guinea, B. Moreno, L. Gonzalez, M.C. Garcia-Alegre, D. Guinea, "Electric modelling and image analysis of channel flow in bipolar plates," *International Journal of Hydrogen Energy* 32 (2007) 1572 – 1581.

VITA

Graduate College  
University of Nevada, Las Vegas

Jianfei Wu

Local Address:

1852 Desert Forest Way,  
Henderson, NV, 89012

Degrees:

Bachelor of Engineering, Automation Engineering, 2005  
Nanjing University of Technology, China.

Selected publications:

- [1] J. F. Wu, J. H. Nie and Y. T. Chen, Optimization Of Fluid Flow In 3d Bipolar Plates, ASME Fluids Engineering Division Summer Conference, FEDSM2008-55040, Jacksonville, Florida, August 10-14, 2008.
- [2] J. H. Nie, J. F. Wu, S. Cohen, B. Carter and Y. T. Chen, Numerical Simulations Of Coupled Flow And Heat Transfer Distributions In A Bipolar Plate Of The Pem Electrolysis Cell, 2008 ASME Fluids Engineering Conference, FEDSM2008-55188, Jacksonville, Florida, August 10-14, 2008.
- [3] J. H. Nie, K. M. Veepuri, Y. T. Chen and J. F. Wu, A New Bipolar Plate Of Pem Electrolysis Cell With Uniform Flow And Heat Transfer Fields, ASME Summer Heat Transfer Conference, HT2008-56362, Jacksonville, Florida, August 10-14, 2008.
- [4] J. F. Wu, J. H. Nie and Y. T. Chen, Three-dimensional fluid flow and coupled heat transfer in simplified bipolar plates, International Mechanical Engineering Congress and Exposition (IMECE 2007), IMECE2007-42360, Seattle, WA, November 14, 2007.

- [5] J. F. Wu, J. H. Nie and Y. T. Chen, 3D fluid flow and coupled heat transfer in PEM bipolar plate electrolyzer cell, 2007 Inaugural Energy Symposium, UNLV, Las Vegas, NV, August 15-16, 2007.
- [6] J. F. Wu, J. H. Nie and Y. T. Chen, Numerical simulations of three-dimensional fluid flow and coupled heat transfer in bipolar plates, 5th Joint ASME/JSME Fluids Engineering Conference, FEDSM2007-37712, San Diego, CA, July 30-August 2, 2007.
- [7] J. F. Wu and M. X. Cheng, Implementation of real-time curve plotting under MiniGUI application and embedded Linux, Computer Engineering, 2006.

Thesis Title:

Three-dimensional Numerical Study of Proton Exchange Membrane Fuel Cell Design

Thesis Examination Committee:

Chairperson, Dr. Yitung Chen, Ph. D.  
Committee Member, Dr. Robert Boehm, Ph. D.  
Committee Member, Dr. Jianhu Nie, Ph. D.  
Graduate College Representative, Dr. Jichun Li, Ph. D.